Alteration at the base of the Siccar Point unconformity and further evidence for an alkaline provenance at Gale crater: Exploration of the Mount Sharp group, Greenheugh pediment cap rock contact with APXS

Lucy M Thompson<sup>1,1</sup>, John G. Spray<sup>1,1</sup>, Catherine D O'Connell-Cooper<sup>1,1</sup>, Jeff A Berger<sup>2,2</sup>, Albert S. Yen<sup>3,3</sup>, Nicholas Boyd<sup>4,4</sup>, Ralf Gellert<sup>4,4</sup>, Michael A. McCraig<sup>4,4</sup>, and Scott J VanBommel<sup>5,5</sup>

November 30, 2022

#### Abstract

Chemical data acquired by Curiosity's Alpha Particle X-ray Spectrometer (APXS) during examination of the contact between the upper Mount Sharp group and overlying Stimson formation sandstones at the Greenheugh pediment reveal compositional similarities to rocks encountered earlier in the mission. Mount Sharp group strata encountered below the Basal Siccar Point group unconformity at the base and top of the section, separated by >300 m in elevation, have distinct and related compositions. This indicates enhanced post-depositional fluid flow and alteration focused along this contact. Sandstone targets exposed immediately above the unconformity have basaltic compositions consistent with previously encountered eolian Stimson formation sandstones, except at the contact, where they show the addition of S. Resistant sandstone outcrops above the contact have higher K, Mn and Na and lower Ni concentrations that primarily reflect changes in provenance. They are compositionally related to cap rock float blocks encountered as Curiosity climbed through the Mount Sharp group, and Bradbury group sandstone outcrops. The higher K, pediment sandstones are interpreted to have a similar provenance to some Bradbury group sandstones, further evidence for widespread, alkaline source rock within and/or in the vicinity of Gale crater. The Bradbury and Siccar Point groups may both be younger than the Mount Sharp group. Alternatively, an alkaline source area in and around Gale crater has been eroded by both water and wind at different times (both before and after deposition of the Mount Sharp group), during the evolution of the crater and its infill.

<sup>&</sup>lt;sup>1</sup>University of New Brunswick

<sup>&</sup>lt;sup>2</sup>NASA Johnson Space Center

<sup>&</sup>lt;sup>3</sup>Jet Propulsion Lab (NASA)

<sup>&</sup>lt;sup>4</sup>University of Guelph

<sup>&</sup>lt;sup>5</sup>Washington University in St. Louis

1 2 3 4 5 6	Alteration at the base of the Siccar Point unconformity and further evidence for an alkaline provenance at Gale crater: Exploration of the Mount Sharp group, Greenheugh pediment cap rock contact with APXS  L. M. Thompson <sup>1</sup> , J. G. Spray <sup>1</sup> , C. O'Connell-Cooper <sup>1</sup> , J. A. Berger <sup>2</sup> , A. Yen <sup>3</sup> , R. Gellert <sup>4</sup> , N. Boyd <sup>4</sup> , M. A. McCraig <sup>4</sup> , and S. J. VanBommel <sup>5</sup>
7	<sup>1</sup> Planetary and Space Science Centre, University of New Brunswick, Fredericton, Canada
8	<sup>2</sup> NASA Johnson Space Center, Houston, USA
9	<sup>3</sup> Jet Propulsion Laboratory, California Institute of Technology, Pasadena, USA
10	<sup>4</sup> Department of Physics, University of Guelph, Ontario, Canada
11 12	<sup>5</sup> Department of Earth and Planetary Sciences, Washington University in St. Louis, St. Louis USA
13	Corresponding author: Lucy Thompson ( <a href="mailto:lthompso@unb.ca">lthompso@unb.ca</a> )
14	Key Points:
15 16	<ul> <li>Enhanced post-depositional fluid flow and alteration of the Mount Sharp group was focused at the Basal Siccar Point group unconformity</li> </ul>
17	<ul> <li>Alkaline source rocks at Gale provided detritus to fluvial and eolian sandstones</li> </ul>
18 19 20	Bradbury and Siccar Point group sandstones may be contemporaneous, and younger than the Mount Sharp group

#### Abstract

21

22

23

24

25

26

27

28

29

30

31

32

33

34

35

36

37

38

39

40

51

Chemical data acquired by Curiosity's Alpha Particle X-ray Spectrometer (APXS) during examination of the contact between the upper Mount Sharp group and overlying Stimson formation sandstones at the Greenheugh pediment reveal compositional similarities to rocks encountered earlier in the mission. Mount Sharp group strata encountered below the Basal Siccar Point group unconformity at the base and top of the section, separated by >300 m in elevation, have distinct and related compositions. This indicates enhanced post-depositional fluid flow and alteration focused along this contact. Sandstone targets exposed immediately above the unconformity have basaltic compositions consistent with previously encountered eolian Stimson formation sandstones, except at the contact, where they show the addition of S. Resistant sandstone outcrops above the contact have higher K, Mn and Na and lower Ni concentrations that primarily reflect changes in provenance. They are compositionally related to cap rock float blocks encountered as Curiosity climbed through the Mount Sharp group, and Bradbury group sandstone outcrops. The higher K, pediment sandstones are interpreted to have a similar provenance to some Bradbury group sandstones, further evidence for widespread, alkaline source rock within and/or in the vicinity of Gale crater. The Bradbury and Siccar Point groups may both be younger than the Mount Sharp group. Alternatively, an alkaline source area in and around Gale crater has been eroded by both water and wind at different times (both before and after deposition of the Mount Sharp group), during the evolution of the crater and its infill.

#### Plain Language Summary

- Chemical data acquired by Curiosity's Alpha Particle X-ray Spectrometer (APXS) during examination of an important regional contact between two rock units in Gale crater, Mars, reveal
- relationships with other rocks encountered much earlier in the mission. These relationships
- 44 provide evidence for erosion by wind and water of various composition source rocks. These
- 45 include more typical martian basaltic and more alkaline composition rocks (e.g., higher
- 46 potassium and sodium). Distinct chemistry within rocks immediately underlying the contact,
- separated by more than 300 m in elevation, indicate enhanced fluid flow and alteration along the
- 48 contact. These relationships provide important insights into regional and crater-scale processes
- 49 and evidence for the long-lived role of water and aqueous alteration and hence, habitable
- 50 environments at Gale.

#### 1 Introduction

- For the last two years, the Mars Science Laboratory (MSL) mission, *Curiosity* rover has
- been exploring a geomorphic trough on the lower slopes of Mount Sharp referred to as "Glen
- Torridon" by the MSL team. The trough overlaps with an area identified from orbit as clay-
- bearing (Anderson and Bell, 2010; Fraeman et al., 2016; Milliken et al., 2010; Thomson et al.,
- 56 2011) and is delineated by Vera Rubin (formerly hematite) ridge (VRR) to the north and the
- 57 Greenheugh pediment and sulfate-bearing unit to the south (also identified from orbit; Milliken

et al., 2014) (Figures 1, 2). Thus, this region potentially records the end of a "wetter" environment on Mars, before a transition to more arid conditions and deposition of the overlying sulfate-bearing strata. The region is therefore one of the primary exploration targets of the MSL mission (Anderson and Bell, 2010; Bibring et al., 2006; Fraeman et al., 2016, Milliken et al., 2010).

As part of the Glen Torridon campaign, *Curiosity's* traverse crossed the contact between the flat-lying strata of the Glen Torridon, clay-bearing unit and the overlying Greenheugh pediment-capping sandstones. The composition of the strata exposed either side of this contact was investigated using the Alpha Particle X-ray Spectrometer (APXS). This work documents the results of that investigation and discusses implications for the alteration history along the contact, and the provenance of the overlying capping sandstones.

# 1.1 Geological background and context

The predominantly sedimentary strata encountered thus far on the mission have been divided into the Bradbury, Mount Sharp and Siccar Point stratigraphic groups (Figure 1b) (Banham et al., 2018; Fraeman et al., 2016; Grotzinger et al., 2015). The Bradbury group encompasses the interfingering lacustrine and fluvio-deltaic strata encountered from landing to arriving at the base of Mount Sharp (up to sol 722; Edgar et al., 2018, 2020; Grotzinger et al., 2014, 2015; Schieber et al., 2017; Williams et al., 2013). The Mount Sharp group comprises the Murray and Carolyn Shoemaker formations, which is in turn overlain by eolian sandstones of the Stimson formation, Siccar Point group (Figure 1b), (Banham et al., 2018, 2021; Fraeman et al., 2016).

The strata explored in Glen Torridon belongs to the upper Murray formation and the Carolyn Shoemaker formation (Figure 1b; Bennett et al., this issue). The Glen Torridon Murray

81

82

83

84

85

86

87

88

89

90

91

92

93

94

95

96

97

98

99

100

101

102

103

formation is a continuation of the Jura member, first encountered on VRR (Fedo et al., 2020). The Jura member is overlain by the Knockfarril Hill and Glasgow members of the Carolyn Shoemaker formation. The Murray formation is characterized by lacustrine mudstones with minor intercalated sandstones (Edgar et al., 2020; Grotzinger et al., 2015; Stack et al., 2019). In contrast, the overlying Carolyn Shoemaker formation comprises more abundant fine sandstone preserving both cross-stratification and symmetrical ripples, as well as mudstone. This is interpreted to have been deposited at least in part, in a higher energy environment (Caravaca et al., this issue; Fedo et al., 2020). The Glasgow member immediately beneath the pediment and exposed on the upper reaches of a butte just to the west of the ascent route is referred to as the Hutton interval, after the Hutton drill hole. It is characterized by a distinctly lighter tone, both from orbit and rover-based imagery (Bennett et al., this issue; Rudolf et al., this issue). The rocks that cap the Greenheugh pediment comprise part of a more extensive, resistant, crater-retaining capping unit originally identified from orbit by Malin and Edgett (2000) who interepreted the unit to lie unconformably on the underlying strata. Curiosity's traverse confirmed the presence of an erosional unconformity between the Mount Sharp group and the overlying eolian Stimson formation, Siccar Point group at the Emerson and Naukluft plateaus and Murray buttes. This is referred to as the Basal Siccar Point group unconformity (Figure 1b, Banham et al., 2018, 2021; Fraeman et al., 2016). Mapping indicates that the unconformity drops in elevation ~140 m over a distance of ~2.3 km between these locations (Watkins et al., 2016).

Based on sedimentology and textures the Greenheugh pediment capping sandstones are interpreted to also belong to the eolian Stimson formation, Siccar Point group (Banham et al., this issue; Figure 1). They have been subdivided into intervals based on their sedimentology: the basal Gleann Beag interval (platy weathering), and the Ladder and Edinburgh intervals

(characterized by their blockier, more massive appearance) (Banham et al., this issue). The basal surface of the pediment, like that of the Stimson formation previously encountered, is interpreted to represent the Basal Siccar Point group unconformity at this location (Banham et al., this issue; Bryk et al., 2019). It might also represent a weathering zone associated with what would have been eroded, exposed Mount Sharp group, prior to deposition of the sandstone. Following deposition and some lithicifcation of the pediment sandstones, the unconformity may also have acted as a focus for later alteration and fluid flow in the underlying, less resistant Mount Sharp group, as has previously been proposed for rocks encountered on VRR (Fraeman et al., 2020; Rampe et al., 2020a; Thompson et al., 2020).

## 1.2 APXS investigation of the Greenheugh pediment area

As part of the Glen Torridon campaign, *Curiosity* was able to drive up to the contact between the Mount Sharp group and the overlying Greenheugh pediment cap rock, and onto the pediment. (Bennett et al., this issue; Figures 1, 2). Obtaining compositional data at this location allows for comparison with the strata previously investigated along this important regional feature. It can help to assess the validity of the hypotheses outlined above. Specifically, elemental compositions measured by APXS can address questions such as:

- 1) Is the composition of the Mount Sharp group strata exposed at the contact with overlying cap rock in family with the rest of the Glen Torridon bedrock and Mount Sharp group, or is it distinct? The answer to this question can aid in determining whether enhanced alteration may have occurred along the contact. Changes in concentration of immobile versus mobile elements can shed light on the nature of any alteration process(es).
- 2) How does the composition of the Mount Sharp group at the Greenheugh, Basal Siccar Point group unconformity location compare to Mount Sharp group strata exposed at lower

stratigraphic levels along the unconformity? A compositional relationship might indicate widespread weathering or alteration associated with the unconformity.

3) Do the Greenheugh pediment capping sandstones all have the same chemistry, or are there differences between the sedimentological intervals that might indicate changing provenance or physical transport/sorting/mixing processes? Distinct chemistry immediately at the unconformity might indicate alteration of the sandstone at the contact, or perhaps incorporation of underlying Mount Sharp group material. How does the chemistry of the pediment capping sandstone compare to that of the Stimson formation sandstone encountered earlier in the mission? Do they have a related provenance? If there are differences in chemistry, do the Greenheugh capping sandstones show any compositional relationship to other sandstones analyzed by APXS during the course of the mission?

#### 2 Methods

# 2.1 Alpha Particle X-ray Spectrometer

The Canadian-built Alpha Particle X-ray Spectrometer (APXS) on *Curiosity* is the third iteration of APXS to fly on a Mars rover. The APXS is located on the end of *Curiosity's* robotic arm, which deploys the instrument to rock and soil targets. Particle induced X-ray emission and X-ray fluorescence techniques are used to induce characteristic X-rays within the sample (i.e., rocks and unconsolidated materials such as sand, soil and drilled samples). The X-rays produced by the sample of interest are detected by a silicon drift detector and the resulting spectrum used to determine composition. Further details of the APXS instrumentation, fundamentals, and calibration are provided by Berger et al. (2020), Campbell et al. (2012, 2014), Gellert et al. (2006, 2015), Reider et al. (2003) and VanBommel et al. (2016, 2017, 2019).

When placed in contact with the target of interest, APXS obtains analyses from a 1.5 cm diameter area. The area analyzed increases up to ~3.6 cm in diameter for a standoff of 2.5 cm from the target. The highest quality measurements (for Na, Mg, Al, Si, P, S, Cl, K, Ca, Ti, Cr, Mn, Fe, Ni, Zn and Br) are obtained when APXS is within 1 cm of the target, at the coldest time of day (overnight) and for integrations times >2-3 hours and typically 8 hours (e.g. VanBommel et al., 2019). Major element (and some minor element) chemistry of a target can be determined with high precision in as little as 10 minutes of integration time during the early morning or evening. Dusty targets can be brushed prior to APXS observations using the Dust Removal Tool (DRT; Davis et al., 2012).

APXS data are reported as weight percent (wt%) oxide except for Cl, which is reported as wt% element, and Ni, Zn and Br (and other trace elements), which are reported in  $\mu g/g$  (parts per million - ppm). APXS does not determine oxidation state and therefore S, Cl, Mn and Fe are reported as SO<sub>3</sub>, Cl, MnO and FeO respectively. Concentrations are normalized to 100%.

#### 2.2 Other instrumentation utilized in this study

For the majority of targets analyzed by APXS, accompanying high-resolution images are obtained. The Mastcam instrument provides context images of the workspace and surrounding area, while the Mars Hand Lens Imager (MAHLI) instrument typically acquires co-located, close-up images of the target of interest. See Edgett et al. (2012) and Malin et al. (2017) and for details of the MAHLI and Mastcam instruments respectively.

Powdered drill samples are delivered to *Curiosity's* internal Chemistry and Mineralogy (CheMin) and Sample Analysis at Mars (SAM) instruments. The CheMin instrument determines the mineralogy of a sample via X-ray diffraction (XRD, Blake et al., 2012), and the SAM instrument the organic and light element content via gas chromatography (GC), mass

spectrometry (MS) and tunable laser spectrometry (TLS) (Mahaffy et al., 2012). Once the CheMin and SAM instruments have received sufficient sample, drill fines remaining in the drill bit assembly are dumped onto the ground and analyzed by APXS, along with any powdered material surrounding the drill hole, thus providing the bulk chemistry of related material ingested by CheMin and SAM.

### 2.3 APXS Sampling

The APXS-derived compositional characteristics of the Bradbury, Mount Sharp and Siccar Point groups encountered up to and including Vera Rubin ridge can be found in Berger et al. (2020) and Thompson et al. (2016, 2020). For a detailed summary of the chemistry of the Glen Torridon, Mount Sharp group, Murray and Carolyn Shoemaker formations as determined by APXS, see O'Connell-Cooper et al. (this issue).

Since the initial descent from VRR down into the Glen Torridon region, APXS has analyzed 153 rock, regolith and drill fines targets within the clay-bearing Mount Sharp group up to and including sol 2776 (sol – martian solar day, which equates to ~24 hours, 39 minutes and 35 seconds) (O'Connell-Cooper et al., this issue). Here we discuss in detail the Mount Sharp group, Glasgow member targets analyzed as we neared the Greenheugh pediment including the Hutton drill samples (Hutton interval, Bennett et al., this issue), as well as targets analyzed just after we left the pediment up to sol 2776, which include the Glasgow drill samples (Figure 2, Table 1a).

A further 22 APXS analyses were obtained on rock and drill fines (Edinburgh drill hole) associated with the Greenheugh pediment cap rock. These included 3 float rocks from a butte encountered prior to *Curiosity's* climb onto the pediment (i.e., Western butte) (Figure 2; Table 1b).

#### 2.4 Treatment of the APXS data

Analyses with atypical alteration and diagenetic features or large veins (>0.5 cm) are distinguished from typical bedrock analyses. Atypical diagenetic and alteration features include irregularly distributed erosion resistant features, and different color patches and halos within the bedrock and associated with vein margins. Regolith analyses are excluded from the main Glen Torridon dataset.

Average, median, maximum and minimum, and  $1\sigma$  standard deviation values are computed for: 1) the Mount Sharp group encountered prior to Glen Torridon, 2) Glen Torridon (GT) Jura and Knockfarril Hill member bedrock combined, 3) Glasgow member bedrock (excluding the targets within 3 m of cap rock, i.e., the Hutton interval), and 4) the Hutton interval (Table 1a).

Average, median, maximum and minimum, and  $1\sigma$  standard deviation values are also derived for: 1) the Stimson formation bedrock from the Emerson and Naukluft plateaus, 2) all Greenheugh pediment cap rock, 3) platy weathering pediment cap rock only (Gleann Beag interval), and 4) blocky pediment cap rock (Ladder and Edinburgh intervals) (Table 1b).

All data is represented in various plots. See §S2.1, 2.3, 2.4, and 2.5 for details of plots. See Table S1 for a list of targets used in this study, Thompson (2022) for all derived data, and §S3 and S4 for relevant Mastcam and MAHLI images.

Statistical F- and t-tests were carried out to compare the variance and the difference/similarity of various subsets of the data (§S2.2, Tables S2 and S3). Relative increases and decreases in elemental concentrations were calculated for certain datasets, e.g., for the Ladder and Edinburgh pediment capping sandstones relative to mean Stimson formation sandstone from the Emerson and Naukluft plateaus (§S2.7; Thompson, 2022). Relative elemental

gains and losses were also derived via a mass balance calculation for select datasets: 1) Hutton interval targets versus the Glasgow DRT target (typical Glasgow member bedrock and drill target), and 2) pediment cap rock diagenetic/alteration features versus the Galloway Hills pediment sandstone target within the Gleann Beag interval (§S2.7; Thompson, 2022). The results of the mass balance and elemental increase/decrease calculations are represented graphically in the main body of the paper.

#### 3 Results

### 3.1 Composition of the Hutton interval targets

The Mount Sharp group targets analyzed by APXS within 3 m of elevation of the pediment, referred to as the Hutton interval (Figures S2, S3, S8), are compositionally distinct for a number of elements from the rest of the Glen Torridon Mount Sharp group and most of the Mount Sharp group encountered prior to the Glen Torridon campaign (Figures 3a, b; Table 1a; Table S2). Hutton, Buchan Haven (Western butte) and other bedrock targets <3 m below the pediment have high Na<sub>2</sub>O concentrations (3.27  $\pm$  0.29 wt%) versus all other Glen Torridon rocks. The Jura and Knockfarril Hill members have a mean Na<sub>2</sub>O concentration of 2.39  $\pm$  0.23 wt% and the Glasgow member, 2.41  $\pm$  0.17 wt%. The Hutton interval targets also exhibit higher Na<sub>2</sub>O concentrations than most of the Mount Sharp group previously analyzed by APXS (2.55  $\pm$  0.25 wt%).

Hutton interval SO<sub>3</sub> concentrations are low compared to all bedrock targets encountered within Glen Torridon ( $2.99 \pm 0.96$  wt% versus  $6.07 \pm 2.70$  wt% for the Jura and Knockfarril Hill members, and  $7.66 \pm 1.85$  wt% for the Glasgow member). SO<sub>3</sub> concentrations are also low compared to the Mount Sharp group preceding the campaign ( $6.40 \pm 2.29$  wt%). SO<sub>3</sub> does not

correlate with CaO ( $R^2 = 0.08$ , R = -0.28), and the Hutton interval targets do not lie on a CaSO<sub>4</sub> addition trend line as is typical for the Mount Sharp group. Instead, the targets plot with excess Ca relative to the CaSO<sub>4</sub> addition trend line, indicating that the Ca is present in another phase (Figure 3c; Thompson et al., 2020).

The bedrock targets just below the pediment also trend to higher MnO and  $P_2O_5$ , and lower Ni  $(0.26\pm0.03 \text{ wt\%}, 1.12\pm0.04 \text{ wt\%}, 689\pm52 \text{ ppm}$  respectively) than the majority of other Glasgow member bedrock targets  $(0.16\pm0.05 \text{ wt\%}, 0.92\pm0.10 \text{ wt\%}, 873\pm117 \text{ ppm}$  respectively) (Figure 3a, b). They have the same characteristically low Zn concentrations as the rest of the Glasgow member (<1550 ppm) compared to the GT Jura and Knockfarril Hill members ( $\leq$ 4400 ppm) (Figure 3b). Unlike the rest of the Mount Sharp group, except for a number of Pahrump Hills member targets at the base of the section, Na correlates with Ti ( $R^2 = 0.8$ ; Figure S1). The APXS bedrock targets with the most similar elemental trends are those encountered at the base of the Mount Sharp group, at Pahrump Hills, within the Pahrump Hills member, and a number of targets from the overlying Hartmann's Valley member (Figures 3a, c; Figure 1 for context). In particular, the Pahrump Hills member, Telegraph Peak and associated targets are the only other Mount Sharp group targets to exhibit the same significantly elevated Na as the Hutton interval (Figure 4a).

Mass balance calculations of the Hutton interval targets relative to the Glasgow DRT target (typical Glasgow member) reveal consistent and significant Na, Mg, Ca, Mn, and Fe gains, and losses of Ni. All the Hutton interval targets, with 2 exceptions, show loss of S, and all targets show less pronounced gains of K and Al (Figure 4b).

### 3.1.1. Diagenetic and vein targets

262

263

264

265

266

267

268

269

270

271

272

273

274

275

276

277

278

279

280

281

282

283

284

The number of features attributed to post-depositional, diagenetic processes observed within the Glasgow member appeared to increase in abundance as *Curiosity* neared the Greenheugh pediment (Bennett et al., this issue; Gasda et al., this issue). The bedrock itself contains abundant, fine-scale (mm-size) resistant features. Larger-scale features analyzed by APXS in the vicinity of the contact with the pediment capping rocks include; 1) Abernethy from the Buchan Haven workspace, Western butte, 2) Moffat Hills and Bogmill Pow, and 3) Dounraey, Liberton Brae and Moorfoot Hills, with 2) and 3) from the Hutton drill workspace (Table 1a; Figures S3, S10, S11 for images). Diagenetic target oxide and elemental abundances are log ratioed to their respective bedrock target in the same workspace (Figure 5). The Abernethy and Dunbartonshire targets, both darker toned and associated with crosscutting vein margins, are compositionally related, with comparable elemental trends relative to their respective bedrock. Both exhibit very high FeO (40.12 and 39.65 wt% respectively) and MnO (5.11 and 6.33 wt% respectively) concentrations. The Fe content is more than double, and the Mn content is sixteen to twenty-four times that measured in the adjacent Buchan Haven and Hutton bedrock targets (16.76 and 18.03 wt% FeO, and 0.32 and 0.25 wt% MnO respectively). The Fe contents are among the highest concentrations measured by APXS at Gale and the Mn concentrations are the highest. Moffat Hills (resistant, knobbly textured with pits) has the same composition as the nearby Trossachs bedrock target, but with slightly elevated P<sub>2</sub>O<sub>5</sub> (1.26 wt% versus 0.92 wt%). It plots with minor excess S relative to the typical Mount Sharp group CaSO<sub>4</sub> addition trend, as does Abernethy (Figure 3c). Bogmill Pow (fine-scale, spherical resistant features) and Moorfoot Hills (irregular shaped, resistant feature immediately adjacent to Liberton Brae) both have elevated Ca and S

relative to the bedrock in the same workspace, consistent with the addition of ~15 and 4 wt% CaSO<sub>4</sub> respectively (Figure 3c). Moorfoot Hills plots off the general CaSO<sub>4</sub> addition trend line, but is consistent with the addition of CaSO<sub>4</sub> to the respective Hutton bedrock target, which also plots with excess Ca relative to other Mount Sharp bedrock (Figure 3c). Other elements are diluted except Mg, Cl, Mn, Fe, Ni, and Zn (Figure 5).

The Liberton Brae and Dounraey features are both light-toned, resistant and smooth compared to the bedrock and are associated with the same vein as the Dunbartonshire and Moorfoot Hills features. They both exhibit elevated MgO and K<sub>2</sub>O (17.11 and 11.36 wt% MgO, and 2.14 and 1.43 wt% K<sub>2</sub>O respectively) relative to the bedrock. Liberton Brae also has elevated Zn, and Dounraey somewhat elevated Mn (Figure 5).

- 3.2 Composition of the Greenheugh pediment cap rocks
- 3.2.1. Previous Stimson formation APXS results

Outcrops of Stimson formation sandstone were first encountered in the vicinity of Pahrump Hills on the Emerson and Naukluft plateaus (Figure 1) and analyzed by APXS between sols 998 and 1351. Stimson formation sandstone exposures were also imaged at Murray buttes, but not analyzed by APXS. The Emerson and Naukluft plateaus are separated by more than 3.5 km lateral distance from the Greenheugh pediment. The Stimson formation is interpreted to represent lithified, basaltic, Mars soil-like composition, eolian sand (Banham et al., 2018, 2021; Thompson et al., 2016; Yen et al., 2017), which has undergone predominantly isochemical alteration (Hausrath et al., 2018; Yen et al., 2017). The exception are targets associated with silica-rich alteration haloes (Yen et al., 2017). We refer to the basaltic, martian sand/soil composition of the Stimson targets encountered at Emerson and Naukluft plateaus as "typical Stimson" (Table 1b). Owing to the soil-like composition of the Emerson/Naukluft plateau

Stimson sandstones, we use Lagrange (typical Gale soil, sol 605) as a comparison target in ratio plots (Figure 6). However, we demonstrate below that not all rocks grouped as Stimson formation based on sedimentological observations conform to typical Stimson, basaltic compositions.

### 3.2.2. Gleann Beag interval (platy)

The two pediment cap rock targets exposed immediately at the contact with the underlying Mount Sharp group (Figures S4, S12) are characterized by elevated S (14.05 and 18.91 wt% SO<sub>3</sub>) relative to typical Stimson formation sandstones (0.65 – 7.17 wt% SO<sub>3</sub>) and the overlying sandstones (5.11 – 7.65 wt% SO<sub>3</sub>) (Table 1b, Figure 6a, 7). The increased S content does not correlate with an increase in Ca (Figure 6a, 7), and therefore cannot be attributed to any appreciable CaSO<sub>4</sub> content. The majority of other elements are diluted relative to typical Stimson formation and the overlying Gleann Beag sandstones, except K, P, and Ni (Figure 6a).

The Gleann Beag interval cap rock sandstones above the high S contact (Figures S5, S13) fall within the same compositional range as typical Stimson formation sandstone (Table 1b; Figure 1, 6a). Nodule-rich areas (Adder targets, Figure S13) have the same composition as the more nodule-free bedrock (Galloway Hills) (Table 1b; Figure 6a). The platy, Gleann Beag sandstones are statistically, compositionally the same as typical Stimson sandstones except for Si, Al, P, Ni, and Zn (see results of t-tests, Table S3). While the Si, Al, P, Ni, and Zn concentrations are statistically distinct, Gleann Beag interval concentrations overlap with typical Stimson for all five elements (Table 1b, Figures 6a, 7).

### 3.2.3. Ladder and Edinburgh intervals (blocky)

In contrast to the sandstones analyzed at the contact, more resistant sandstones exposed higher up the section within the Ladder and Edinburgh intervals weather in a blockier fashion

(Figures S6, S7, S14) and have distinct compositions as illustrated in Figures 6b, 7, and 8. T-tests reveal that the blocky sandstones are statistically different than the typical Stimson for every element except Mg, Ca, S, and Cl (Table S3).

The Ladder and Edinburgh sandstones have significantly increased (up to 2.6 times)  $K_2O$  concentrations (0.92  $\pm$  0.08 wt%) compared to typical Stimson formation sandstones (0.42  $\pm$  0.06 wt%) and the platy pediment cap rock exposed within the Gleann Beag interval (0.46  $\pm$  0.04 wt%). MnO concentrations are also elevated (0.54  $\pm$  0.05 wt%) within the Ladder and Edinburgh interval compared to typical Stimson (0.38  $\pm$  0.03 wt%) and the Gleann Beag interval (0.36  $\pm$  0.10 wt%). The Ladder and Edinburgh sandstones also trend to higher Na<sub>2</sub>O (3.16  $\pm$  0.20 wt%), FeO (20.92  $\pm$  1.06 wt%), and Cr<sub>2</sub>O<sub>3</sub> (0.49  $\pm$  0.06 wt%) concentrations compared to typical Stimson formation sandstones (2.81  $\pm$  0.20 wt% Na<sub>2</sub>O, 19.00  $\pm$  1.55 wt% FeO, 0.43  $\pm$  0.07 wt% Cr<sub>2</sub>O<sub>3</sub>) and Gleann Beag sandstones (2.64  $\pm$  0.18 wt% Na<sub>2</sub>O, 19.16  $\pm$  1.51 wt% FeO, 0.41  $\pm$  0.08 wt% Cr<sub>2</sub>O<sub>3</sub>). They are also characaterized by lower TiO<sub>2</sub>, P<sub>2</sub>O<sub>5</sub>, and Ni concentrations (0.84  $\pm$  0.05 wt%, 0.70  $\pm$  0.07 wt% and 370  $\pm$  45 ppm respectively) than Stimson (0.92  $\pm$  0.05 wt%, 0.85  $\pm$  0.08 wt% and 468  $\pm$  67 ppm respectively) and Gleann Beag sandstones (0.92  $\pm$  0.09 wt%, 0.91  $\pm$  0.03 wt% and 567  $\pm$  24 ppm respectively).

The Ladder and Edinburgh sandstones are also distinguished by moderate correlations between Na and K, and Na and Al ( $R^2 = 0.5$  for both). This is in contrast to typical Stimson, which shows no correlation for Na and K ( $R^2 = 0.2$ ), and only a very weak correlation between Na and Al ( $R^2 = 0.4$ ) (Figure 8). The Gleann Beag sandstones plot with the Emerson and Naulkluft plateau Stimson targets for Na<sub>2</sub>O versus K<sub>2</sub>O and Al<sub>2</sub>O<sub>3</sub>.

3.2.4 Float cap rock from Western butte

Several loose blocks were analyzed on Western butte, the most likely origin for which is the morphologically and texturally similar cap rock exposure at the top of the butte (Figures 1d; S2, S9). The Blackwaterfoot target has the same elemental trends as the Ladder and Edinburgh interval sandstones from the pediment (Table 1b; Figure 6c, 8). The Lomond Hills and Heinrich Waenke rocks also have elevated  $K_2O$  (2.37 and 2.28 wt%), but concentrations are more than five times the  $K_2O$  of average Stimson (0.42  $\pm$  0.08 wt%) (Figure 6d, 8). Lomond Hills and Heinrich Waenke have lower  $Cr_2O_3$  (0.28 and 0.32 wt%), and trend to higher  $Na_2O$  (4.17 and 3.36 wt%), Ni (716 and 889 ppm) and Zn (1367 and 1876 ppm) concentrations than Blackwaterfoot and the Ladder and Edinburgh interval sandstones on the pediment (274 – 522 ppm Zn; see 3.2.2. for Cr, Na, and Ni concentrations) (Figure 6d, 8).

### 3.2.5 Compositionally related targets to pediment cap rock

The blocky pediment capping sandstones and Western butte, Blackwaterfoot cap float block reveal related elemental trends to sandstone targets analyzed on Bradbury rise in the vicinity of Yellowknife Bay, as well as more resistant weathering, crater retaining cap rock encountered before *Curiosity* reached Pahrump Hills. Float cap rocks from the Mount Sharp group traverse, just below the Emerson plateau, also reveal comparable compositions (Figures 6e, 8, 9). Similarly, the Lomond Hills and Heinrich Waenke float cap rocks from Western butte exhibit elemental trends that are related to a number of sandstone, cap and float rock targets previously encountered on the mission; many of them also Bradbury group (Figure 6f, 8, 9).

### 4 Discussion and Implications

The APXS results from the investigation of the contact between the Mount Sharp group and Greenheugh pediment capping sandstones have revealed a number of compositional

similarities to rocks encountered earlier in the mission. We discuss the significance and implications of these relationships.

4.1 Hutton interval relationship to previous Mount Sharp group along the Basal Siccar Point group unconformity

The notably elevated Na, low S, and excess Ca not associated with CaSO<sub>4</sub> within the Hutton interval immediately underlying the pediment, is also characteristic of several targets analyzed by APXS at the base of the Mount Sharp group, within the Pahrump Hills and Hartmann's Valley members. These include the bedrock targets: Topanga, Mescal, Puente, Pickhandle and Telegraph Peak (Pahrump Hills member), and Mirabib, Inamagando and Oudam (Hartmann's Valley member) (Table S1). More than 300 m of elevation and 3.5 km lateral distance separates the Pahrump Hills and Hartmann's Valley targets from the Hutton interval at the pediment contact (Figure 1). With reference to questions 1) and 2) in §1.2, what might the compositional relationship between these targets infer regarding provenance or sorting versus weathering and/or alteration associated with the Basal Siccar Point unconformity?

The Pahrump Hills targets are also in proximity to capping sandstones and other blocky, likely erosional remnants of alkaline cap rocks (Figure 9a, b). Specifically, the resistant Salsberry Peak sandstones (represented by the APXS target, Little Devil) are exposed just above the Telegraph Peak drill site (Figures 9a, b). The Mirabib, Hartmann's Valley target was the last Mount Sharp group target analyzed by APXS before *Curiosity's* initial ascent onto the Naukluft Plateau, Stimson formation sandstones, and Oudam and Inamagando are situated just below the western extent of the plateau (Figures 9a, c). All the lower Mount Sharp group targets discussed here are within 1 to 3 m elevation of overlying capping sandstones (Salsberry Peak or Stimson). Previous work has interpreted the Salsberry Peak sandstones to be a lens within the Mount Sharp

group (Kronyak et al., 2019; Stack et al., 2019) and therefore unrelated to the deposition of the Stimson sandstones. Construction of a cross section between the Salsberry Peak and Marias Pass area (where *Curiosity* first encountered Stimson formation sandstones), reveals that the sandstones are exposed at a similar elevation and could therefore be contemporaneous (Figure 10a), both overlying the Basal Siccar Point group unconformity.

398

399

400

401

402

403

404

405

406

407

408

409

410

411

412

413

414

415

416

417

418

419

The distinct chemistry preserved at these widely dispersed, separate stratigraphic intervals could be the result of changes in provenance and/or sedimentological processes, or conversely, related to proximity to the unconformity? If the compositional differences within the Hutton interval were the result of primary sedimentary processes, we would expect the zone to mimic the underlying, flat-lying stratigraphy (Stein et al., 2020). Instead, extrapolating the Hutton interval from Buchan Haven on Western butte to the Hutton drill site just below the pediment, reveals that it is dipping and cross-cuts the flat-lying stratigraphy. Furthermore, the dip of the Hutton interval mimics that of the unconformity, if extrapolated from the pediment to Western butte (Figure 10b). This indicates that at least at this location, the distinct chemistry is unlikely to be related to provenance or depositional processes, but is a result of proximity to the unconformity. Supporting this are the lack of obvious, sedimentological changes observed within the Hutton interval, relative to the rest of the Glasgow member. Furthermore, laterally equivalent Glasgow member targets analyzed by APXS after Curiosity drove east, away from the pediment, do not exhibit the same distinct chemistry as the Hutton interval, but instead reveal typical Glasgow member compositions (O'Connell-Cooper et al., this issue). Laterally equivalent Glasgow member targets also exhibit the same spectral signatures as the rest of the Glen Torridon Mount Sharp group (Rudolf et al., this issue).

420

421

422

423

424

425

426

427

428

429

430

431

432

433

434

435

436

437

438

439

440

441

442

The proximity of all the Mount Sharp group targets discussed above to the Basal Siccar Point group unconformity could be consistent with that erosional surface extending from the pediment, down to the lower Mount Sharp group at Pahrump Hills and Hartmann's Valley (Figure 11). Weathering along the exposed erosional surface prior to the deposition of the Siccar Point group could be responsible for the related chemistry. The distinct chemistry could also be the result of fluids interacting with the Mount Sharp bedrock immediately underlying the unconformity, both at the base of the Mount Sharp group and at the Hutton interval, after deposition and at least some lithification of the overlying sandstones.

At least for the Hutton interval, these rocks would have undergone the same burial and diagenesis as the rest of the Glasgow member, prior to erosion, and weathering (physical and possibly chemical) and/or alteration along the subsequent Basal Siccar Point group unconformity. Therefore, we can compare the chemistry of the Hutton interval to the Glasgow DRT target to look for indicators of one process over another. Weathering typically follows Cl>SO<sub>4</sub>>Na>Ca>Mg>K>Si>Fe>Al>Ti with respect to mobility of ions (decreasing mobility from left to right; Hudson 1995). This results in concentration of the immobile elements, e.g., Ti, Al, Fe, Si, and depletion of the more mobile ions e.g., Na, Ca, Mg, in the weathered horizon (e.g., Nesbitt & Wilson, 1992; Nesbitt & Young, 1982). On Mars, weathering of the dominantly basaltic crust is expected to result in liberation of Ca, Mg, Fe, S, and Cl, leaving residual Al, Fe, and Si (McLennan et al., 2003, 2019). However, compared to Glasgow, the Hutton interval targets show higher concentrations of the mobile elements (Na, Ca, and Mg) and approximately the same or lower concentrations of the immobile elements (Si, Al, and Ti) (Table 1a, Figures 3a, b). Furthermore, the mass balance comparison of Hutton interval targets relative to Glasgow DRT indicates gains of the mobile elements, Na, Ca, and Mg, as well as Fe and Mn, and the loss

of S (Figure 4b). The lower concentrations of Si, Al, and Ti are considered to be the result of addition of the mobile elements. It therefore seems unlikely that chemical weathering has played a significant role in the alteration of the Glasgow member rocks, and by inference, the similar composition Pahrump Hills and Hartmann's Valley member rocks that would have been exposed along the erosional surface.

### 4.1.1 Mineralogy and composition

The compositional relationships between the Hutton interval and lower Mount Sharp group, Pahrump Hills targets are reflected in the mineralogy of the Hutton and Telegraph Peak drilled samples, as determined by CheMin. The crystalline components of both samples are dominated by plagioclase, pyroxene, magnetite>hematite, crystalline SiO<sub>2</sub> phases and potassium feldspar (Rampe et al., 2017; Thorpe et al., this issue). Along with Buckskin (high SiO<sub>2</sub> Pahrump Hills member drill sample), they are the only Mount Sharp group drill samples with magnetite as the dominant Fe-oxide phase detected. Both have minor fluorapatite and minor to absent crystalline CaSO<sub>4</sub> phases, consistent with the P, Ca, and S measured by APXS.

The Hutton and Telegraph Peak samples, along with Oudam, Buckskin and Highfield (grey/blue Jura member drill sample from Vera Rubin ridge), have the lowest clay mineral abundances detected of the Mount Sharp group drill samples (<6 wt %) (Rampe et al., 2020b; Thorpe et al., this issue). The Buckskin drill hole is located only 0.2 m from the contact with the unconformably overlying Stimson formation sandstone and the Highfield drill site is interpreted to have been situated just below the extrapolation of the pediment capping sandstone over the Vera Rubin ridge (Figure 11) (Bryk et al., 2019; Fraeman et al., 2020).

Opal-CT is also only detected in the low clay abundance Mount Sharp group drill samples listed above (4-11 wt %), and not in any other Mount Sharp group drill sample (Rampe

et al., 2020b). In contrast to Hutton, the Glasgow drill sample, situated ~6 m below the pediment, has 23.5 wt% clay mineral abundance, hematite>magnetite, calcium sulphates, only ~1 wt% crystalline SiO<sub>2</sub>, and no opal-CT; the same as other Glen Torridon drill samples (Thorpe et al., this issue).

The plagioclase abundances are also distinct for Hutton versus Glasgow (26.5 versus 15.4 wt% respectively), as are their derived compositions (An<sub>25</sub> and An<sub>47</sub>, respectively; Thorpe et al., this issue). The more sodic plagioclase composition of the Hutton drill sample is consistent with the elevated Na measured by APXS. Therefore, most of the excess Ca (which is not associated with CaSO<sub>4</sub> phases) in the Hutton sample cannot be attributed to differences in plagioclase content (i.e., higher calcic plagioclase abundance in Hutton). Instead it is probably related to the higher pyroxene abundance in the Hutton sample, the detection of fluorapatite and the greater CaO content of the amorphous component of Hutton versus Glasgow. Telegraph Peak also has a more sodic plagioclase component compared to the other Pahrump Hills drill samples (Rampe et al., 2017), consistent with the elevated Na measured by APXS in that sample and related targets (Thompson et al. 2020).

### 4.1.2 Implications

The proximity of the Hutton interval and other geochemically and mineralogically related Mount Sharp group targets to the Basal Siccar Point group unconformity suggests that the contact provided a conduit for enhanced fluid flow. The absence of appreciable CaSO<sub>4</sub> and low clay content are consistent with an alteration event associated with the unconformity that resulted in the dissolution of those phases after deposition of the cap rock and post-dating the process that concentrated clay and CaSO<sub>4</sub> minerals throughout the rest of the Mount Sharp group (e.g., Achilles et al., 2020; Bedford et al., 2019; Bristow et al., 2018, 2021; Hurrowitz et al., 2017;

Rampe et al 2017, 2020b; Thorpe et al., this issue). Based on the chemistry, the silica phases detected by CheMin in the Hutton drill sample are not the result of the addition of silica, but must instead be the result of the dissolution of pre-existing silicates, which could include clay minerals. The fluid responsible for the alteration would have been concentrated in the mobile cations Na, Ca, and Mg and to a lesser extent Fe and Mn.

489

490

491

492

493

494

495

496

497

498

499

500

501

502

503

504

505

506

507

508

509

510

511

The presence of opal-CT and coarse grained, grey hematite in the Highfield and Oudam drilled samples has been proposed by Achilles et al. (2020) and Rampe et al. (2020a) to be the result of alteration by relatively warm (~100°C) diagenetic fluids. While grey hematite has not been detected by CheMin within the Hutton drilled sample, Rudolf et al. (this issue) observe spectral signatures within Hutton interval strata consistent with grey hematite. Therefore, we suggest that the related chemistry and mineralogy observed within the Hutton interval is the result of interaction with similar diagenetic fluids. The occurrence of magnetite, cristobalite, opal-CT, sodic feldspar compositions and the lack of CaSO<sub>4</sub> are consistent with alteration by relatively warm, near neutral pH, possibly briney fluids. Bonyadia & Sadeghib (2020) describe sodic and calcic alteration associated with the formation of hydrothermal iron oxide deposits in the Bafq iron deposits, Iran. Minerals formed during the alteration include sodic plagioclase, magnetite and apatite; minerals detected by CheMin in the Hutton sample. They invoke the hydrothermal heating of brines, derived from evaporite basins and the action of fluids with high Na/K and Cl/S ratios. The action of a briney fluid would also be consistent with lack of CaSO<sub>4</sub> detected by either APXS or CheMin. Brines enhance the solubility of CaSO<sub>4</sub> (Klimchouck, 1996).

We are not suggesting that the processes and tectonic setting resulting in the alteration described by Bonyadia & Sadeghib (2020) are analogous to those here, but that there are

512

513

514

515

516

517

518

519

520

521

522

523

524

525

526

527

528

529

530

531

532

533

534

scenarios within Gale crater that could produce similar chemistry, relatively warm, briney fluids. The sources of diagenetic fluids within Gale crater have previously been debated (e.g., Achilles et al., 2020; Bristow et al., 2018, 2021; Fraeman et al., 2020; Gasda et al., this issue; Rampe et al., 2017, 2020b; Yen et al., 2017, 2021). We propose that relatively warm fluids, possibly sourced from remnant hydrothermal systems within the Gale crater central uplift, could have flowed down along, and be confined to the basal Siccar Point unconformity. Hydrothermal systems could have persisted for at least 30,000 years (Schwenzer et al., 2012), and possibly for >2.5 million years after impact (Kring et al., 2020). The hydrothermal fluids would probably have interacted with the sulfate-bearing strata that adorns much of the central uplift, thus resulting in briney chemistry. As a result of exposure and physical weathering, the Mount Sharp group within 1-3 m of the contact could have enhanced porosity and permeability relative to both the underlying Mount Sharp group strata, and the overlying, well cemented, resistant, cliffforming, pediment capping sandstones and be more susceptible to alteration. This is just one possible scenario; future work will aim to attempt to further constrain fluid chemistry, temperature and alteration conditions.

The Moorfoot Hills diagenetic target indicates addition of CaSO<sub>4</sub> to a Hutton-like bedrock with pre-existing excess CaO. This is consistent with the CaSO<sub>4</sub> addition occurring after the event that resulted in the excess CaO in the Hutton interval bedrock. The association of the Moorfoot Hills, Liberton Brae, Dunbartonshire and Dounraey targets with the same vein that cross-cuts the Hutton workspace, and the compositionally related, cross-cutting Abernethy vein target in the Buchan Haven workspace, is further evidence for the late-stage timing. If the vein system was emplaced prior to the CaO enrichment of Hutton interval bedrock, we might expect all the analyses to plot with excess Ca, which they do not. The distinct and varied chemistries of

the different diagenetic features within the Hutton workspace suggest complicated and multistage fluid interactions associated with their formation, necessarily including the mobility of Fe, Mn, Mg, and K.

Similar veins and diagenetic features to those within the Hutton drill workspace were not observed within the overlying pediment-capping sandstones. This might indicate that the vein system was emplaced prior to the deposition and lithification of the sandstones, contradicting the above argument. However, *Curiosity* has only examined a relatively small area of the overlying pediment-capping sandstones, so the presence of similar features cannot be discounted. They may also be more difficult to identify within the darker grey, more resistant pediment-capping sandstones. The sandstones may also have had a different response to the stresses that formed the veins in the underlying Hutton interval.

- 4.2 Compositional relationship of Greenheugh pediment cap rock to Stimson formation
- 4.2.1 Gleann Beag interval sandstones

The Gleann Beag interval is interpreted to represent the remnants of oblique compound dunes, with the same wind transport direction (to the northeast) as the those preserved at Murray buttes (Banham et al., this issue). The Gleann Beag sandstones are compositionally in family with Stimson formation sandstones previously analyzed on the Emerson and Naukluft plateaus. On A-CN-K and A-CNK-FM diagrams (Nesbitt &Young, 1984; Figure 12) they overlap with, and lie on the same trend as, both the Emerson and Naukluft Stimson sandstones and modern, eolian Gale sand samples. The Gale sand samples define a trend that parallels the CN-A axis on the A-CN-K plot, consistent with variable plagioclase versus mafic mineral content, interpreted to be the result of eolian sorting (e.g., O'Connell-Cooper et al., 2018). Given the compositional and sedimentological relationship between the Gleann Beag interval and Stimson sandstones from

lower down the section, both could have been deposited in a similar environment as proposed by Banham et al. (this issue). They may also share a related provenance, not dissimilar to the Bagnold sands, which have a basaltic source (O'Connell-Cooper et al., 2017). Whether the sandstones exposed within the Gleann Beag section on the pediment are contemporaneous with those observed at Murray buttes cannot be determined from the available data; however, it can also not be ruled out. The statistically distinct Si, Al, P, Ni, and Zn concentrations of the pediment capping Gleann Beag sandstones from typical Stimson sandstones might support an interpretation that they were not deposited at the same time, perhaps under somewhat different depositional regimes (Banham et al. 2018 and 2021). However, the Si, Al, P, Ni, and Zn concentrations of the two overlap and a minor change in the sediment input or sorting and transport processes, and/or slightly contrasting post-depositional diagenesis of the sandstones could also account for the compositional differences.

## 4.2.1.1. Diagenesis/alteration of the Gleann Beag sandstones

The nodular sandstone targets analyzed within the Gleann Beag section have related compositions to the less nodular Galloway Hills target, as well as Naukluft and Emerson Plateau Stimson sandstones. This indicates that their formation was associated with essentially isochemical processes. In contrast, high S detected in the two targets analyzed immediately at the contact with the underlying Mount Sharp group indicates interaction with S-rich fluids, focused along the contact. The mass balance calculation relative to the Galloway Hills target indicates addition of significant S, some K and P, and the possible loss of Mn and Cr (Figure 13a). Hence the additional S is not associated with CaSO<sub>4</sub> (Figure 13 b). Investigation of the more nodular targets via the same mass balance calculation suggests the same relationships, but far less

pronounced. This might indicate that the same fluids were responsible for the formation of the nodules, but that the fluid became rapidly diluted away from the contact.

The underlying Hutton interval targets all exhibit low sulfur concentrations relative to the rest of the Glasgow member, other Glen Torridon rocks, and most of the Mount Sharp group (§3.1, Figures 3, 13b). Sulfur may have been mobilized during alteration of the Hutton interval strata along the Basal Siccar Point group unconformity and precipitated in the sandstones immediately overlying the contact, perhaps in response to a change in porosity/permeability. If this is the case, it supports alteration of the underlying Mount Sharp group after deposition of the overlying sandstone. It also provides some constraints on the source of fluids responsible for the alteration of the underlying Hutton interval. They are unlikely to have passed through the pediment capping sandstones prior to interaction with the Hutton interval, and instead were probably focused just beneath the contact, along the unconformity, with only limited migration into the overlying sandstones.

### 4.2.2. Ladder and Edinburgh interval sandstones

The blocky pediment sandstones (Ladder and Edinburgh intervals; Banham et al., this issue) are compositionally distinct from the basal (Gleann Beag) sandstones and the Stimson formation sandstones encountered earlier in the mission. The different chemistry of these sandstones is consistent with their contrasting sedimentology (Banham et al., this issue). The sandstones exposed within the Ladder interval (APXS targets: Forsinard Flows and Machir Bay) represent straight-crested simple dunes, with a southerly wind transport direction. The Edinburgh interval sandstones (APXS targets: Glen Feshie, Assynt Window, Edinburgh, and Eshaness) are trough cross-bedded and were deposited in a westerly wind transport direction. These transport directions are in contrast with the north-northeast directions preserved within the basal Gleann

Beag interval sandstones and the Stimson formation sandstones exposed on the Naukluft and Emerson plateaus and at Murray buttes (Banham et al., 2018, 2021). There are indications, based on analysis of MAHLI images (Figure S14), that the higher K sandstones are also generally coarser grained, and preserve somewhat more rounded grains than the basal Gleann Beag sandstones, although there is significant overlap in grainsize (Banham et al., this issue). On an A-CN-K diagram (Figure 12a) the Ladder/Edinburgh interval sandstones are offset from the other eolian sandstones, and Bagnold sands, which all lie on the same trend. Therefore, the compositional and sedimentological differences between the lower and upper pediment sandstones are most likely reflecting changes in provenance and/or depositional environment.

## 4.2.2.1 Mineralogy and composition

The higher potassium feldspar abundance of the Edinburgh drill sample (3.4 wt%; Thorpe et al., this issue) compared to the Stimson formation Big Sky (1.1 wt%) and Okoruso (1.9 wt%) drill samples from the Naukluft plateau (Yen et al., 2017) is consistent with the elevated K measured by APXS. Plotting the data on an A-CN-K diagram also indicates the addition of potassium feldspar (Figure 12a). The Ladder/Edinburgh interval sandstones are offset, parallel to the plagioclase-potassium feldspar tie line towards potassium feldspar, from the both the basaltic Gleann Beag and Emerson/Naukluft plateau sandstones, and modern Gale sands. The detection of olivine (8.3 wt%) and smectite (7 wt%) (Thorpe et al., this issue), phases not found above detection limits in the Big Sky and Okoruso samples (Yen et al., 2017), might explain the higher Fe, Mn and Cr measured by APXS if the olivine and/or smectite were relatively Fe-rich. SAM EGA and CheMin data indicate that the Edinburgh phyllosilicate is an Fe-rich dioctahedral smectite (Sutter et al., 2020; Rampe et al., 2020c). The Ladder/Edinburgh and Gleann Beag interval standstones overlap on an A-CNK-FM plot (Figure 12b), indicating similar

olivine/orthopyroxe versus feldspar contents. Both overlap with the Emerson/Naukluft plateau sandstones and Gale sand, but plot with the more mafic targets, closer to the FM apex, consistent with the higher CheMin olivine detection in the Edinburgh drill sample.

626

627

628

629

630

631

632

633

634

635

636

637

638

639

640

641

642

643

644

645

646

647

648

The coarser grain size of the high-K sandstones (Banham et al., this issue) indicates that transport/sorting processes may be responsible for at least some of the differences in chemistry. However, as discussed above, the Ladder/Edinburgh sandstones are offset from the eolian sorting trend line exemplified by the the modern Bagnold sand on the A-CN-K plot. Both the Gleann Beag sandstones and previous Stimson sandstones lie on this sorting trend line. Thus provenance is most likely responsible for the observed compositional and mineralogical changes, at least with respect to K and potassium feldspar. Plagioclase and potassium feldspar have similar hardness, density and cleavage and would not be expected to segregate from one another during transport. The higher K and addition of potassium feldspar could also be the result of authigenic/diagenetic processes, but authigenic potassium feldpspar would be expected to result in a microcline-structure, not the sanidine structure detected by CheMin. The alternative is that the sanidine structure feldspar is hydrothermal, as proposed by Morris et al. (2020) for at least some of the Gale crater drill samples, based on Maunakea analogue samples. However, it is unlikely that formation of hydrothermal sanidine would have occurred insitu within the Edinburgh/Ladder interval sandstones, given the preservation of olivine, and would therefore have to be detrital.

The detection of olivine could be consistent with the coarser grain size measured within the Ladder and Edinburgh intervals. Olivine is more resistant to mechanical breakdown than softer minerals and those with cleavage; it would therefore be expected to reside in the coarser eolian size fraction (unless originally present as fine crystals in the igneous source rock), as has

been observed for the active Bagnold sands (O'Connell-Cooper at al., 2017). However, the high-K sandstones plot with the basaltic composition Gleann Beag sandstones on the A-CNK-FM diagram (Figure 12b), indicating no significant sorting of olivine between the intervals.

If potassium feldspar formed relatively large crystals in an igneous source rock compared to plagioclase, this could also explain the concentration of potassium feldspar in coarser sand fractions, and the higher K concentrations measured by APXS. However, this would still require a change in source rock for the high K pediment sandstones versus the Emerson/Naukluft sandstones and Gale sand. A coarser grain size might also indicate a more proximal source, although all pediment sandstones show rounded grains, which would suggest no significant change in transport distance. However, the Ladder and Edinburgh sandstones are described as exhibiting somewhat more rounding of grains than the basal Gleann Beag sandstones (Banham et al., this issue). This could be consistent with reworking of already rounded grains from a more proximal, pre-existing sedimentary rock.

Big Sky, Okoruso and Edinburgh all have potassium feldspar (1-3 wt%); neither the inactive Rocknest soil, nor the two active sand samples contain potassium feldspar above the detection limits of CheMin (Achilles et al., 2017; Rampe et al., 2018). The high K, Windjana sandstone comprises 26 wt% potassium feldspar (Treiman et al., 2016). Could the potassium feldspar detected in the ancient eolian deposits be derived from erosion of pre-existing Gale crater, high-K sandstones (e.g., Windjana), and mixing of this material with more basaltic source rocks? In this scenario, the higher-K pediment sandstones contain more of this locally derived detritus than the rest of the Stimson formation and modern sand. The Windjana sandstone also contains 10% smectite (Treimann et al., 2016) and the majority of the Mount Sharp group drilled

samples contain significant clay mineral abundances (Thorpe et al., this issue). Thus, at least the phyllosilicate detected within the Edinburgh sample might reflect a more proximal input.

Given the correlation of the chemistry with detrital mineralogy, weathering is unlikely to have played a significant role in the differences observed. Potassium feldspar is more resistant to weathering than plagioclase (Goldich, 1938). Its detection could therefore indicate increased weathering either at source or post-depositionally for the Ladder and Edinburgh interval sandstones relative to the rest of the Stimson. However, the olivine detection in the Edinburgh drill sample is not consistent with this; the preservation of olivine indicates only minimal weathering and aqueous alteration. Minimal weathering is also supported by plotting the data on A-CN-K and A-CNK-FM diagrams with the CIA index superimposed (Figure 12). The pediment capping sandstones (and Western butte float) do not follow chemical weathering trends (towards the Al<sub>2</sub>O<sub>3</sub> apex).

Hausrath et al. (2018) attribute the lack of olivine, and greater magnetite content of the drilled Big Sky and Okoruso Stimson samples versus the eolian Rocknest and Gobabeb samples to diagenesis by near-neutral pH aqueous solutions. They propose the dissolution of olivine and precipitation of magnetite by solutions enriched in sulfate and chloride. They do not consider weathering/alteration of the source material prior to erosion, differences in igneous mineralogy at the source, sorting/transport processes, nor the fact that magnetite could be detrital and a primary igneous mineral. Applying their model to the Edinburgh drill sample is not consistent with both the high magnetite and olivine content detected by CheMin, unless there was significantly more olivine in the sand prior to diagenesis.

4.3 Compositional relationship of the high-K pediment capping rocks to other Gale crater lithologies

The Ladder and Edinburgh interval sandstones, and Blackwaterfoot float from Western butte reveal elemental trends related to a number of Bradbury group sandstones and float cap rock targets analyzed along the Mount Sharp group traverse (Figures 6c, 8, 12). These including Bell Island (sandstone exposed just above Yellowknife Bay) and Howells and Eqaluik (Shaler fluvial sandstone, also just above Yellowknife Bay – Bradbury group), South Park (example of Bradbury group, capping unit sandstone analyzed just before Pahrump Hills), and the Ravalli float cap rock analyzed as we traversed the Hartmann's Valley member adjacent to the Emerson Plateau (Table S1; Figures S17, S20, S24).

The Lomond Hills and Heinrich Waenke cap float rock targets analyzed on Western butte are also compositionally related to other Bradbury group sandstones and cap rock targets (Figures 6d, 8, 12). These include Minginish (float rock on VRR), Little Devil (interpreted to represent the Salsberry Peak cap sandstone at Pahrump Hills), Stirling and Thimble (capping unit sandstone analyzed nearby South Park, prior to Pahrump Hills), Bathurst and Rocknest 3 (Bradbury group sandstones just above Yellowknife Bay), and Ravalli (see above) (Table S1; Figures S18, S19, S21, S22, S24).

The locations of these compositionally related targets previously encountered by *Curiosity* are shown on Figure 9. Note that a number of them are in the vicinity of one another, and that all the cap rock float targets on the Mount Sharp group traverse (except Minginish) are in proximity to either the Emerson or Naukluft plateaus or Murray buttes Stimson formation. Minginish is a small boulder within the Bressay blocky deposit on VRR, which also included a sandstone target, Rousay (sol 2019), with a typical Stimson composition. Many of these rocks are also texturally alike, appearing relatively smooth, resistant to weathering, and blockier in appearance than typical Stimson sandstone and the sandstones exposed at the base of the

pediment capping unit (see images in §S3 and S4). The comparable composition Bradbury sandstones also share similar oribital characteristics with the pediment capping sandstones; they are both manifest as crater-retaining units.

#### 4.3.1 Implications

The comparable compositions and textures of the higher K pediment capping, Siccar Point sandstones and the Western butte float rocks to Bradbury group rocks and float, indicate that they could be related to one another. The proximity of the Bradbury-like float rocks encountered along the Mount Sharp traverse to Stimson formation sandstones and the occurrence of both typical basaltic Stimson and high-K composition sandstones on the pediment also point to a relationship.

The Bradbury group sandstones analyzed just above Yellowknife Bay are separated by more than 9 km laterally and ~400 m in elevation, from the pediment capping sandstones. The large lateral separation is most easily explained by shared provenance and/or depositional processes for the sandstones versus the same style of post-depositional alteration. This is supported by the relationship between the composition and detrital mineralogy of the Edinburgh samples. The Bradbury group is interpreted to have been derived from the mixing of multiple, diverse igneous source rocks including basaltic and more alkaline and silica rich lithologies (Bedford et al., 2019; Cousin et al., 2017; Edwards et al., 2017; Sautter et al., 2015; Schmidt et al., 2014; Stolper et al., 2013; Thompson et al., 2016; Treiman et al., 2016). We therefore propose that the Ladder and Edinburgh interval sandstones, as well as the float rocks analyzed on Western butte, are derived from similar source rocks to the Bradbury group sandstones, which includes a more alkaline component.

The current stratigraphic column depicts the Bradbury group as being older than the Mount Sharp group. However, given the argument above, could the Bradbury group and the Stimson formation both be younger than the Mount Sharp group and related (Figure 11)? The Mount Sharp group might represent relatively old lacustrine/fluvial deposits, which were buried, lithified and then eroded, before deposition of the Bradbury and Siccar Point groups onto that erosional surface, thus explaining the differences in elevation between the two groups. This is not the first time such a scenario has been proposed. Wiens et al. (2020) suggest that at least parts of the Bradbury group, i.e., the layered rocks at Bathurst Inlet, and other similar composition, layered float rocks from the Bimbe heterolithic deposit (another blocky deposit on the Mount Sharp Group), have the same provenance and were deposited at the same time. In their model, both are younger than, and would have overlain, the Stimson formation and along with it, draped over the underlying erosional topography.

An alternative is that there is at least one, more alkaline (than an average martian basaltic) source area in and around Gale crater that has been eroded by both water and wind at different times during the history of the evolution of the crater and its infill. The Bradbury group alkaline sedimentary rocks would have been deposited prior to the more basaltic Mount Sharp group, followed by the basaltic and alkaline Siccar Point group eolian rocks (Figure 11). Both scenarios are consistent with widespread evidence at Gale crater for the presence of multiple igneous source rocks.

#### 4.3.2 Relationship to Gediz Vallis ridge

The Gediz Vallis ridge, south of the pediment (Figure 2) appears to contain abundant large, dark blocks and boulders. (Bryk et al., 2019; Hughes et al., 2020). Could the Gediz Vallis ridge be the source of the high-K and -Na Lomond Hills/Heinrich Waenke float cap

rocks and the material that capped Western butte? If so, what is the relationship between the boulders within the Gediz Vallis ridge, cap rocks and Bradbury group targets previously encountered on the mission? Bryk et al. (2019) have proposed that the Gediz Vallis ridge deposit could once have extended to VRR and may be the source of the Bressay boulder deposit containing the high-K, Minginish, and Stimson-like composition, Rousay float blocks. The Bradbury group has generally been interpreted to have been sourced from the Gale crater rim or beyond (Palucis et al., 2014), whereas the material that comprises the Gediz Vallis ridge is thought to have been sourced from higher up on Mount Sharp (Bryk et al., 2019), which does not seem to fit with them being genetically related. If the Western butte cap float rocks did originate in Gediz Vallis, the valley could be sourcing material/boulders from some overlying strata that was once more extensive and related to Bradbury group rocks.

### 4.3.3 The role of diagenesis

Another scenario is that the blockier, high-K, pediment-capping sandstones underwent more diagenesis/cementation than the low-K pediment sandstones, and that this is the source of the distinct chemistry. This would be consistent with their blockier and smoother appearance and would imply that a K- (and Mn-, Na-) rich fluid may have been involved. However, following the argument in §4.2.2.1. the potassium feldspar detected by CheMin is not consistent with authigenic processes and is most likely detrital and igneous, or hydrothermal in origin.

The Edinburgh drill sample contains phyllosilicate, which was not detected in previous Stimson drill samples (Rampe et al., 2018; Thorpe et al., this issue). If the phyllosilicate is authigenic, it implies a different post-depositional diagenetic/alteration history for the blocky pediment sandstones versus the Stimson formation at the Naukluft and Emerson plateaus. However, given the arguments in §4.2.2.1. the phyllosilicate is most likely reflecting a local detrital input.

Coarser sandstones would be expected to have had higher initial porosity and permeability than finer grained sandstones at the time of deposition, and might therefore undergo more diagenesis. Therefore, the coarser Ladder and Edinburgh section sandstones might be expected to be better cemented than the somewhat finer grained Gleann Beag sandstones. Given the sedimentological differences between the Gleann Beag, and Ladder and Edinburgh interval sandstones, the correlation of the chemistry with the detrital mineralogy, and the relationship to rocks encountered much earlier in the mission, this is not the most plausible explanation. However, even if provenance and sedimentary processes are primarily responsible for the difference in chemistry of the capping sandstones versus the Emerson and Naukluft Plateau Stimson sandstones, the distinct detrital mineralogy might have driven different post-depositional diagenetic reactions.

4.4 Proposed series of events

Figure 14 outlines the proposed series of events, based on the compositional, mineralogical and sedimentological data.

#### **5 Conclusions**

Curiosity's investigation of the Greenheugh pediment capping rocks and immediately underlying strata, and the compositional data acquired by APXS have revealed relationships with a number of lithologies examined earlier in the mission. These relationships provide important insights into regional and crater-scale processes within Gale crater and evidence for the long-lived role of water and aqueous alteration and hence, habitable environments.

The Stimson formation strata encountered on the pediment preserves a record of eolian transport and deposition of both more basaltic and alkaline detritus; the basaltic sand being sourced from the south, and the more alkaline sand from the north. The relationship of the

alkaline composition, pediment-capping Stimson formation to Bradbury group sandstones and cap rock lends further credence to the presence of alkaline igneous source rocks within, and in the vicinity of Gale crater, concentrated to the north of *Curiosity's* location. This source rock would have provided the sediment input to both fluvial and eolian sandstones, which may have been deposited more or less contemporaneously. In this scenario, the Bradbury group and Siccar Point group are both younger than the Mount Sharp group. Alternatively, erosion and transport of alkaline source rock by both wind and water may have occurred at different times during the evolution of Gale crater, separated by millions of years, i.e., the Bradbury group is older than both the Mount Sharp and Siccar Point groups.

Identification of compositionally and mineralogically distinct Mount Sharp group strata only exposed within 3 m elevation of the Basal Siccar Point group unconformity, both at the base of, and more than 300 m higher up the section, indicates a relationship to that unconformity. We suggest fluid flow focused along the contact between the Mount Sharp group rocks and the overlying, relatively impermeable Siccar Point group sandstones, altered Mount Sharp group strata within 3 m of the contact. This alteration resulted in the loss of S and addition of Ca, Mg and Na to typical Mount Sharp group strata, manifest by the loss of clay minerals and calcium sulfate and the formation of magnetite, opal-CT and cristobalite, and more sodic plagioclase. The fluid had limited interaction with immediately overlying sandstones, resulting in the addition of S to strata within 10s of cms of the contact. Cross-cutting dark-toned veins and associated features provide evidence for complicated, late stage alteration, with multiple distinct chemistries.

Curiosity will soon transition onto the Greenheugh pediment again, at a lateral distance of ~1 km and an elevation gain of ~100 m from the original ascent. The discovery of Mount Sharp

832

833

834

835

836

837

838

839

840

841

842

843

844

845

846

847848

849

850

851

852

853

854

855

856

857

858

859

860

group exposures within 3 m of the unconformity, compositionally related to the Hutton interval and lower Mount Sharp group targets previously sampled along the Basal Siccar Point unconformity would support the hypothesis presented here. Curiosity is expected to drive through a stratigraphic sequence related to the Siccar Point grp we document in this study. Will we see the same stratigraphy, sedimentology and chemistry within the pediment capping rocks as observed on our initial ascent of the Greenheugh pediment? Will we again observe compositional and textural similarities to Bradbury group rocks encountered much earlier in the mission, lending further support to a relationship between the Siccar Point and Bradbury groups? Curiosity's planned traverse should also access slightly higher stratigraphic sections within the Siccar Point group; we might discover in situ high-K and -Na rocks equivalent to the Western butte float rocks. Curiosity will also investigate the edge of the Gediz Vallis deposit. There could be a compositional relationship between the Gediz Vallis deposit and the high-K float cap rocks encountered on Western Butte, and other heterolithic blocky deposits. Acknowledgments We thank the two anonymous reviewers and editors for constructive comments that helped improve this work. MSL APXS is managed and financed by the Canadian Space Agency (CSA). We acknowledge the important role of the engineers at JPL, the MSL science team and everyone involved in operations with respect to obtaining APXS data. Mastcam mosaics were processed by the Mastcam team, and MAHLI images and mosaics were processed by the MAHLI team at Malin Space Science Systems. Science team member funding for Thompson, Boyd, Gellert, O'Connell-Cooper, and Spray is provided by the CSA. Yen acknowledges that a portion of this research was carried out at the Jet Propulsion Laboratory, California Institute of Technology, under a contract with the National Aeronautics and Space Administration. Berger was funded by a NASA Postdoctoral Program fellowship administered by USRA. VanBommel was supported by NASA/Caltech/JPL Contract 1549716 to Washington University in St. Louis for participation in the Mars Science Laboratory Science Team. **Data Availability** 

All MSL, raw data are available at the planetary data system:

https://pds-geosciences.wustl.edu/missions/msl/index.htm

- https://an.rsl.wustl.edu/msl/mslbrowser/an3.aspx
- All raw and derived APXS data used in this study is available at the planetary data system:
- https://pds-geosciences.wustl.edu/msl/msl-m-apxs-4\_5-rdr-v1/mslapx\_1xxx/data/ and
- 864 <a href="https://doi.org/10.17189/1519534">https://doi.org/10.17189/1519440</a> (Gellert, 2012, 2013)
- All APXS Murray formation data upto and including VRR presented in this paper is available at:
- 867 Thompson, L. (2020). Alpha Particle X-ray spectrometer geochemistry of the Murray formation
- and Vera Rubin ridge, Gale crater, Mars. https://doi.org/10.25545/ZXDJZ7, UNB, V1,
- UNF:6:bL/a2qTZBu6DNJlzkmGAbg==[fileUNF]
- All tables within the manuscript and supporting information, as well as derived data can be found
- at: Thompson, Lucy, 2022, "Alpha Particle X-ray spectrometer geochemistry of rocks associated
- with the Basal Siccar Point group unconformity, Glen Torridon region, Gale crater,
- 873 Mars", <a href="https://doi.org/10.25545/FXZOZ0">https://doi.org/10.25545/FXZOZ0</a>, UNB, V1, UNF:6:9gSkKeCmJKxFD9m0RbmtFg==
- 874 [fileUNF]

- 875876 Other manuscripts sub
- Other manuscripts submitted to this special issue referenced herein
- Manuscripts without a JGR identifier were uploaded with the revised files.
- Banham et al., (this volume), Evidence for seasonal- to millennial-scale wind fluctuations in an
- ancient aeolian dune field: Reconstruction of the Hesperian Stimson formation at the
- 880 Greenheugh pediment, Gale crater, Mars.
- Bennett et al., (this volume), An Overview of the Curiosity rover's Campaign in Glen Torridon,
- 882 Gale Crater, Mars. 2022JE007185
- Caravacal et al., (this volume), From lake to river: Documenting an environmental transition
- across the Jura/Knockfarril Hill members boundary in the Glen Torridon region of Gale crater
- 885 (Mars). 2021JE007093
- Gasda et al., (this volume), Overview of the morphology and chemistry of diagenetic features in
- the clay-rich Glen Torridon unit of Gale crater, Mars. 2021JE007097
- 888 O'Connell-Cooper et al., (this volume), Statistical analysis of APXS-derived chemistry of the
- 889 clay-bearing Glen Torridon region and Mount Sharp group, Gale crater, Mars
- 890 2021JE007177
- Rudolf, et al., (this volume), The distribution of clay minerals and their impact on diagenesis in
- 892 Glen Torridon, Gale crater, Mars.
- Thorpe, et al., (this volume), Mars Science Laboratory CheMin data from the Glen Torridon
- region and the significance of lake-groundwater interactions in interpreting mineralogy and
- sedimentary history. 2021JE007099
- 896 References
- Achilles, C. N., Downs, R. T., Ming, D. W., Rampe, E. B., Morris, R. V., Treiman, A. H., et al.
- 898 (2017), Mineralogy of an active eolian sediment from the Namib dune, Gale crater, Mars.
- 399 *Journal of Geophysical Research, Planets 122*(11), doi.org/10.1002/2017JE005262
- Achilles, C. N., Rampe, E. B., Downs, R. T., Bristow, T. F., Ming, D. W., Morris, R. V., et al.
- 901 (2020), Evidence for multiple diagenetic episodes in ancient fluvial-lacustrine sedimentary rocks

- 902 in Gale crater, Mars. Journal of Geophysical Research, Planets 125(8),
- 903 doi:10.1029/2019JE006295
- Anderson, R. B., & Bell, J. F. III (2010), Geologic mapping and characterization of Gale crater
- and implications for its potential as a Mars Science Laboratory landing site. *Mars* 5, 76–128.
- 906 doi.org/10.1555/mars.2010.0004
- Banham, S.G., Gupta, S., Rubin, D.M., Watkins, J.A., Sumner, D.Y., Edgett, K.S., et al. (2018),
- Ancient martian aeolian processes and palaeomorphology reconstructed from the Stimson
- formation on the lower slope of Aeolis Mons, Gale crater, Mars. Sedimentology, 65, 993–1042.
- 910 doi.org/10.1111/sed.12469
- 911 Banham, S. G., Gupta, S., Rubin, D. M., Edgett, K. S., Barnes, R., Van Beek, J., et al. (2021), A
- 912 rock record of complex aeolian bedforms in a Hesperian desert landscape: The Stimson
- 913 formation as exposed in the Murray buttes, Gale crater, Mars. *Journal of Geophysical Research*:
- 914 Planets, 126 (4): e2020JE006554. Doi
- Banham, S. G., Gupta, S., Rubin, D. M., Bedford, C. C., Edgar, L., Bryk, A., et al. (this issue),
- 916 Evidence for seasonal- to millenial-scale wind fluctuations in an ancient aeolian dune field:
- Reconstruction of the Hesperian Stimson formation at the Greenheugh pediment, Gale crater,
- 918 Mars. Journal of Geophysical Research: Planets
- 919 Bedford, C. C., Bridges J. C., Schwenzer, S. P., Wiens, R. C., Rampe, E. B., Frydenvang, J. &
- 920 Gasda, P. J. (2019), Alteration trends and geochemical source region characteristics preserved in
- 921 the fluviolacustrine sedimentary record of Gale crater, Mars. Geochimica et Cosmochimica Acta,
- 922 246, 234-266. doi.org/10.1016/j.gca.2018.11.031
- 923 Berger, J.A., R. Gellert, N.I. Boyd, P.L. King, M.A. McCraig, C.D. O'Connell-Cooper, et al.
- 924 (2020), Elemental composition and chemical evolution of geologic materials in Gale crater,
- 925 Mars: APXS results from Bradbury Landing to the Vera Rubin Ridge. *Journal of Geophysical*
- 926 Research: Planets, 12(12), doi: 10.1029/2020JE006538
- 927 Bibring, J-P., Langevin, T., Mustard, J. F., Poulet, F., Arvidson, R., Gendrin, A., et al. (2006),
- 928 Global mineralogical and aqueous Mars history derived from OMEGA/Mars Express data.
- 929 Science 312(5772), 400-404. doi:10.1126/science.1122659
- Blake, D.F., Vaniman, D., Achilles, C., Anderson, R., Bish, D., Bristow, T., et al. (2012),
- 931 Characterization and calibration of the CheMin mineralogical instrument on Mars Science
- 932 Laboratory. Space Science Reviews 170: 341-399. doi:10.1007/s11214-012-9905-1
- Bonyadia, Z., & Sadeghib, R. (2020), Hydrothermal alteration associated with magnetite
- mineralization in the Bafq iron deposits, Iran. Journal of Asian Earth Sciences, 189, 104152.
- 935 doi.org/10.1016/j.jseaes.2019.104152
- 936 Bristow, T.F., Rampe, E.B., Achilles, C.N., Blake, D.F., Chipera, S.J., Craig, P. et al. (2018),
- 937 Clay mineral diversity and abundance in sedimentary rocks of Gale crater, Mars. Science
- 938 *Advances*, 4(6), article ear3330, doi:10.1126/sciadv.aar3330
- 939 Bristow, T.F., J. P. Grotzinger, E. B. Rampe, J. Cuadros, S. J. Chipera, G. W. Downs, et al.
- 940 (2021), Brine-driven destruction of clay minerals in Gale crater, Mars. *Science*, 373(6551),
- 941 doi:10.1126/science.abg5449

- 942 Bryk, A. B., Dietrich, W. E., Lamb, M. P., Grotzinger, J. P., Vasavada, A. R., Stack, K. M., et al.
- 943 (2019), What was the original extent of the Greenheugh pediment and Gediz Vallis ridge
- 944 deposits in gale crater, mars? Paper presented at Ninth International Conference on Mars.
- 945 Abstract 6296. Pasadena, California.
- Campbell, J. L., Perrett, G. M., Gellert, R., Andrushenko, S. M., Boyd, N. I., Maxwell, J. A., et
- al. (2012), Calibration of the Mars Science Laboratory alpha particle X-ray spectrometer. Space
- 948 Science Reviews, 170, 319–340. doi.org/10.1007/s11214-012-9873-5
- 949 Campbell, J. L., King, P. L., Burkemper, L., Berger, J. A., Gellert, R., Boyd, N. I., et al. (2014),
- 950 The Mars Science Laboratory APXS calibration target: Comparison of Martian measurements
- with the terrestrial calibration. *Nuclear Instruments and Methods in Physics Research Section B:*
- Beam Interactions with Materials and Atoms, 323, 49–58. doi.org/10.1016/j.nimb.2014.01.011
- 953 Caravaca, G., Mangold, N., Dehouck, E., Schieber, J., Zaugg, L., Bryk, A.B., et al. (this issue),
- From lake to river: Documenting an environmental transition across the Jura/Knockfarril Hill
- 955 members boundary in the Glen Torridon region of Gale crater (Mars). Journal of Geophysical
- 956 Research: Planets, 2021JE007093
- 957 Cousin, A., Sautter, V., Payre, V., Forni, O., Mangold, N., Le Diet, L., et al. (2017),
- 958 Classification of igneous rocks analyzed by ChemCam at Gale Crater, Mars. *Icarus* 288, 265-
- 959 283. doi:10.1016/j.icarus.2017.01.014
- Davis, K., Herman, J., Maksymuk, M., Wilson, J., Chu, P., Burke, K., Jandura, L., & Brown, K.
- 961 (2012), Mars Science Laboratory Dust Removal Tool. Paper presented at the 41<sup>st</sup> Aerospace
- 962 Space Mechanisms Symposium, Paper #12, Pasadena, California.
- Edgar, L.A., Fedo, C. M., Gupta, S., Banham, S.G., Fraeman, A.A. Grotzinger, J.P et al. (2020),
- A lacustrine paleoenvironment recorded at Vera Rubin ridge, Gale crater: Overview of the
- sedimentology and stratigraphy observed by the Mars Science Laboratory Curiosity rover.
- Journal of Geophysical Research, Planets, 125(3) doi: 10.1029/2019JE006307
- Edgar, L.A., Gupta, S., Rubin, D.M., Lewis, K.W., Kocurek, G.A., Anderson, R.B., et al. (2018),
- 968 Shaler: in situ analysis of a fluvial sedimentary deposit on Mars. Sedimentology, 65(1):96-122,
- 969 doi:10.1111/sed.12370
- 970 Edgett, K. S., Yingst, R. A., Ravine, M. A., Capilinger, M. A., Maki, J. N., Ghaemi, F. T., et al.
- 971 (2012), Curiosity's Mars Hand Lens Imager (MAHLI) Investigation. Space Science Review, 170:
- 972 259. https://doi.org/10.1007/s11214-012-9910-4
- 973 Edwards, P. H., Bridges, J. C., Wiens, R., Anderson, R., Dyar, D., Fisk, M., et al. (2017), Basalt-
- 974 trachybasalt samples in Gale crater, Mars. *Meteoritics and Planetary Science*, 52 2931-2410.
- 975 doi.org/10.1111/maps.12953
- 976 Fedo, C.M., J.P. Grotzinger, A. Bryk, L.A. Edgar, K. Bennett, V. Fox, N. Stein, A. Fraeman, S.
- Banham, S. Gupta, K. Edgett, et al. (2020), Ground-based stratigraphic correlation of the Jura
- and Knockfarril Hill members of the Murray formation, Gale crater: Bridging the Vera Rubin
- 979 ridge-Glen Torridon divide. Paper presented at 51<sup>st</sup> Lunar and Planetary Science Conference,
- 980 Abstract # 2345, Woodlands, Texas.
- 981 Fraeman, A. A., Ehlmann, B. L., Arvidson, R. E., Edwards, C. S., Grotzinger, J. P., Milliken, R.
- 982 E., Quinn, D. P., & Rice, M. S. (2016), The stratigraphy and evolution of lower Mount Sharp

- 983 from spectral, morphological, and thermophysical orbital data sets. *Journal of Geophysical*
- 984 Research, Planets, 121, 1713–1736. doi:10.1002/2016JE005095
- Fraeman, A.A., Edgar, L.A., Rampe, E. B., Thompson, L. M., Frydenvang, J., Fedo, C. M., et al.
- 986 (2020), Evidence for a diagenetic origin of Vera Rubin ridge, Gale crater, Mars: Summary and
- 987 synthesis of Curiosity's exploration campaign. Journal of Geophysical Research Planets doi:
- 988 10.1029/2020JE006527
- Gasda, P. J., Comellas, J., Essunfeld, A., Das, D., Bryk, A. B., Dehouck, E., et al. (this issue).
- 990 Overview of the Morphologyand Chemistry of Diagenetic Features in the Clay-Rich Glen
- 991 Torridon Unit of Gale Crater, Mars. Journal of Geophysical Research: Planets
- 992 https://doi.org/10.1029/2021JE007097
- 993 Gellert, R. (2012) MSL Mars Alpha Particle X-ray Spectrometer 2 EDR v1.0 [Data set]. NASA
- 994 Planetary Data System. https://doi.org/10.17189/1519534
- 995 Gellert, R. (2013) MSL Mars Alpha Particle X-ray Spectrometer 4/5 RDR v1.0 [Data set].
- 996 NASA Planetary Data System. https://doi.org/10.17189/1519440
- 997 Gellert, R., Rieder, R., Brückner, J., Clark, B.C., Dreibus, G., Klingelhöfer, G., et al. (2006),
- Alpha Particle X-Ray Spectrometer (APXS): Results from Gusev crater and calibration report.
- 999 *Journal of Geophysical. Research, Planets, 111*, E02S05. doi.org/10.1029/2005JE002555
- 1000 Gellert, R., Clark, B.C. III, & Mars Science Laboratory (MSL) Science Team (2015), In situ
- 1001 compositional measurements of rocks and soils with the Alpha Particle X-ray Spectrometer on
- 1002 NASA's Mars rovers. *Elements 11*, 39–44. https://doi.org/10.2113/gselements.11.1.39
- Goldich, S. S. (1938), A Study in Rock-Weathering. The Journal of Geology, 46 (1): 17–
- 1004 58. doi:10.1086/624619
- 1005 Grotzinger, J.P., Sumner, D. Y., Kah, L. C., Stack, K., Gupta, S., Edgar, L., et al. (2014), A
- habitable fluvio-lacustrine environment at Yellowknife Bay, Gale Crater, Mars. Science,
- 1007 343(6169), 1242777. doi:10.1126/science.1242777.
- 1008 Grotzinger, J. P., Gupta, S., Malin, M.C., Rubin, D.M., Schieber, J., Siebach, K., et al. (2015),
- Deposition, exhumation, and paleoclimate of an ancient lake deposit, Gale Crater, Mars. Science,
- 1010 350(6257), aac7575. doi:10.1126/science.aac7575.
- Hausrauth, E. M., Ming, D. W., Peretyazhko, T. S., & Rampe, E. B. (2018) Reactive transport
- and mass balance modeling of the Stimson sedimentary formation and altered fracture zones
- 1013 constrain diagenetic conditions at Gale crater, Mars. Earth and Planetary Science Letters, 491, 1-
- 1014 10. doi.org/10.1016/j.epsl.2018.02.037
- Hudson, B. D. (1995), Reassessment of Polynov's ion mobility series. Soil Science Society of
- 1016 America Journal, 59, 1101-1103. doi.org/10.2136/sssaj1995.03615995005900040022x
- Hughes, M. N., Arvidson, R. E., Bryk, A. B., Dietrich, W. E., Lamb, M. P., & Catalano, J. G.
- 1018 (2020), Mass Movements and Debris Deposits in the Grand Canyon and Gediz Vallis, Gale
- 1019 Crater, Mars. Paper presented at 51st Lunar and Planetary Science Conference, Abstract #2426,
- 1020 Woodlands, Texas.
- Hurowitz, J. A., Grotzinger, J. P., Fischer, W. W., McLennan, S. M., Milliken, R. E., Stein, N., et
- al. (2017), Redox stratification of an ancient lake in Gale crater, Mars. Science, 356, eaah6849

- Klimchouck, A. (1996), The dissolution and conversion of gypsum and anhydrite. *International*
- 1024 Journal of Speleology 25 (3-4), 21-36. doi.org/10.5038/1827-806X.25.3.2
- Kring, D. A., Tikoo, S. M., Schmieder, M., Riller, U., Rebolledo-Vieyra, M., Simpson, S. L., et
- al. (2020). Probing the hydrothermal system of the Chicxulub impact crater. Science Advances,
- 1027 6(22), eaaz3053. doi:10.1126/sciadv.aaz3053
- Kronyak, R.E., Kah, L.C., Edgett, K.S., VanBommel, S.J., Thompson, L.M., Wiens, R.C., Sun,
- 1029 V.Z., & Nachon, M. (2019), Mineral-filled fractures as indicators of multigenerational fluid flow
- in the Pahrump Hills member of the Murray formation, Gale crater, Mars. Earth and Space
- 1031 *Science*, 6, 238–265. https://doi.org/10.1029/2018EA000482
- 1032 Mahaffy, P. R., Webster, C. R., Cabane, M., Conrad, P. G., Coll, P., Atreya, S. K., et al. (2012),
- 1033 The sample analysis at Mars investigation and instrument suite. Space Science Reviews, 170(1-
- 1034 4), 401-478.
- 1035 Malin, M.C., & Edgett. K.S. (2000), Sedimentary rocks of early Mars. *Science*, 290, 1927-1937.
- 1036 doi: 10.1126/science.290.5498.1927
- Malin, M.C., Ravine, M.A. Caplinger, M.A. Ghaemi, F.T. Schaffner, J.A. Maki, J.N., et al.
- 1038 (2017), The Mars Science Laboratory (MSL) Mast cameras and Descent imager: Investigation
- and instrument descriptions. Earth and Space Science, 4(8):506-539,
- 1040 doi:10.1002/2016EA000252
- 1041 Mc Lennan, S. M. (2003), Sedimentary silica on Mars. Geology 31:315–318. doi:10.1130/0091-
- 1042 7613
- Mc Lennan, S. M., Grotzinger, J. P., Hurowitz, J. A., & Tosca, N., J. (2019), The sedimentary
- 1044 cycle on early Mars. Annual Review of Earth and Planetary Sciences, 47: 91-118,
- 1045 doi.10.1146/annurev-earth-053018-060332
- 1046 Milliken, R. E., Grotzinger, J. P., & Thomson, B. J. (2010), Paleoclimate of Mars as captured by
- the stratigraphic record in Gale Crater. *Geophysical Research Letters*, 37(4), L04201.
- 1048 doi:10.1029/2009GL041870
- Milliken, R.E., Ewing, R.C., Fischer, W.W., and Hurowitz, J. (2014), Wind-blown sandstones
- 1050 cemented by sulfate and clay minerals in Gale Crater, Mars. Geophysical Research Letters, v. 41,
- 1051 p. 1149–1154, doi.org/10.1002/2013GL059097.
- Morris, R. V., Rampe, E. B., Vaniman, D. T., Christoffesren, R., Yen, A. S., Morrison, S. M., et
- al. (2020) Hydrothermal precipitation of sanidine (adularia) having full Al, Si structural disorder
- and specular hematite at Maunakea volcano (Hawai'i) and at Gale crater (Mars). Journal of
- 1055 Geophysical Research Planets, 125(9), doi.org/10.1029/2019JE006324
- Nesbitt, H.W., & Wilson, R.E. (1992), Recent chemical weathering of basalt. *American Journal*
- 1057 of Science, 292, 740–777.
- Nesbitt, H. W., & Young, G. M. (1982), Early Proterozoic climates and plate motions inferred
- from major element chemistry of lutites. *Nature*, 299(5885), 715–717. doi.org/10.1038/299715a0
- Nesbitt, H. W., & Young, G. M. (1984), Prediction of some weathering trends of plutonic and
- 1061 volcanic rocks based on thermodynamic and kinetic considerations. Geochimica et
- 1062 Cosmochimica Acta, 48(7), 1523-1534, doi:10.1016/0016-703(84)90408-3

- 1063 O'Connell-Cooper, C.D., Spray, J.G., Thompson, L.M., Gellert, R., Berger, J.A., Boyd, N.I., et
- al., (2017), APXS-derived chemistry of the Bagnold dune sands: Comparisons with Gale Crater
- soils and the global Martian average. Journal of Geophysical Research Planets, 122(12):2623-
- 1066 2643, doi:10.1002/2017JE005268
- 1067 O'Connell-Cooper, C.D., Thompson, L.M., Spray, J.G., Berger, J.A., VanBommel, S. J., Gellert,
- 1068 R., et al. (2018), Chemical diversity of sands within the linear and barchan dunes of the Bagnold
- Dunes, Gale Crater, as revealed by APXS onboard Curiosity. Geophysical Research Letters,
- 1070 45(18):9460-9470, doi:10.1029/2018GL079026
- 1071 O'Connell-Cooper, C.D., Thompson, L.M., Spray, J.G., Berger, J.A., VanBommel, S. J.,
- Gellert, R., et al. (this issue), Statistical analysis of APXS-derived chemistry of the clay-bearing
- 1073 Glen Torridon region and Mount Sharp group, Gale crater, Mars. Journal of Geophysical
- 1074 Research Planets, https://doi.org/10.1002/essoar.10510270.1 (ESSOAr Preprint)
- Palucis, M. C., Dietrich, W. E., Hayes, A. G., Williams, R. M., Gupta, S., Mangold, N., et al.
- 1076 (2014), The origin and evolution of the Peace Vallis fan system that drains to
- the Curiosity landing area, Gale Crater, Mars. *Journal of Geophysical Research Planets 119*(4):
- 1078 705-728, doi.org/10.1002/2013JE004583
- Rampe, E.B., Ming, D.W., Blake, D.F., Bristow, T.F., Chipera, S.J., Grotzinger, J.P., et al.
- 1080 (2017), Mineralogy of an ancient lacustrine mudstone succession from the Murray formation,
- Gale crater, Mars. Earth and Planetary Science Letter,s 471, 172–158.
- 1082 doi.org/10.1016/j.epsl.2017.04.021
- Rampe, E.B., Lapotre, M. G. A., Bristow, T.F., Arvidson, R. E., Morris, R. V., Achilles, C. N., et
- al. (2018), Sand mineralogy within the Bagnold dunes, Gale crater, as observed in situ and from
- orbit. Geophysical Research Letters, 45(18), 9488-9497. doi.org/10.1029/2018GL079073
- Rampe, E. B., Bristow, T. F., Morris, R. V., Morrison, S. M., Achilles, C. N., Ming, D. W., et al.
- 1087 (2020a), Mineralogy of Vera Rubin Ridge from the Mars Science Laboratory CheMin
- Instrument. Journal of Geophysical Research-Planets. doi:10.1029/2019JE006306
- Rampe, E. B., Blake, D.F., Bristow, T. F., Ming, D. W., Vaniman, D. T., Morris, R. V., et al.
- 1090 (2020b), Mineralogy and geochemistry of sedimentary rocks and eolian sediments in Gale crater,
- 1091 Mars: A review after six Earth years of exploration with Curiosity. *Geochemistry*, 80(2).
- 1092 doi:10.1016/j.chemer.2020.125605
- Rampe, E. B., Yen, A., Bristo, T, Blake D. F., Vaniman, D., Achilles, C. N., et al. (2020c),
- Mineralogy of the Greenheugh Pediment and Underlying Murray Formation from the Mars
- 1095 Science Laboratory CheMin Instrument. Paper presented at American Geophysical Union Fall
- 1096 Meeting, December 2020. Abstract P070-09.
- Rieder, R., Gellert, R., Brückner, J., Klingelhöfer, G., Dreibus, G., Yen, A. & Squyres, S. W.
- 1098 (2003), The new Athena alpha particle X-ray spectrometer for the Mars Exploration Rovers.
- 1099 Journal of Geophysical Research, Planets, 108, E12, 8066.
- 1100 https://doi.org/10.1002/2015GL066675
- 1101 Rudolf, A., Horgan, B., Johnson, J., Bennett, K., Haber, J., Bell III, J. F., et al. (this issue), The
- distribution of clay minerals and their impact on diagenesis in Glen Torridon, Gale crater, Mars.
- 1103 Journal of Geophysical Research, Planets

- Sautter, V., Toplis, M. J., Wiens, R. C., Cousin, A., Fabre, C., & Gasnault, O. (2015), In situ
- evidence for continental crust on early Mars. *Nature Geoscience*, 8(8), 605.
- Schieber, J., Bish, D. L., Coleman, M., Reed, M., Hausrauth, E. M., Cosgrove, J., et al. (2017),
- Encounters with an unearthly mudstone: Understanding the first mudstone found on Mars.
- 1108 Sedimentology, 64, p. 311-358. doi:10.1111/sed.12318.
- 1109 Schmidt, M. E., Campbell, J. L., Gellert, R., Perrett, G. M., Treiman, A. H., Blaney, D. L. et al.
- 1110 (2014), Geochemical diversity in first rocks examined by the Curiosity rover in Gale crater:
- 1111 Evidence for and significance of an alkali and volatile-rich igneous source, *Journal of*
- 1112 Geophysical Research Planets, 119(1):64-81, doi:10.1002/2013JE004481
- 1113 Schwenzer, S. P., Abramov, O., Allen, C. C., Bridges, J. C., Clifford, S. M., Filberto, J., et al.
- 1114 (2012), Gale crater: Formation and post-impact hydrous environments. *Planetary and Space*
- 1115 Science, 70, 84-95. http://dx.doi.org/10.1016/j.pss.2012.05.014
- 1116 Stack, K.M., Grotzinger, J.P., Lamb, M.P., Gupta, S., Rubin, D.M., Kah, L.C., et al. (2019),
- Evidence for plunging river plume deposits in the Pahrump Hills member of the Murray
- 1118 formation, Gale crater, Mars. *Sedimentology* 66, 1768–1802. https://doi.org/10.1111/sed.12558
- Stein, N.T., Quinn, D.P., Grotzinger, J.P., Fedo, C., Ehlmann, B.L., Stack, K. M., et al. (2020),
- Regional structural orientation of the Mt. Sharp group revealed by in-situ dip measurements and
- stratigraphic correlations on the Vera Rubin ridge. Journal of Geophysical Research, Planets,
- 1122 *125*(5), doi: 10.1029/2019JE006298
- Stolper, E. M., Baker, M. B., Newcombe, M. E., Schmidt, M. E., Treiman, A. H., Cousin, A., et
- al. (2013), The petrochemistry of Jake M: A martian mugearite. Science 341 (6153), 1239463.
- 1125 doi:10.1126/science.1239463
- Sutter, B., McAdam, A.C., Archer, P. D., Ming, D.W., Eigenbrode, J. L., Rampe, E.B., et al.
- 1127 (2020), Geochemical Processes Along and Above the Glen Torridon/Greenheugh Pediment,
- 1128 Unconformity, Gale Crater, Mars: Results from the Sample Analysis at Mars Instrument. Paper
- presented at American Geophysical Union Fall Meeting, December 2020. Abstract P070-07
- Thomson, B. J., Bridges, N. T., Milliken, R., Baldridge, A., Hook, S. J., Crowley, J. K., et al.
- 1131 (2011), Constraints on the origin and evolution of the layered mound in Gale Crater, Mars using
- 1132 Mars Reconnaissance Orbiter data. *Icarus*, 214(2), 413–432.
- 1133 doi.org/10.1016/j.icarus.2011.05.002
- 1134 Thompson, L. (2020), Alpha Particle X-ray spectrometer geochemistry of the Murray formation
- and Vera Rubin ridge, Gale crater, Mars. <a href="https://doi.org/10.25545/ZXDJZ7">https://doi.org/10.25545/ZXDJZ7</a>, UNB, V1,
- 1136 UNF:6:bL/a2qTZBu6DNJlzkmGAbg==[fileUNF]
- 1137 Thompson, L. (2022) Alpha Particle X-ray spectrometer geochemistry of rocks associated with
- the Basal Siccar Point group unconformity, Glen Torridon region, Gale crater,
- Mars. https://doi.org/10.25545/FXZOZ0, UNB, V1, UNF:6:9gSkKeCmJKxFD9m0RbmtFg==
- 1140 [fileUNF]
- Thompson, L. M., J.A. Berger, J.G. Spray, A.A. Fraeman, M.A. McCraig, C.D. O'Connell-
- 1142 Cooper, et al. (2020), APXS-derived compositional characteristics of Vera Rubin Ridge and
- Murray formation, Gale crater, Mars: Geochemical implications for the origin of the ridge.
- 1144 *Journal of Geophysical Research: Planets, 125*(10), doi: 10.1029/2019JE006319

- Thompson, L. M., Schmidt, M. E., Spray, J. G., Berger, J. A., Fairén, A. G., Campbell J. L., et al.
- 1146 (2016), Potassium-rich sandstones within the Gale impact crater, Mars: The APXS perspective.
- 1147 Journal of Geophysical Research Planets, 121(10):1981-2003, doi:10.1002/2016JE005055
- Thorpe, M. T., Bristow, T. F., Rampe, E. B., Tosca, N. J., Grotzinger, J. P., Bennett, K., A., et
- al., (this issue), Mars Science Laboratory data from the Glen Torridon region and the
- significance of lake-groundwater interactions in interpreting mineralogy and sedimentary history.
- Journal of Geophysical Research Planets 2021JE007099
- 1152 Treiman, A. H., Bish, D. L., Vaniman, D. T., Chipera, S. J., Blake, D. F., Ming, D. W., et al.
- 1153 (2016), Mineralogy, provenance and diagenesis of a potassic basaltic sandstone on Mars:
- 1154 CheMin X-ray diffraction of the Windjana sample (Kimberley area, Gale Crater). *Journal of*
- 1155 Geophysical Research, 121(1), p.75 106. doi:10.1002/2015JE004932
- VanBommel, S.J., Gellert, R., Berger, J.A., Campbell, J.L., Thompson, L.M., Edgett, K.S., et al.
- 1157 (2016), Deconvolution of distinct lithology chemistry through oversampling with the Mars
- 1158 Science Laboratory Alpha Particle X-ray Spectrometer. X-Ray Spectrometry, 45, 155–161.
- 1159 https://doi.org/10.1002/xrs.2681
- VanBommel, S.J., Gellert, R., Berger, J.A., Thompson, L.M., Edgett, K.S., McBride, M.J., et al.
- 1161 (2017), Modeling and mitigation of sample relief effects applied to chemistry measurements by
- the Mars Science Laboratory Alpha Particle X-ray Spectrometer. X-Ray Spectrometry, 46, 229–
- 236. https://doi.org/10.1002/xrs.2755
- VanBommel, S.J., Gellert, R., Boyd, N.I., & Hanania, J.U. (2019), Empirical simulations for
- further characterization of the Mars Science Laboratory Alpha Particle X-ray Spectrometer: An
- 1166 Introduction to the ACES program. *Nuclear Instrumentation and Methods, B* 441, 79–87.
- 1167 https://doi.org/10.1016/j.nimb.2018.12.040
- Watkins, J. A., Grotzinger, J., Stein, N., Banham, S. G., Gupta, S., Rubin, D., Stack, K. M.,
- Edgett, K. S. (2016), Paleotopography of Erosional Unconformity, Base of Stimson Formation,
- Gale Crater, Mars. Paper presented at the 47th Lunar and Planetary Science Conference,
- 1171 Abstract #2939, Woodlands, Texas
- Wiens, R. C., et al. (2020), Origin and composition of three heterolithic boulder- and cobble-
- bearing deposits overlying the Murray and Stimson formations, Gale Crater, Mars. *Icarus*, 350,
- 1174 113897. doi.org/10.1016/j.icarus.2020.113897
- Williams, R.M.E., Grotzinger, J.P., Dietrich, W.E., Gupta, S., Sumner, D.Y., Wiens, R.C., et al.
- 1176 (2013), Martian fluvial conglomerates at Gale crater. *Science* 340, 10681072.
- 1177 https://doi.org/10.1126/science.1237317
- 1178 Yen, A.S., Ming, D.W., Vaniman, D.T., Gellert, R., Blake, D.F., Morris, R.V., et al. (2017),
- Multiple stages of aqueous alteration along fractures in mudstone and sandstone strata in Gale
- 1180 crater, Mars. Earth and Planetary Science Letters, 471, 186–198. doi:10.1016/j.epsl.2017.04.033
- Yen, A.S., Morris, R.V., Ming, S.P., Schwenzer, Sutter, B., D.W., Vaniman, et al. (2021),
- Formation of tridymite and evidence for a hydrothermal history at Gale crater, Mars. *Journal of*
- 1183 Geophysical Research Planets, 126, e2020JE006569. doi:1.1029/2020JE006569
- 1184 Supporting Information References

- Brimhall, G. H., & Dietrich, W. E. (1987), Constitutive mass balance relations between
- chemical composition, volume, density, porosity, and strain in metasomatic hydrochemical
- systems: results on weathering and pedogenesis. Geochimica et Cosmochimica Acta, 51(3), 567–
- 1188 587.

## Figure Captions

- Figure 1. a) HiRISE imagery with Curiosity's traverse to sol 2940, turquoise arrow shows the
- approximate extent of the Bradbury group; b) Stratigraphic column for the sedimentary strata
- encountered within Gale crater up to sol 2776, with zoomed in section (right) showing the Glen
- 1194 Torridon Mount Sharp group and Greenheugh pediment capping sandstones.
- Figure 2. a) Close-up HiRISE with details of Curiosity's traverse, Vera Rubin ridge, Glen
- 1196 Torridon, the sulfate-bearing unit, Greenheugh pediment and Gediz Vallis ridge; b) HiRISE with
- 1197 Curiosity's traverse overlain showing the area of interest (white box in a), Hutton interval targets,
- Glasgow, Greenheugh pediment capping sandstone targets, as well as cap float rock targets
- analyzed on Western butte (WB) encountered prior to ascending on to the pediment; c) Part of a
- Mastcam mosaic (sol 2633, mcam013796) looking towards the pediment and Mnt Sharp,
- showing location of APXS targets of interest (circles) d) Part of Mastcam mosaic (sol 2620,
- mcam013767) Western butte with
- Figure 3. a) Log ratio plot (relative to average Mount Sharp group (grp) pre Glen Torridon
- 1204 (GT)) showing the compositional range for GT Jura and Knockfarril Hill (KH) members
- 1205 (grey dashed lines), the range of Glasgow member compositions (solid grey lines), Hutton
- interval targets within 3 m of the pediment contact (purples), and lower Mount Sharp grp,
- Pahrump Hills and Hartmann's Valley member targets with similar elemental trends (greens).
- Note the elevated Na, and moderate Ca, but relatively low S associated with the Hutton interval
- targets, as well as many of the lower Mount Sharp grp targets; b) Select oxide and element
- 1210 concentrations for the GT Jura, Knockfarril Hill and Glasgow member targets plotted versus
- elevation (up to and including Glasgow drill fines; sol 2776). Hutton interval targets are in
- purple. Larger, thicker outlined Glasgow target is Glasgow DRT. Verical blue line indicates
- average Mount Sharp grp pre-GT, and the blue shaded area the  $1\sigma$  standard deviation; c) CaO
- versus SO<sub>3</sub> plot for the Mount Sharp grp to GT, and the GT Jura, Knockfarril Hill and Glasgow
- members. Note that Hutton interval targets within 3 m of the pediment (purple), and the related
- Pahrump Hills and Hartmann's Valley targets (green diamonds) plot with excess CaO relative to
- the CaSO<sub>4</sub> addition trend line (orange)
- Figure 4. a) Plot showing % increases and decreases in Na<sub>2</sub>O relative to average Mount Sharp
- group for the various members; b) Plot showing % gains and losses of Na, Mg, Ca, Mn, Fe, Al,
- 1220 K, Ni and S for Hutton interval targets compared to the Glasgow DRT target (see §S2.8, Table
- 1221 S4)
- Figure 5. Log ratio plot (relative to the bedrock target in the same workspace) showing relative
- increases and decreases in oxide and element concentrations of the diagenetic features analyzed
- in the upper Mount Sharp grp. Abernethy and Dunbartonshire (reds) both show very high Fe and
- Mn concentrations, and Dounreay and Liberton Brae (yellow/orange) exhibit elevated Mg and K.
- 1226 **Figure 6.** Log ratio plots (relative to Lagrange, typical Gale soil target from sol 605) with the
- 1227 compositional range of typical Stimson sandstone APXS targets from the Naukluft and Emerson
- plateaus (brown lines) and a) capping sandstones at the pediment contact (oranges), lighter
- orange elemental traces are the two targets analyzed immediately at the contact; **b)** showing the

- addition of pediment capping sandstones analyzed higher up the section from the Ladder and
- Edinburgh intervals (blue); c) Ladder and Edinburgh interval sandstones and Blackwaterfoot
- float cap rock (yellow); d) with the addition of Lomond Hills and Heinrich Waenke float cap
- rocks (red); e) compositionally related targets to the Ladder and Edinburgh interval sandstones
- encountered earlier in the mission; and f) compositionally related targets to Lomond Hills and
- Heinrich Waenke encountered earlier in the mission (RN3 Rocknest 3).
- Figure 7. Plot showing % elemental increases and decreases relative to average
- 1237 Emerson/Naukluft plateau, Stimson formation for; the Ladder and Edinburgh interval cap rock
- 1238 (blue), and the Gleann Beag interval cap rock (solid brown). The lighter brown denotes the two
- high S targets at the contact with the underlying Hutton interval. Shaded brown areas represent
- mimimum and maximum concentrations for the Stimson formation.
- 1241 **Figure 8.** Emerson/Naukluft plateau Stimson formation, Gleann Beag, Ladder and Edinburgh
- interval cap rocks, Western butte float cap rocks, and Bradbury rocks and float cap rock on K<sub>2</sub>O
- versus Na<sub>2</sub>O (left), and Na<sub>2</sub>O versus Al<sub>2</sub>O<sub>3</sub> (right) plots. In contrast to the Emerson/Naukluft
- plateau Stimson formation, the Ladder and Edinburgh interval cap rocks show moderate
- 1245 correlations of K and Na, and Na and Al.
- Figure 9. a) Locations on HiRISE imagery of previously encountered APXS targets that are
- 1247 compositionally related to pediment cap rock and the Hutton interval; **b)** Portion of Mastcam
- mosaic (mcam03214 sol 747) showing the context of the Mount Sharp group at Pahrump Hills
- including the Telegraph Peak target and surrounding terrain, including Salsberry Peak capping
- sandstones and blocky float rocks, including the Little Devil float rock target; c) Portion of
- Mastcam mosaic (mcam06679 sol 1367) showing the context of the Hartmann's Valley, Mount
- Sharp group just below the capping, Naukluft Plateau, Stimson sandstone at the Oudam drill site.
- 1253 Image credit for Mastcams: NASA/Caltech-JPL/MSSS
- Figure 10. Schematic cross-sections from a) Salsberry Peak (left) to Marias Pass (right). Note
- that the Stimson formation sandstones exposed at Marias Pass are at a similar elevation to
- Salsberry Peak capping sandstones and might also overly the Basal Siccar Point group
- unconformity (see Figures 9a & b for location of cross-section); b) Western butte (left) to where
- 1258 Curiosity ascended the pediment (right) (see Figure 2 for location of cross-section). Circles
- represent select APXS targets. Note how the compositionally distinct Hutton interval (purple)
- mimics the dip of the pediment erosional surface extended to the butte and cuts across the
- underlying flat-lying stratigraphy of the Mount Sharp group. All sandstones (Salsberry Peak,
- Marias Pass and the pediment) exhibit sub-horizontal bedding planes (Banham et al., 2018, 2021,
- 1263 this issue; Kronyak et al., 2019; Stack et al., 2019.)
- Figure 11. Cross-sections drawn through A-A' shown on HiRise image top left; from the
- Yellowknife Bay area (left) to the pediment (right). Top cross-section depicts the scenario
- whereby both the Bradbury group and Stimson formation are younger than, and deposited onto
- the irregular erosional surface of the flat-lying Mount Sharp group. Bottom cross-section depicts
- the Bradbury group as older than the Mount Sharp group, with the Stimson formation being the
- 1269 youngest. Both show Basal Siccar Point group unconformity extrapolated from Pahrump Hills
- 1209 youngest. Both show Basar Siccar Form group uncomorning extrapolated from Familing IIII
- 1270 upto the pediment. Diamonds depict altered Mount Sharp group strata lying just below the
- unconformity. Stimson at Pahrump Hills and pediment-capping sandstones exhibit sub-
- horizontal bedding planes (Banham et al., 2018, 2021, this issue)
- Figure 12. a) Molar A-CN-K plot showing offset of the Ladder/Edinburgh, high-K sandstones
- and Western butte (WB) float along the plagioclase potassium feldspar join, away from

- basaltic sand, Stimson fm and Gleann Beag interval targets; **b)** Molar A-CNK-FM plot showing
- high-K sandstones plotting with basaltic sand, Stimson fm and Gleann Beag interval targets.
- 1277 **Figure 13. a)** Plot representing the results of a mass balance calculation for the high S and
- nodular sandstones relative to Galloway Hills (Table S4 and §S2.8.). Note change of scale above
- 1279 100%; **b)** Plots of CaO and SO<sub>3</sub> concentrations versus elevation for the GT Mount Sharp group
- and pediment capping sandstones. Note the very low S associated with the Hutton interval
- targets and the elevated S in the two pediment sandstones immediately above the Basal Siccar
- 1282 Point group unconformity.
- 1283 Figure 14. Proposed series of events: a) Deposition of the Mount Sharp group sediment in a
- predominantly lacustrine environment followed by burial (probably by the upper Mount Sharp
- sediment), and diagenesis/alteration to give the clay-rich, CaSO<sub>4</sub>-bearing, relatively
- homogeneous in composition, Mount Sharp group; b) Followed by physical weathering and
- erosion of the Mount Sharp group (and overlying sulfate and yardang unit), which could have
- resulted in increased porosity and permeability of the uppermost, exposed section; c) later
- deposition of eolian sand (Siccar Point group, Stimson formation, and possibly the Bradbury
- group sand) onto that erosional surface, both with basaltic and more alkaline composition
- provenance. The sands were then subject to at least some burial and diagenesis, prior to fluid
- flow focused along the Basal Siccar Point group unconformity (blue arrows). The fluid may be
- derived from the interaction of post-impact hydrothermal fluids with the sulfate unit. Fluids
- interact with the Mount Sharp grp rocks immediately adjacent to the unconformity (within ~3 m
- and over at least 4 km laterally) resulting in destruction of both clay and calcium sulfate
- minerals. The localized dark veins and associated diagenetic features within the Hutton interval
- 1297 (e.g. Dounraey-Dumbartonshire), and crosscutting CaSO<sub>4</sub> veins were the last to form, with
- distinct fluid chemistries from those responsible for the alteration of the Hutton interval strata; d)
- Finally, the surface was eroded to its current level. The green outlined area corresponds with the
- 1300 cross-sections depicted in Figure 11.

## **TableCaptions**

1301

1302

1308

- Table 1. APXS compositional data for a) the Mount Sharp group (grp) pre-Glen Torridon (GT);
- Glen Torridon, Mount Sharp grp Jura and Knockfarril Hill members (mbrs); Glasgow mbr
- including the Hutton interval and diagenetic features; and **b)** Stimson formation (fm)
- encountered at Emerson and Naukluft plateaus, and the pediment capping rocks. See supporting
- information for details. All data reported as wt% except Ni, Zn and Br (ppm).

Figure :	1.
----------	----

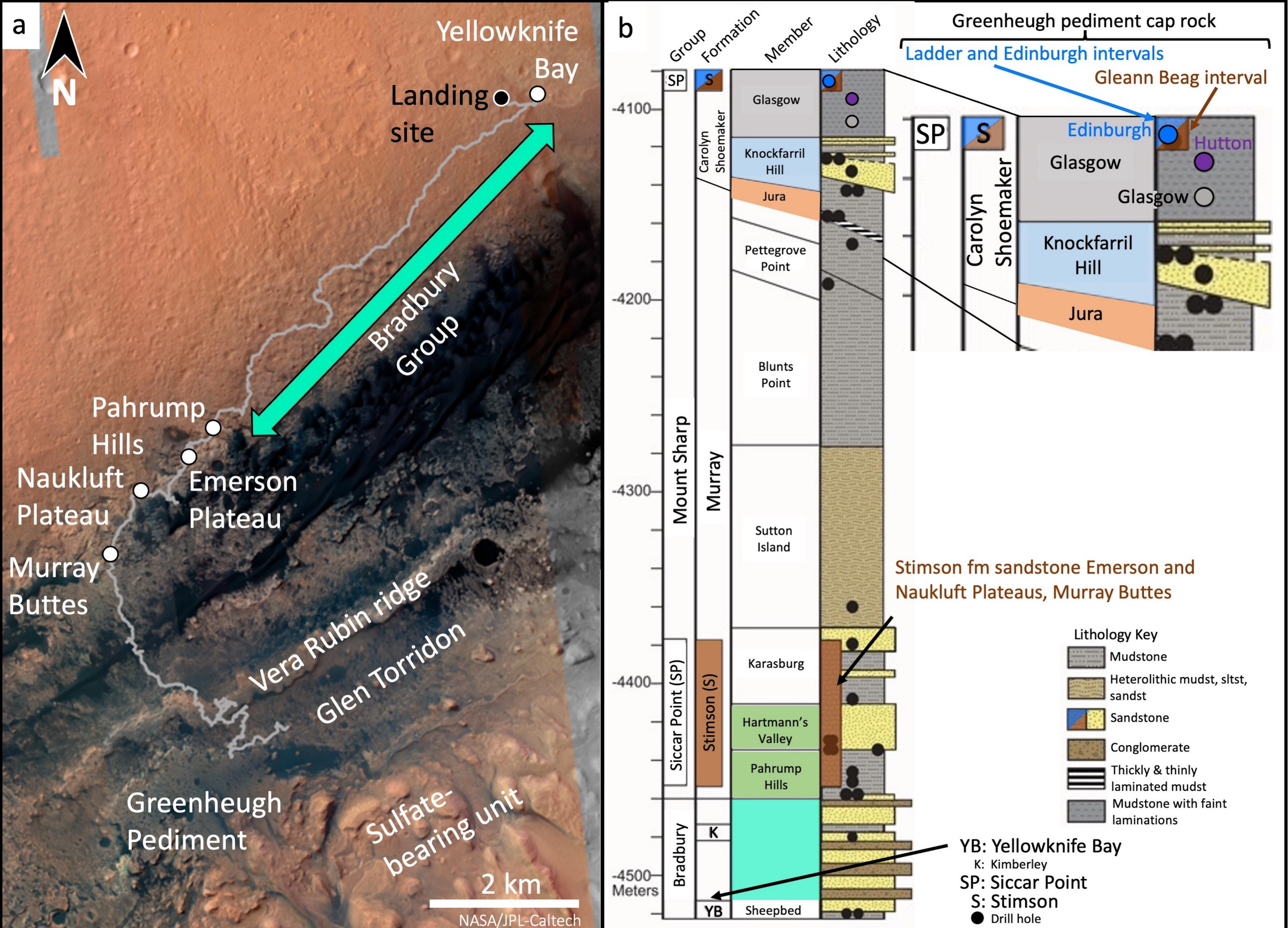


Figure 2	2.
----------	----

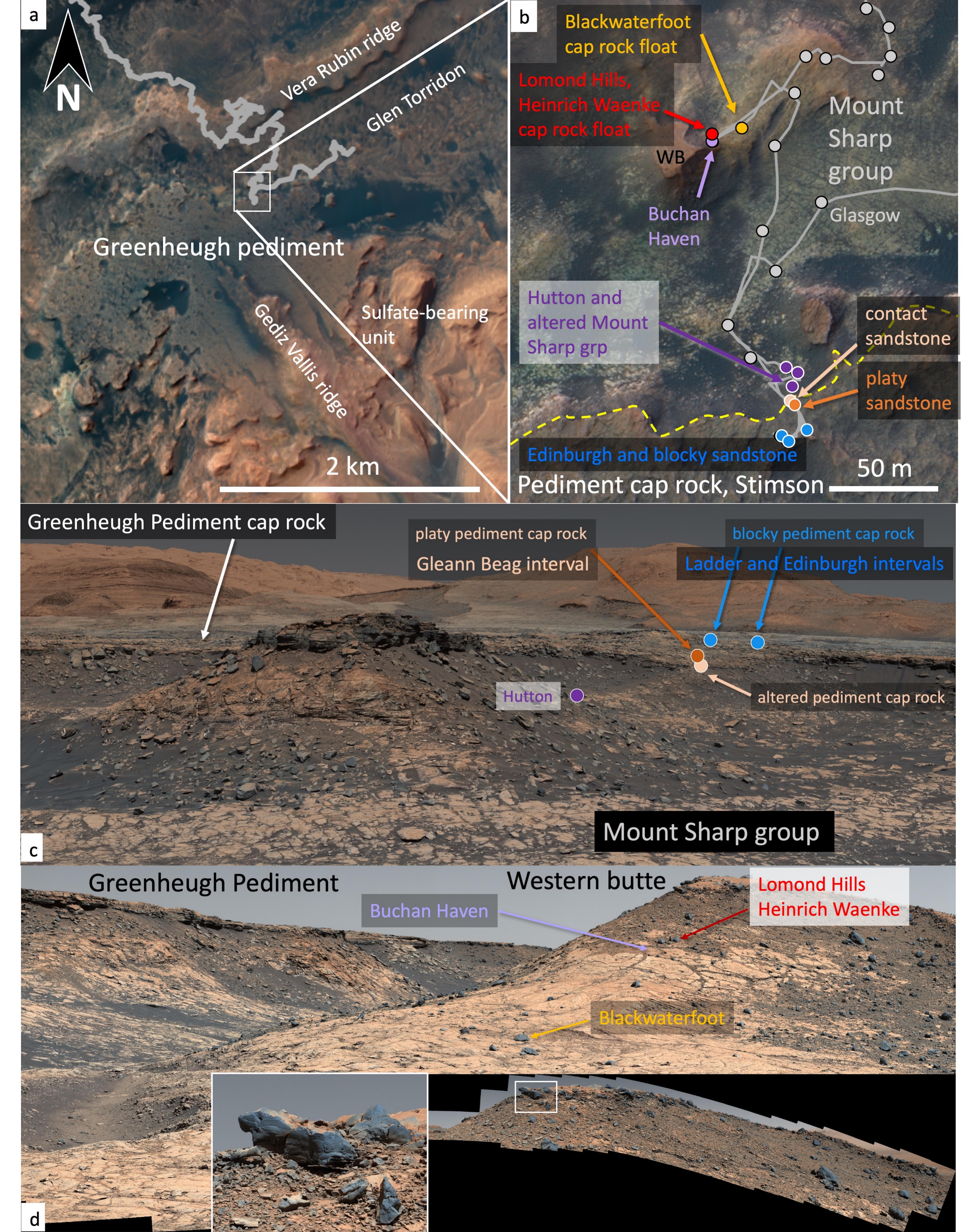


Table 1a		SiO <sub>2</sub>	TiO <sub>2</sub>	$Al_2O_3$	Cr <sub>2</sub> O <sub>3</sub>	FeO	MnO	MgO	CaO	Na <sub>2</sub> O	K <sub>2</sub> O	$P_2O_5$	SO <sub>3</sub>	Cl	Ni	Zn	Br
Mount Sharp grp to GT	Average	48.31	1.04	9.29	0.32	18.53	0.22	5.56	4.40	2.55	0.89	0.96	6.40	1.21	870	1172	225
	Median	48.30	1.04	9.11	0.32	18.51	0.21	5.54	4.31	2.55	0.88	0.93	6.19	1.12	879	1084	125
า=302	Stdev	2.92	0.08	0.95	0.04	2.70	0.10	0.99	1.18	0.24	0.13	0.24	2.15	0.53	186	440	239
	Max	55.80	1.29	13.22	0.45	26.80	0.77	8.65	8.61	3.66	1.22	2.51	15.44	3.07	1832	2472	1396
	Min	41.05	0.79	7.22	0.24	9.13	0.06	2.66	2.08	1.99	0.58	0.48	1.85	0.30	231	397	14
GT Mount Sharp grp	Average	46.76	1.12	8.78	0.33	20.38	0.22	6.03	4.39	2.39	0.95	0.84	6.07	1.30	838	1936	541
ura and Knockfarril Hill	Median	47.36	1.13	8.79	0.34	20.04	0.20	5.94	3.89	2.45	1.01	0.81	5.38	1.35	845	1631	479
members	Stdev	3.21	0.06	0.62	0.03	1.67	0.12	0.92	1.70	0.23	0.21	0.14	2.70	0.38	116	1090	361
n=94	Max	53.17	1.30	10.17	0.40	26.24	0.61	8.06	9.98	2.73	1.36	1.35	16.19	2.12	1168	4411	1609
	Min	37.04	0.91	6.26	0.25	15.93	0.06	4.34	2.32	1.35	0.54	0.57	2.86	0.32	568	505	27
Glasgow member	Elevation/m	1															
Kirkcudbrightshire	-4118.12	45.29	1.14	8.53	0.36	18.42	0.22	7.65	5.22	2.52	0.72	0.93	7.32	1.32	840	1187	747
Stonehive	-4117.47	41.51	0.98	8.09	0.28	17.22	0.16	5.91	8.14	2.47	0.75	0.90	12.15	1.24	560	632	183
Jpperhill_DRT	-4117.47	47.96	1.05	8.36	0.30	20.91	0.19	4.78	4.21	2.31	1.05	0.85	6.17	1.47	960	1037	1125
Glen_Mark	-4118.14	44.34	1.03	8.33	0.29	18.20	0.14	7.11	6.00	2.46	0.79	0.97	8.66	1.21	820	874	428
Conachair_DRT	-4119.31	47.26	1.15	8.77	0.38	18.27	0.20	7.09	4.76	2.32	0.78	0.89	6.54	1.16	892	1452	209
onachair_offset	-4119.31	44.08	1.12	8.78	0.31	15.52	0.22	7.68	6.95	2.55	0.66	1.04	9.72	1.09	729	1210	84
ourhope	-4118.12	46.37	1.11	8.84	0.33	18.26	0.21	6.30	4.95	2.40	0.85	0.93	7.98	1.20	857	1191	78
leneagles	-4119.31	45.65	1.05	8.17	0.32	20.15	0.17	6.40	4.79	2.40	0.95	0.80	7.61	1.10	1115	1340	573
oggy_Moss	-4118.12	48.06	1.09	9.41	0.34	18.72	0.12	5.40	4.44	2.25	0.92	0.94	6.69	1.31	935	1175	128
Vell_Run	-4119.19	47.98	1.03	9.10	0.26	19.38	0.18	5.73	4.19	2.38	0.94	1.03	6.37	1.11	890	1147	165
taxigoe	-4117.94	48.25	1.19	8.99	0.38	17.87	0.15	6.45	4.19	2.64	0.87	0.81	6.37	1.46	895	1274	435
cotnish_DRT	-4115.99	46.69	1.06	8.47	0.30	17.64	0.11	4.23	5.55	2.16	1.02	0.76	10.78	0.94	732	894	213
enfrewshire	-4114.39	47.28	1.05	8.89	0.33	17.53	0.11	5.09	5.08	2.31	0.95	0.81	8.94	1.27	783	1287	19
lenmard_Wood	-4110.72	44.21	1.07	8.93	0.33	20.12	0.19	6.76	5.13	2.51	0.62	0.81	7.88	1.14	1073	1074	122
orth_Esk	-4109.56	45.74	0.99	8.64	0.28	17.75	0.12	6.17	5.85	2.51	0.66	0.80	8.99	1.05	848	781	189
en_Arnaboll_DRT	-4108.57	45.48	0.86	8.67	0.27	16.69	0.25	5.95	6.37	2.42	0.73	0.86	10.22	0.72	772	1332	178
ennedys_Pass	-4109.26	48.86	1.01	9.05	0.25	18.61	0.13	5.87	4.12	2.38	0.78	0.98	6.39	1.30	838	810	356
rbroath	-4109.49	49.86	1.00	9.42	0.34	16.93	0.10	5.75	3.94	2.61	0.84	0.88	6.63	1.25	910	984	54
rossachs_DRT	-4109.49	50.02	1.08	8.86	0.31	18.27	0.14	4.98	3.93	2.68	0.88	0.92	5.86	1.71	898	946	1040
auchiehall_DRT	-4108.74	49.18	1.06	8.88	0.29	16.84	0.11	4.02	5.59	2.19	0.94	0.91	8.95	0.77	845	907	75
annoch_Moor	-4108.74	46.90	1.03	9.02	0.31	18.79	0.15	6.91	4.15	2.62	0.79	0.95	6.62	1.22	926	890	540
Marchmont (	-4104.84	43.75	0.94	8.32	0.30	18.52	0.20	6.16	6.55	2.28	0.68	0.86	10.11	0.86	981	659	42
ullivoe DRT	-4098.16	50.41	0.99	9.57	0.28	17.22	0.27	7.60	3.94	2.80	0.89	0.92	4.24	0.61	684	970	69
Glasgow1_tailings	-4107.93	47.51	1.10	8.69	0.41	19.02	0.22	4.71	6.22	2.11	0.78	1.05	6.99	0.91	916	876	29
Glasgow1_dump_corrected	-4107.93	46.87	1.08	8.74	0.38	18.82	0.17	4.74	6.11	2.23	0.91	1.03	7.48	1.12	964	1039	200
lasgow_1_DRT	-4107.93	53.11	1.12	9.50	0.32	17.28	0.11	4.65	3.47	2.32	0.96	1.19	4.46	1.15	1080	1103	607
lasgow_1_offset	-4107.93	48.32	1.00	8.73	0.29	15.98	0.11	4.76	5.79	2.33	0.86	1.03	9.16	1.27	913	972	494
eefstand_Hill_DRT	-4105.43	50.95	1.04	9.51	0.29	19.14	0.15	4.31	3.71	2.37	0.88	0.99	5.82	0.58	828	935	74
eefstand_Hill_offset	-4105.43	49.41	1.03	9.11	0.29	19.20	0.15	4.86	3.85	2.26	0.84	0.94	7.16	0.65	830	956	82
=29	Average	47.29	1.05	8.84	0.31	18.18	0.16	5.79	5.08	2.41	0.84	0.92	7.66	1.11	873	1032	294
	Median	47.28	1.05	8.84	0.31	18.27	0.15	5.87	4.95	2.38	0.85	0.92	7.32	1.15	890	984	183
	Stdev	2.49	0.07	0.40	0.04	1.22				0.17		0.10	1.85	0.27	117	203	296
	Max	53.11	1.19	9.57	0.41	20.91	0.27	7.68	8.14	2.80	1.05	1.19	12.15	1.71	1115	1452	1125
	Min	41.51	0.86	8.09	0.25	15.52	0.10	4.02	3.47	2.11	0.62	0.76	4.24	0.58	560	632	19
ilasgow mbr, Hutton interva	ıl																
uchan_Haven_DRT	-4106.37	51.62	0.94	9.83	0.28	16.76	0.32	6.30	5.80	3.05	0.91	1.15	2.26	0.50	587	1547	89
erwickshire_DRT	-4095.43	47.50	0.94	8.73	0.29	20.10				2.94		1.16	3.71	1.19	712	946	506
airnbulg	-4095.43	47.27	0.93	9.05	0.28	19.19				2.96		1.14	4.18	1.11	716	907	107
utton_DRT_centre	-4095.37	50.50	1.00	9.53	0.28	18.03	0.25	6.16	5.05	3.38	0.94	1.12	2.63	0.88	658	938	219
utton_dump_centre	-4095.37	49.29	1.07	9.27	0.28	18.68	0.26	5.39	6.10	3.51	0.93	1.04	2.99	0.91	716	1191	70
utton_dump_corrected	-4095.37	46.64	1.07	9.29	0.31	19.94	0.27	6.29	5.88	3.39	0.89	1.09	3.71	0.91	739	1598	131
utton_tailings	-4095.37	50.55	1.06	9.46	0.31	19.23	0.25	5.58	5.28	3.68	0.96	1.12	1.43	0.84	698	988	21
=7	Average	49.05	1.00	9.31	0.29	18.85	0.26	6.40	5.35	3.27	0.92	1.12	2.99	0.91	689	1159	163
	Median	49.29	1.00	9.29	0.28	19.19	0.25	6.29	5.28	3.38	0.93	1.12	2.99	0.91	712	988	107
	Stdev	1.93	0.07	0.35	0.01	1.16	0.03	0.85	0.58	0.29	0.03	0.04	0.96	0.22	52	298	163
	Max	51.62	1.07	9.83	0.31	20.10	0.32	7.69	6.10	3.68	0.96	1.16	4.18	1.19	739	1598	506
	Min	46.64	0.93	8.73	0.28	16.76	0.24	5.39	4.62	2.94	0.89	1.04	1.43	0.50	587	907	21
Jpper Glasgow member diag			0.93	8.73	0.28	16.76	0.24	5.39	4.62	2.94	0.89	1.04	1.43	0.50	587	907	21

Moffat Hills	-4109.49	47.36	0.98	9.19	0.30	19.03	0.18			2.18		1.26	8.34	0.95	878	960	65
Bogmill_Pow	-4098.17	36.15	0.94	8.12	0.28	19.49	0.27		7.70	2.58	0.37	0.87	13.49	1.34	1153	1403	397
Liberton_Brae	-4095.37	40.60	0.85	7.62	0.25	16.25	0.25	####	3.31	1.86	2.14	0.97	6.67	1.42	1052	3433	486
Moorfoot_Hills	-4095.37	42.04	0.92	8.54	0.30	20.69	0.33		7.27	2.89	0.74	1.00	5.46	1.68	749	1097	765
Dunbartonshire_refined	-4095.37	26.38	0.58	5.09	0.14	39.65	6.33	8.57	3.60	1.57		0.62	4.89	1.97	893	1593	750
Dounreay	-4095.37	40.01	1.00	7.95	0.27	19.88	0.49	####	5.07	2.04	1.43	1.09	6.73	2.18	1283	1613	822
Table 1b		SiO <sub>2</sub>	TiO <sub>2</sub>	$Al_2O_3$	Cr <sub>2</sub> O <sub>3</sub>	FeO	MnO	MgO	CaO	Na₂O	K <sub>2</sub> O	P <sub>2</sub> O <sub>5</sub>	SO <sub>3</sub>	Cl	Ni	Zn	Br
Stimson fm from Emerson/	Average	43.72	0.92	10.00	0.43	19.00	0.38	8.75	6.43	2.81	0.42	0.85	4.95	1.20	468	333	235
Naukluft plateaus	Median	43.66	0.92	9.46	0.42	19.23	0.39	8.76	6.51	2.76	0.43	0.87	5.24	1.19	448	314	194
	Stdev	1.20	0.05	1.39	0.07	1.55	0.03		0.50		0.06	0.08	1.60	0.35	67	64	138
	Max	47.31	1.05	13.29	0.70	22.13	0.44	####	7.42	3.23	0.51	0.98	7.17	1.94	640	478	722
n=26	Min	41.63	0.81	8.18	0.33	14.80	0.29	6.88	4.98	2.56	0.29	0.72	0.65	0.61	386	217	76
Western butte float cap rock	Elevation/m	1															
Blackwaterfoot	-4108.57	44.42	0.77	9.16	0.63	19.13	0.48	8.74	7.25	3.22	1.21	0.9	3.23	0.74	293	373	57
Lomond_Hills	-4106.37	46.64	0.92	10.2	0.28	17.06	0.35	7.89	6	4.17	2.37	1.31	1.9	0.58	716	1367	74
Heinrich_Waenke	-4106.37	45.49	1.01	9.09	0.32	18.72	0.43	7.44	7.05	3.36	2.28	1.13	2.66	0.66	889	1876	38
Glaen Baeg interval (platy) ca	ap rock																
Huttons_Section	-4092.79	37.24	0.75	7.47	0.3	16.77	0.19	7.32	6.4	2.3	0.48	0.88	18.91	0.76	564	360	168
Clach_Glas	-4092.79	39.71	0.87	8.2	0.33	17.52	0.23	7.99	5.92	2.69	0.53	0.95	14.05	0.84	536	358	161
Galloway_Hills_DRT	-4091.75	41.72	1	8.58	0.56	21.05	0.46	9.91	6.37	2.65	0.39	0.86	5.11	1.18	593	465	60
Adder_raster3 (nodular)	-4090.90	41.52	0.95	8.97	0.39	19.83	0.41	9.43	6.59	2.78	0.45	0.93	6.54	1.05	560	448	46
Adder_raster2 (nodular)	-4090.90	42.03	0.97	8.77	0.42	20.08	0.42	9.28	6.47	2.8	0.44	0.92	6.06	1.17	567	448	73
Adder_raster1 (nodular)	-4090.90	40.99	0.92	8.92	0.42	19.13	0.4	9.65	6.4	2.76	0.46	0.89	7.65	1.24	545	419	53
Ladder and Edinburgh interv	als (bocky) ca	p rock															
Forsinard_Flows_offset	-4088.78	40.98	0.77	8.57	0.58	20.43	0.66	9.05	6.93	3.02	0.94	0.75	6.27	0.95	301	513	68
Forsinard_Flows	-4088.78	42.36	0.83	9.11	0.51	19.79	0.59	8.81	6.51	3.18	1.00	0.70	5.48	0.97	298	522	59
Machir_Bay_DRT	-4088.78	42.24	0.81	8.63	0.51	19.31	0.52	8.84	6.81	3.03	0.94	0.77	6.43	1.01	343	471	48
Edinburgh_dump_corrected	-4088.69	41.54	0.87	9.25	0.46	22.71	0.53	9.09	6.14	3.55	0.99	0.69	3.18	0.84	455	476	68
Edinburgh_tailings	-4088.69	39.54	0.87	8.86	0.42	22.67	0.54	9.36	7.10	3.45	1.09	0.59	4.58	0.81	408	353	77
Edinburgh_dump_2	-4088.69	41.85	0.92	9.36	0.40	21.25	0.49	8.58	6.23	3.29	0.96	0.69	4.79	1.04	387	407	56
Edinburgh_dump_1	-4088.69	41.70	0.83	9.22	0.45	20.10	0.52	8.44	6.25	3.05	0.81	0.84	6.37	1.17	390	375	50
Eshaness_DRT	-4088.69	39.18	0.84	8.22	0.55	21.58	0.56	9.25	6.36	3.08	0.84	0.64	7.18	1.61	357	331	93
Edinburgh_DRT	-4088.69	42.59	0.77	8.24	0.50	20.84	0.48	9.76	5.90	3.00	0.86	0.68	4.60	1.67	406	274	54
Edinburgh_offset	-4088.69	41.96	0.82	7.94	0.57	21.48	0.52	9.96	5.80	2.87	0.83	0.68	4.85	1.60	385	338	50
Assynt_Window_DRT	-4088.46	42.85	0.83	9.00	0.50	20.34	0.51	9.02	5.75	3.29	0.90	0.63	4.90	1.37	368	340	85
Glen_Feshie	-4088.46	40.98	0.90	8.82	0.46	20.53	0.51	8.71	6.34	3.15	0.89	0.76	6.49	1.33	345	329	32
All pediment cap rock	Average	41.22	0.87	8.68	0.46	20.27	0.47	9.01	6.36	2.97	0.75	0.78	6.86	1.14	443	404	72
(Gleann Beag, Ladder &	Median	41.70	0.87	8.78	0.46	20.34	0.51	9.05	6.37	3.02	0.84	0.76	6.27	1.09	406	407	60
Edinburgh intervals)	Min	37.24	0.75	7.47	0.30	16.77	0.19			2.30	0.39	0.59	3.18	0.76	298	274	32
-	Max	42.85	1.00	9.36	0.58	22.71	0.66	9.96	7.10	3.55	1.09	0.95	18.91	1.67	601	522	168
	Stdev	1.40	0.07	0.49	0.08	1.48	0.11	0.66	0.37	0.32	0.24	0.12	3.65	0.27	104	70	36
Ladder & Edingburgh	Average	41.48	0.84	8.77	0.49	20.92	0.54	9.07	6.34	3.16	0.92	0.70	5.43	1.20	370	394	62
intervals only	Median	41.78	0.83	8.84	0.50	20.69	0.52	9.04	6.30	3.12	0.92	0.69	5.19	1.11	377	364	58
•	Min	39.18	0.77	7.94	0.40	19.31				2.87		0.59	3.18	0.81	298	274	32
	Max	42.85	0.92	9.36	0.58	22.71				3.55		0.84	7.18	1.67	455	522	93
	Stdev	1.15	0.05	0.46	0.06	1.06				0.20		0.07	1.14	0.31	45	82	17
Gleann Beag interval only	Average	40.78	0.92	8.53	0.41	19.16				2.64		0.91	9.31	1.05	567	421	89
	Median	41.52	0.95	8.77	0.42	19.75				2.69		0.92	6.84	1.09	564	448	65
	Min	37.24	0.75	7.47	0.30	16.77				2.30		0.86	5.11	0.76	536	358	46
	Max	42.22	1.00	8.97	0.56	21.05				2.80		0.95	18.91		601	465	168
	Stdev	1.77	0.09	0.53	0.08	1.51				0.18		0.03		0.18	24	45	52
	3.00.	,,	5.05	0.55	5.00		0.10	5.55	J.2 F	5.15	0.0 .	5.55	5.15	0.10		.5	-

Figure	3.
--------	----

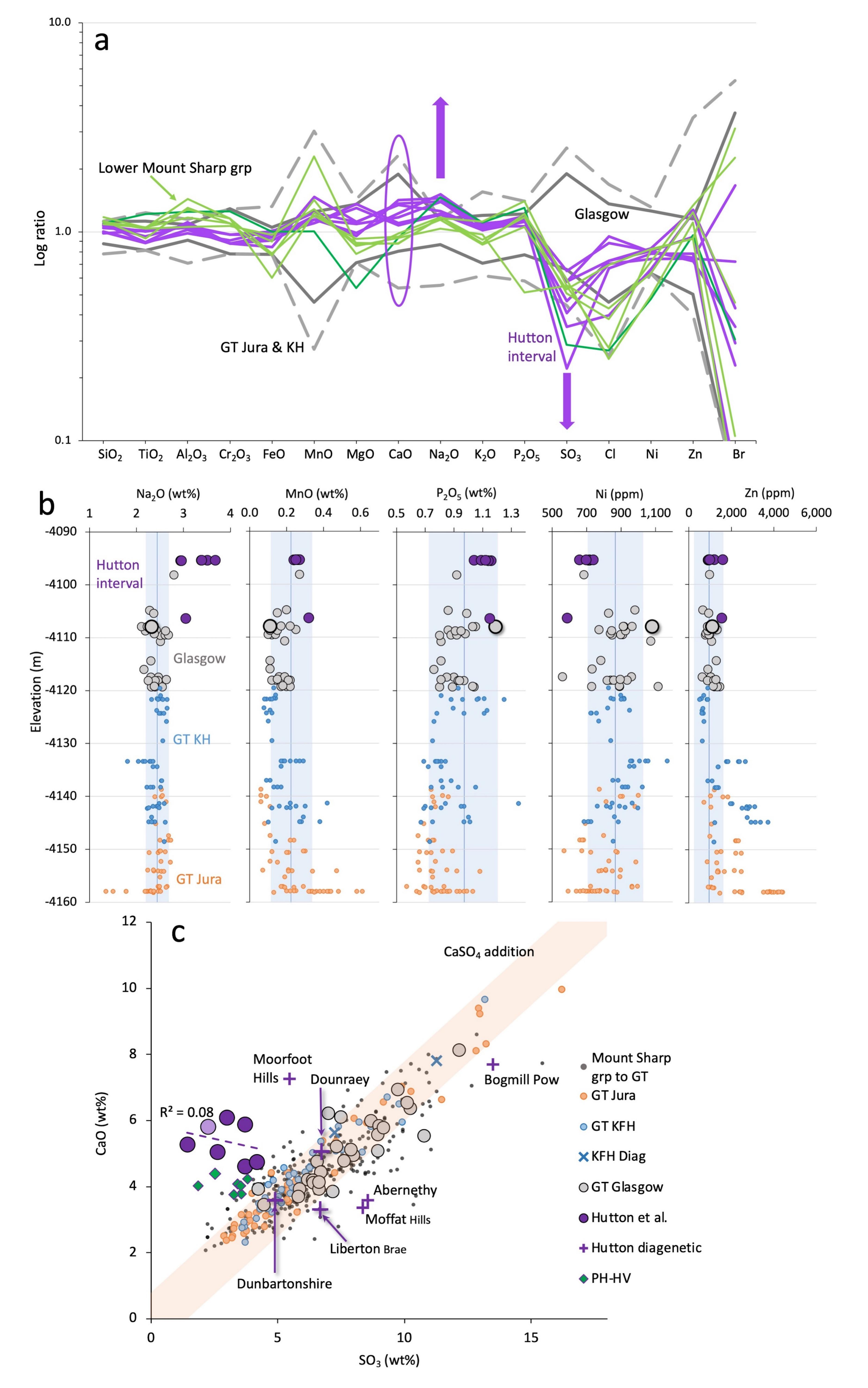


Figure 4	١.
----------	----

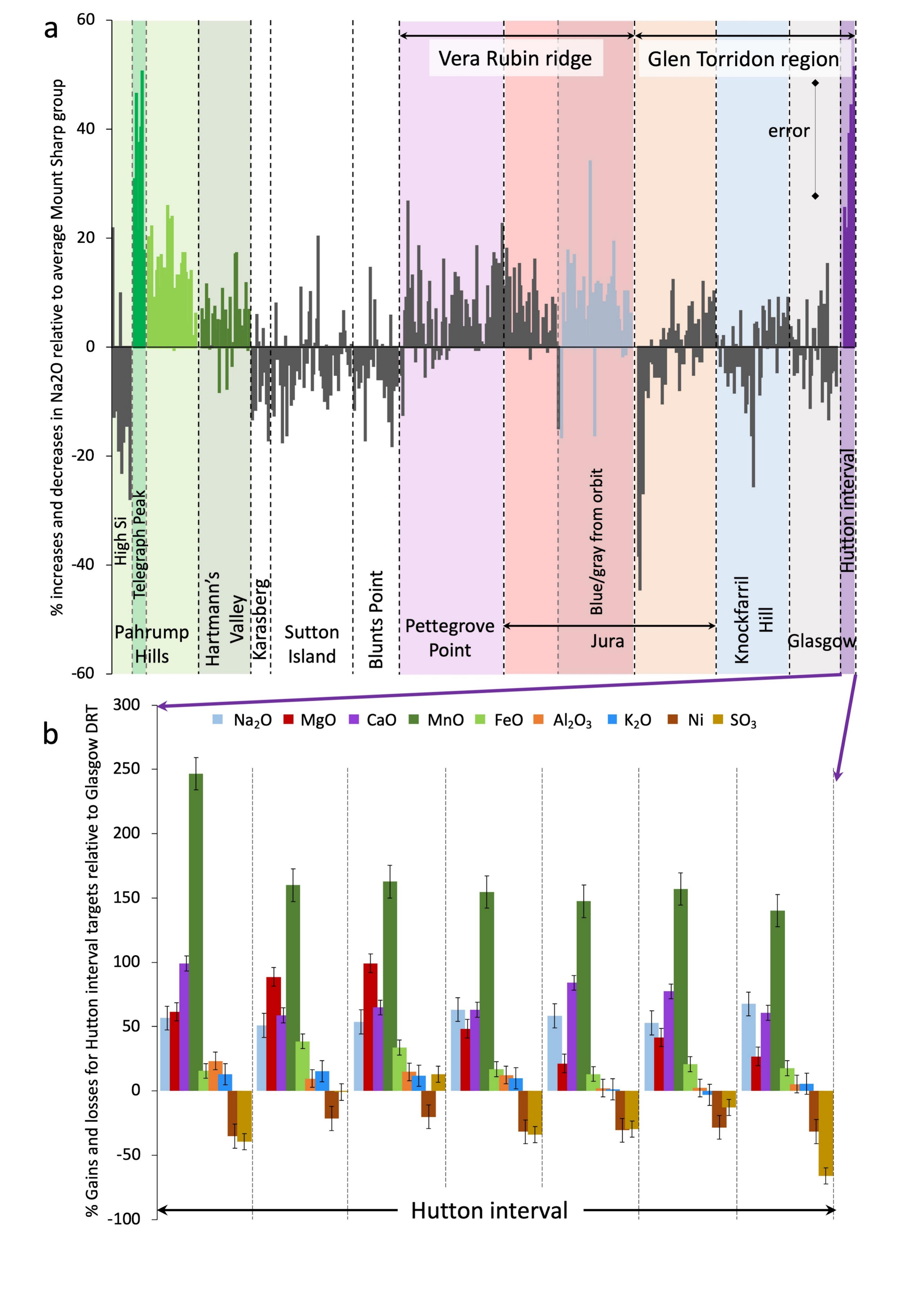


Figure 5.	
-----------	--

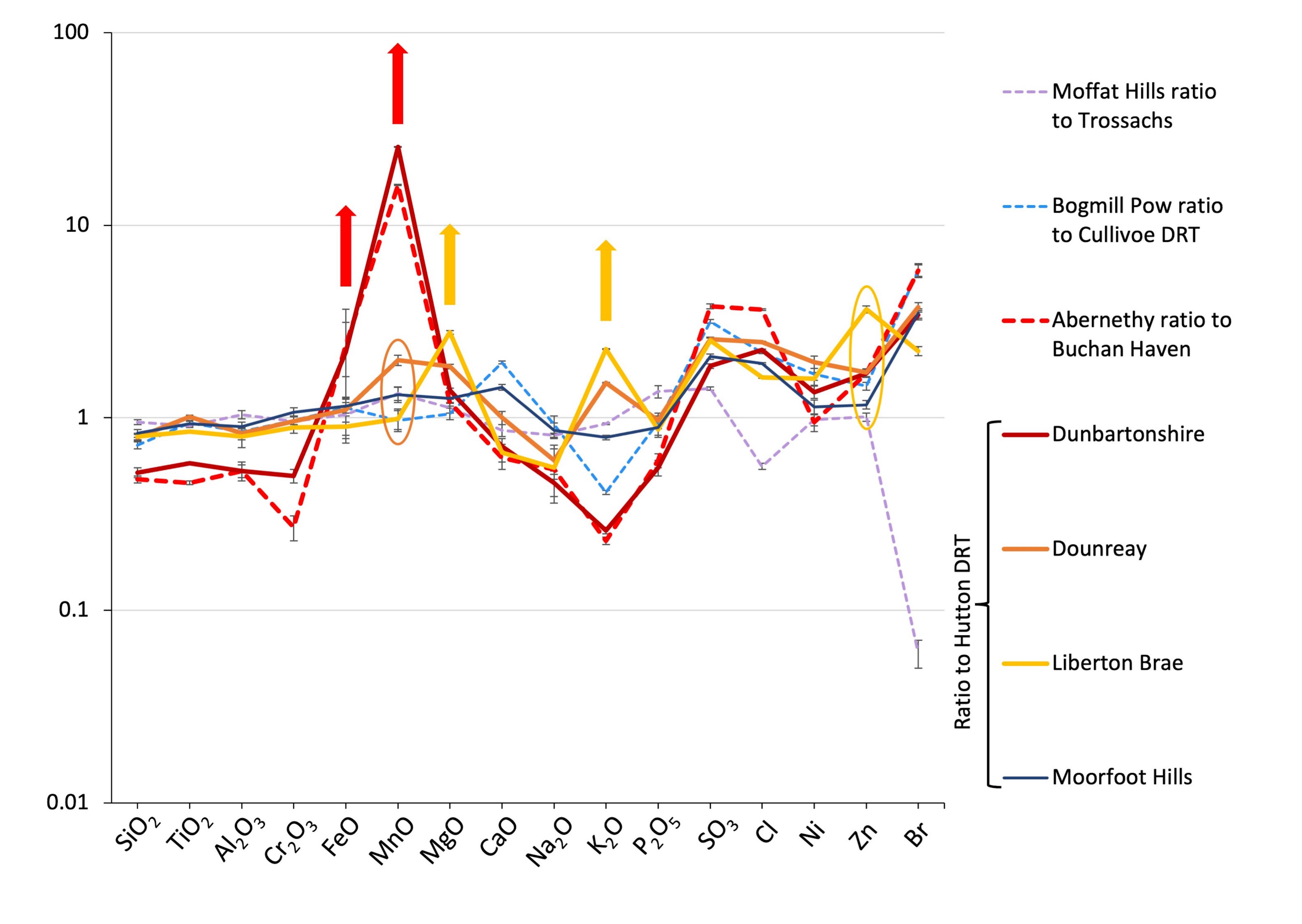


Figure 6	5.
----------	----

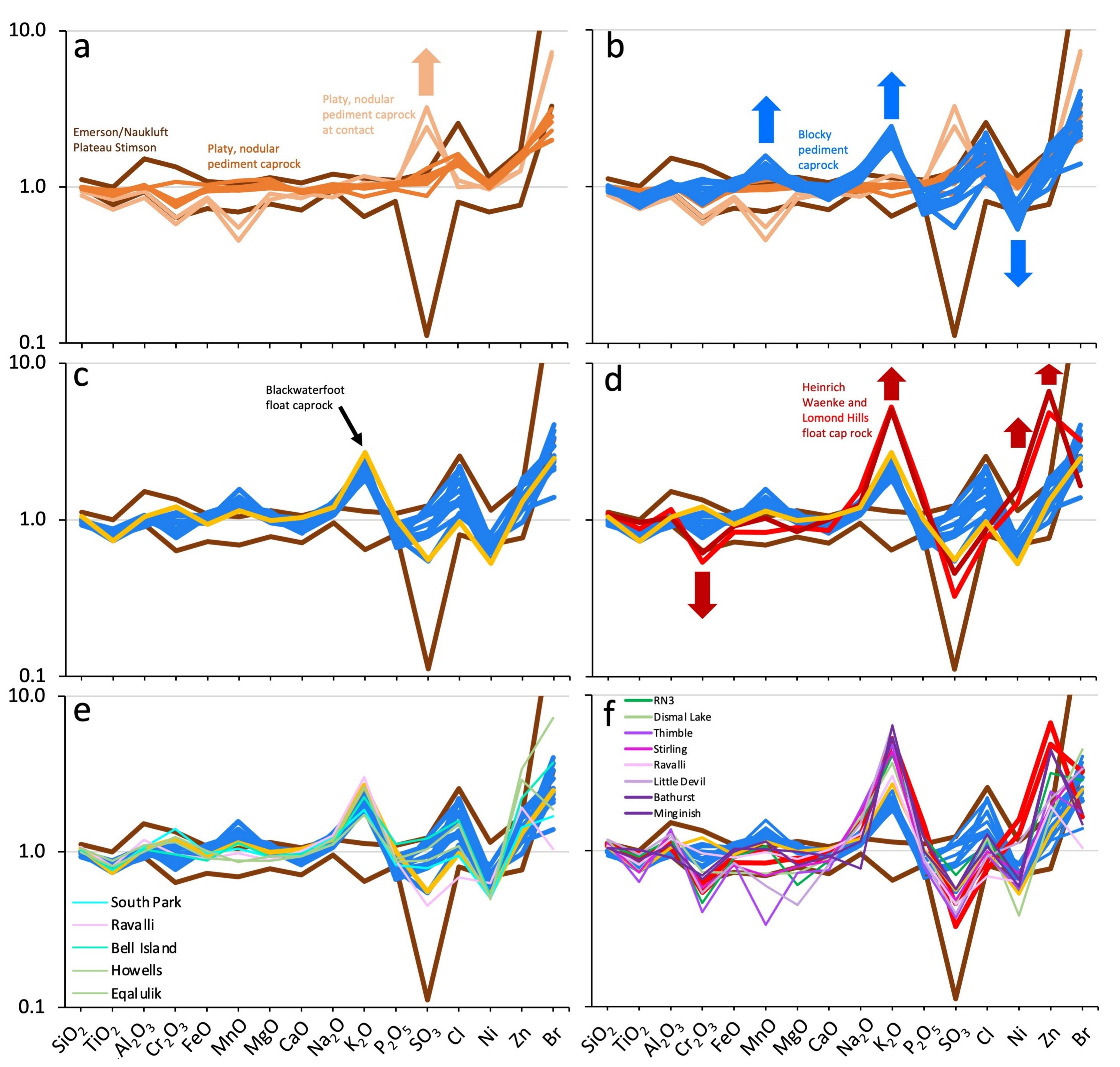


Figure 7.	
-----------	--

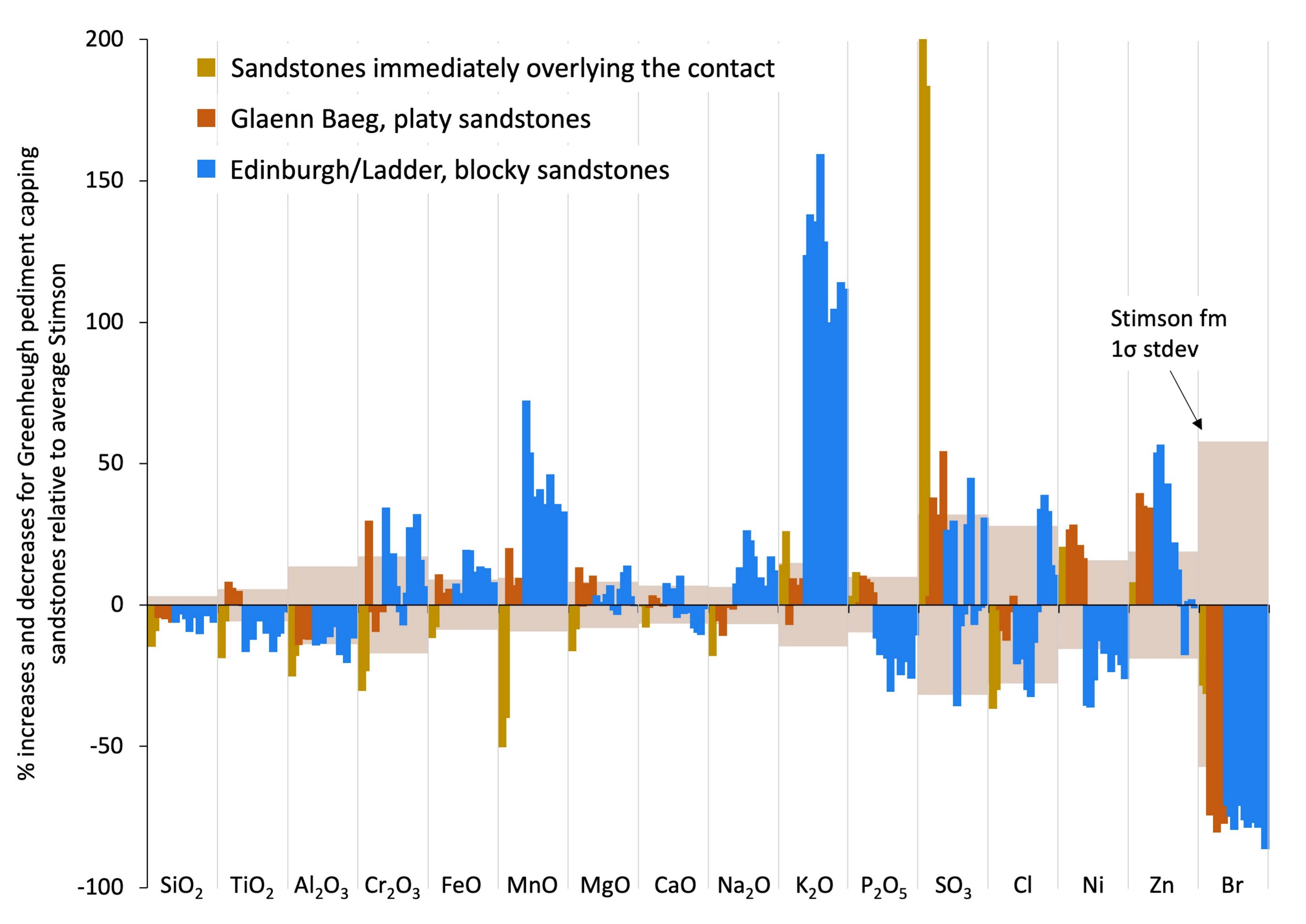


Figure 8.	
-----------	--

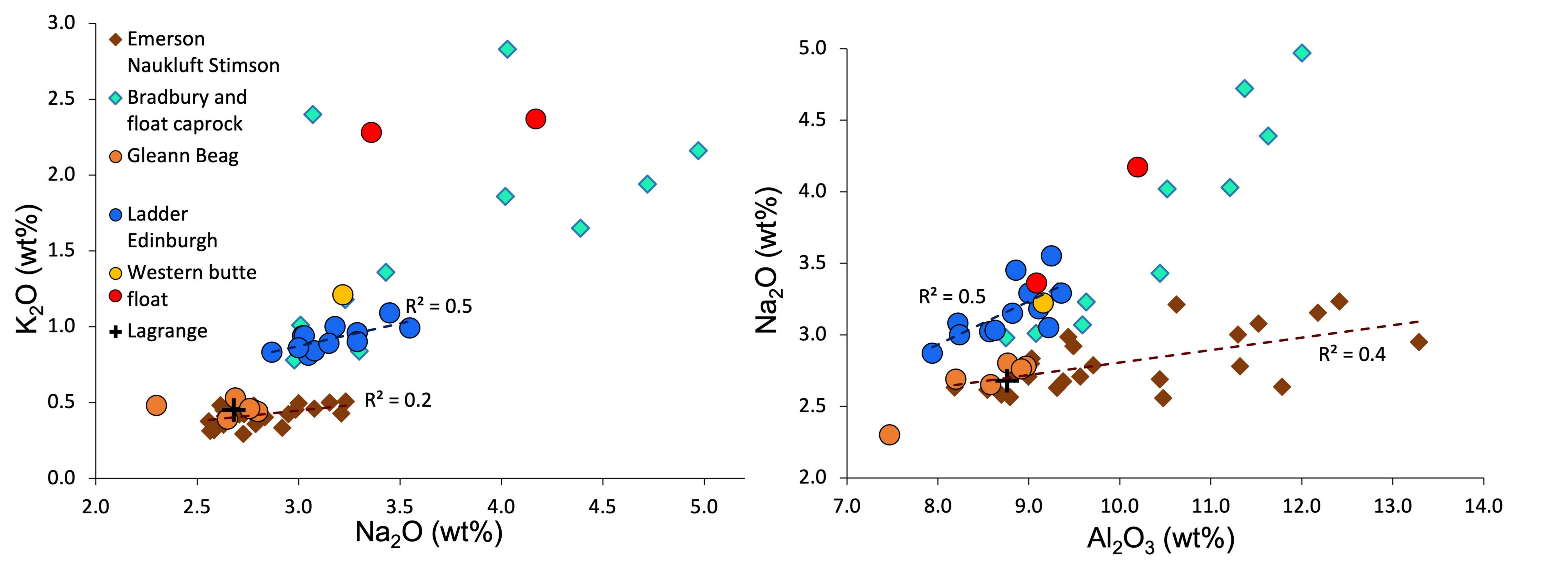


Figure 9.	
-----------	--

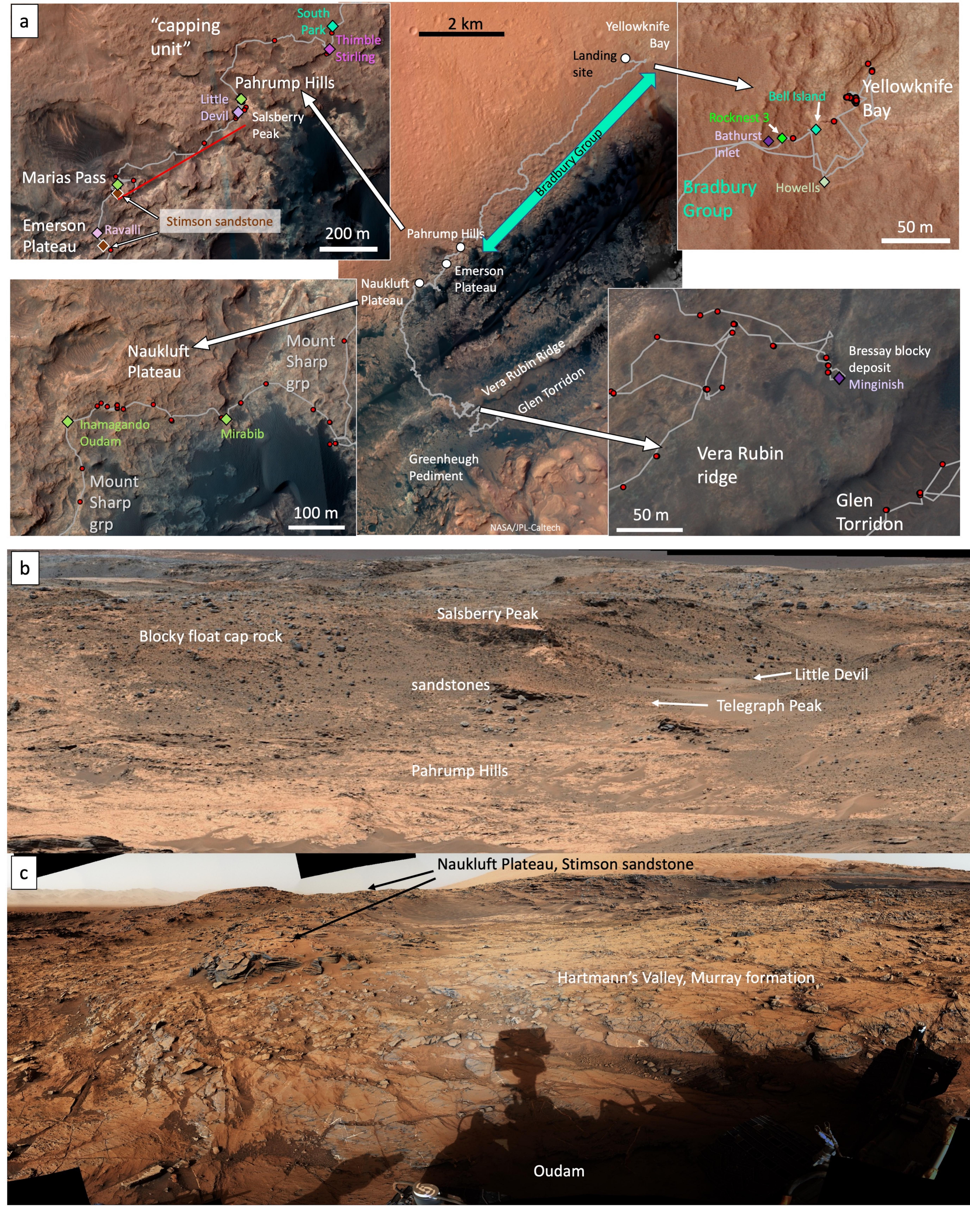
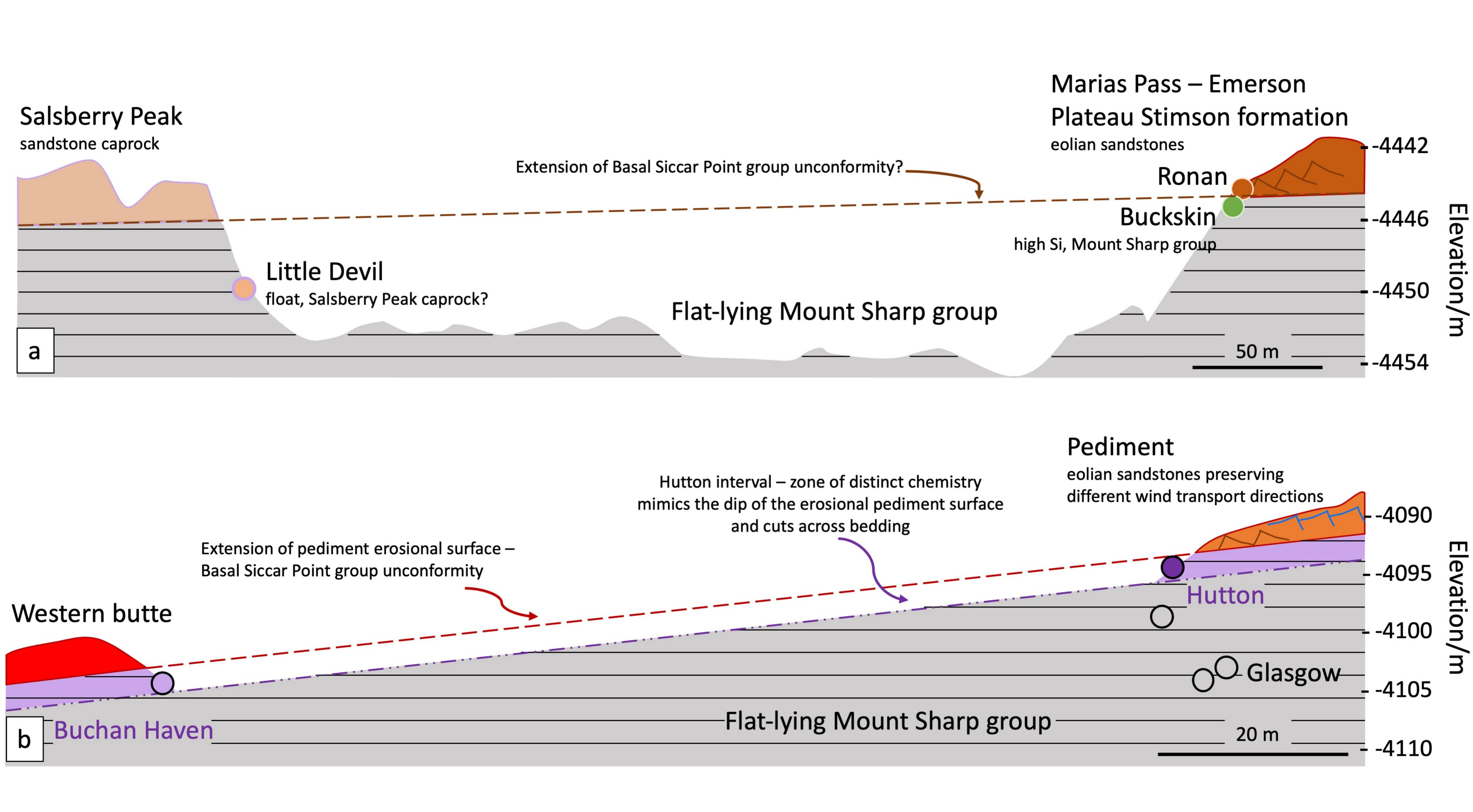


Figure	10.
--------	-----



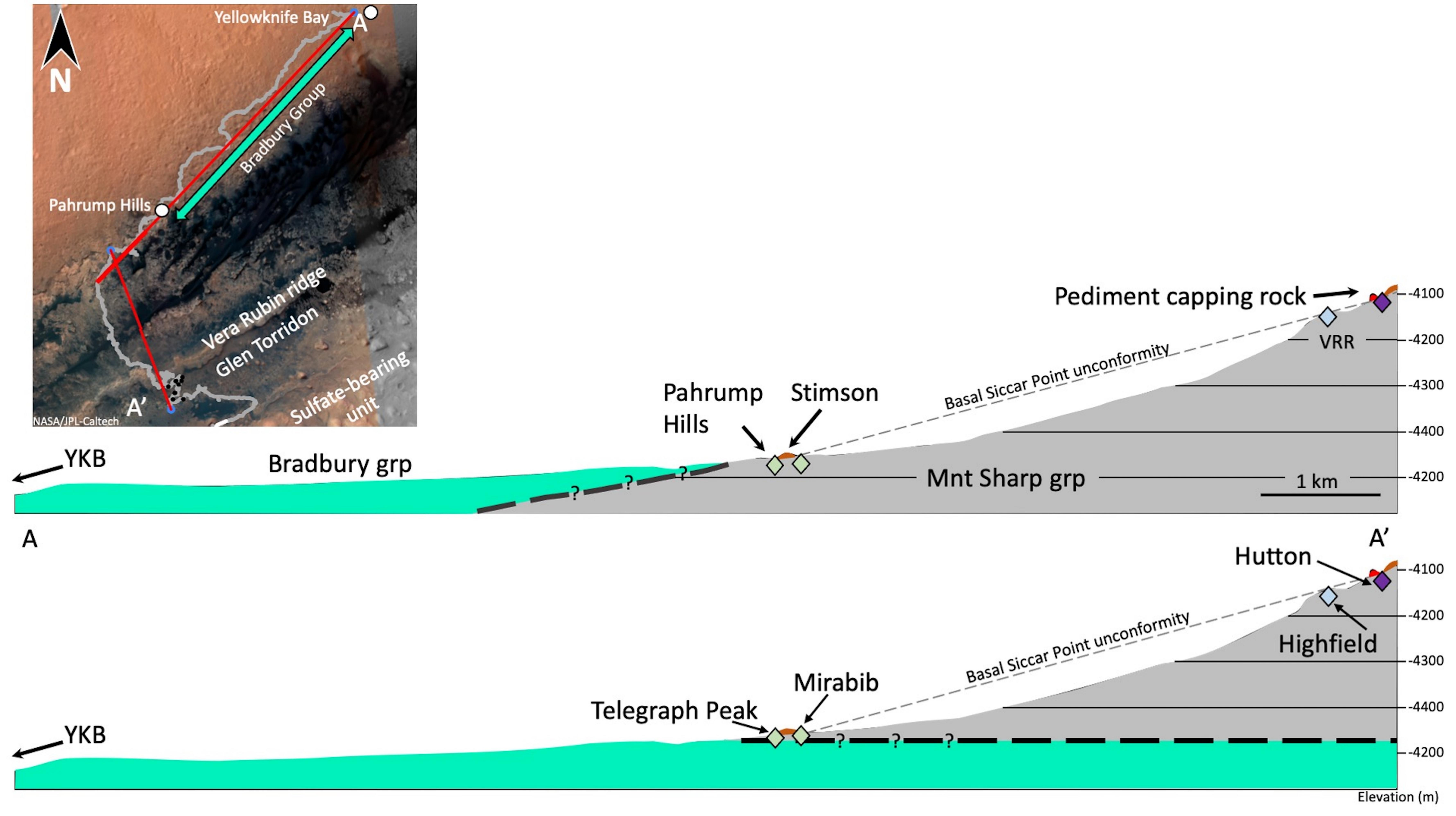


Figure	12.
--------	-----

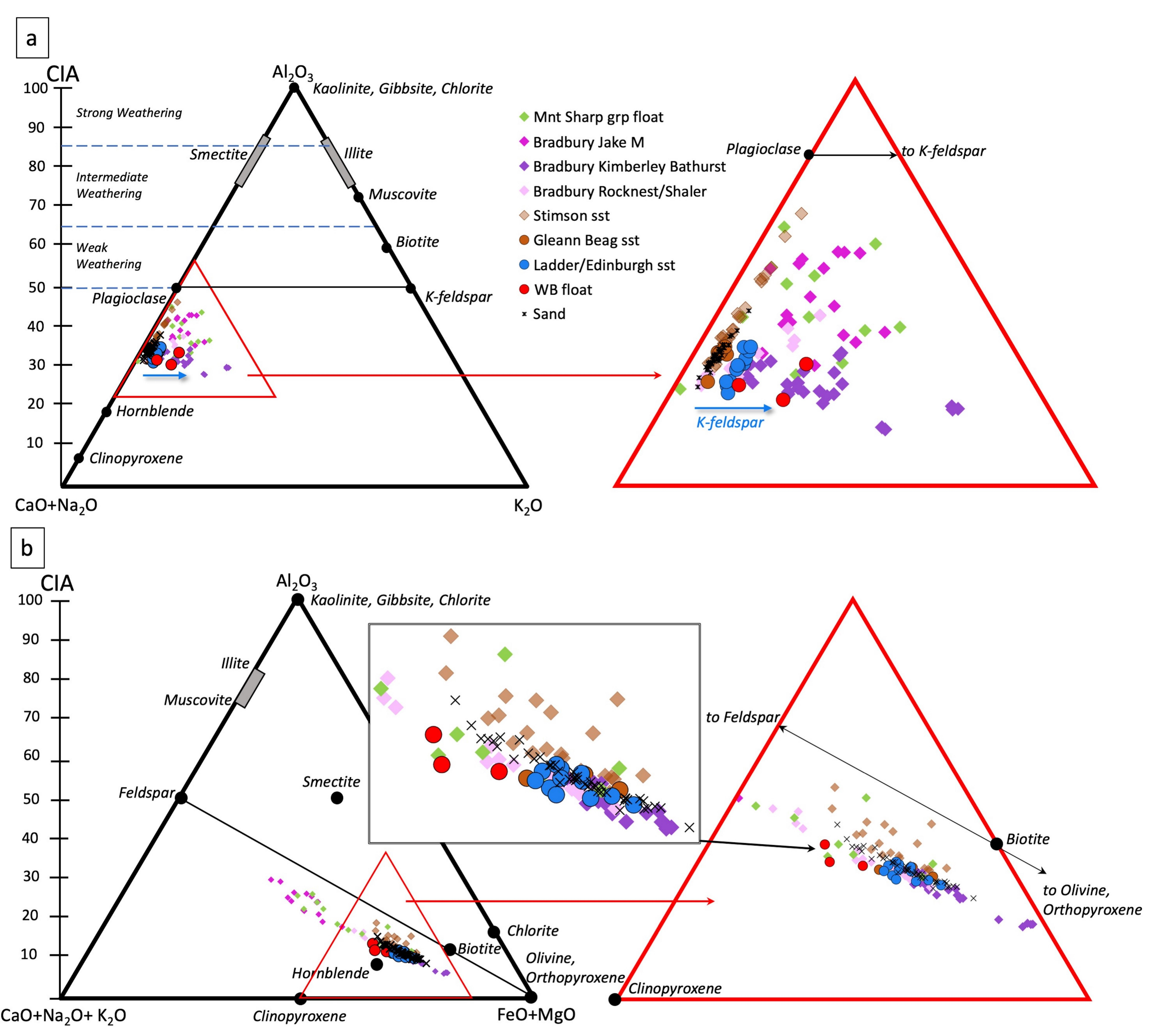


Figure	13.	
--------	-----	--

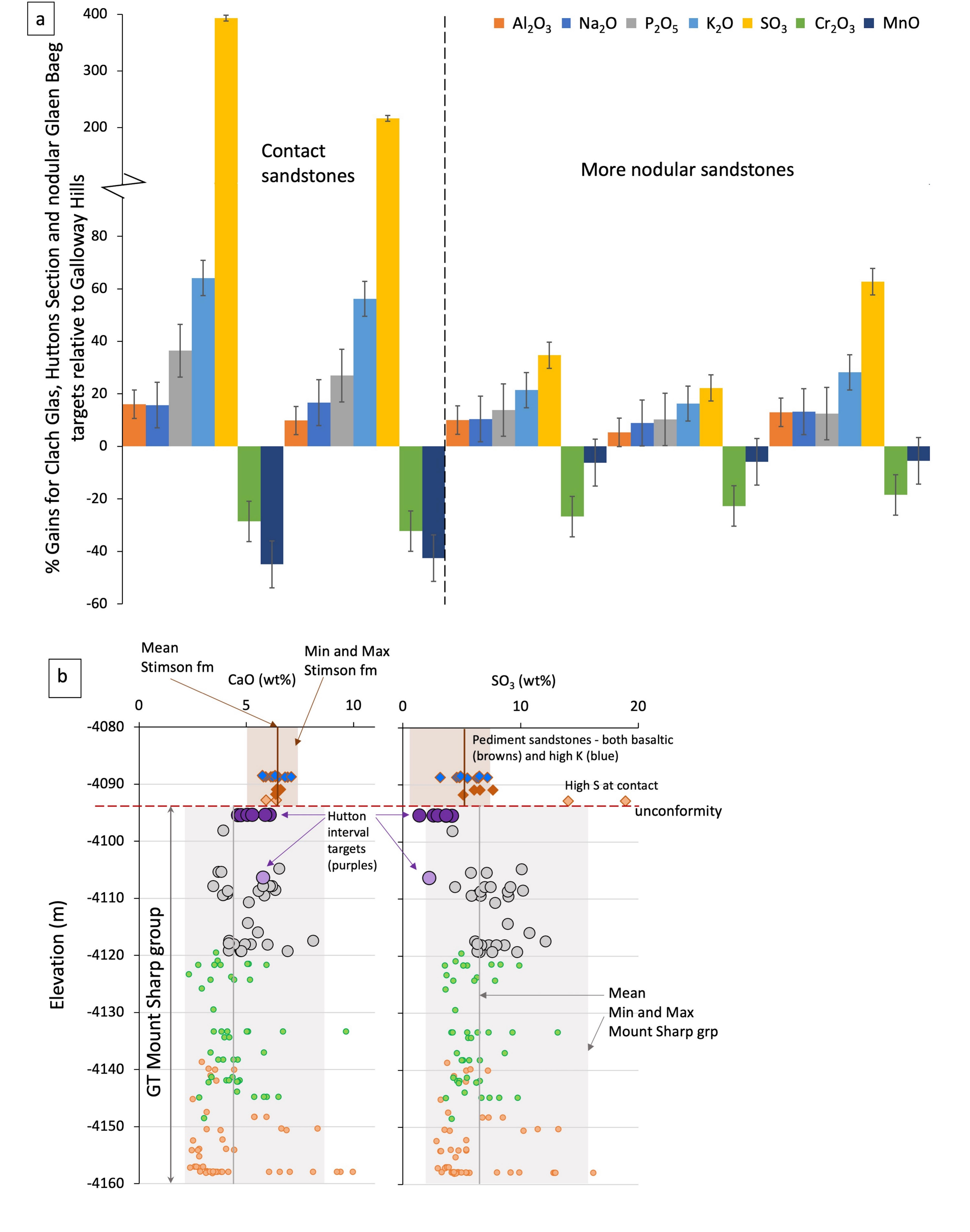
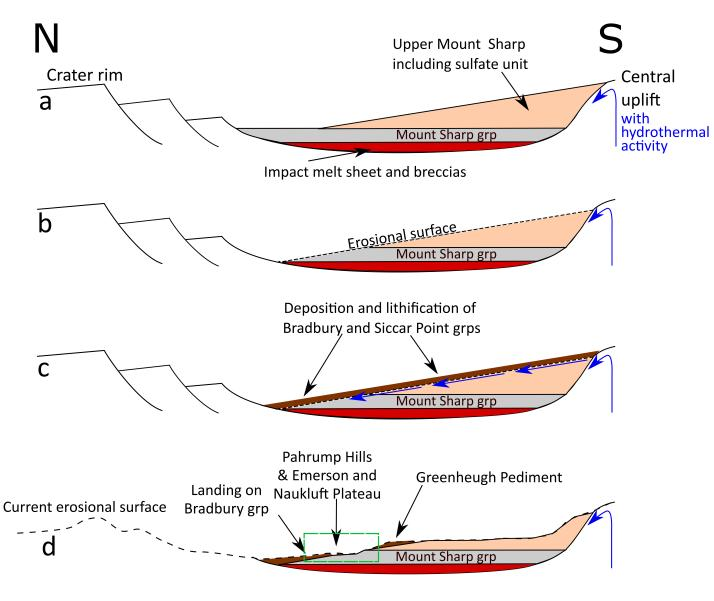


Figure	14.





#### [Journal of Geophysical Research, Planets]

#### Supporting Information for

# Alteration at the base of the Siccar Point unconformity and further evidence for an alkaline source rock at Gale crater: Exploration of the Mount Sharp group, Greenheugh pediment cap rock contact with APXS

L. M. Thompson<sup>1</sup>, J. G. Spray<sup>1</sup>, C. O'Connell-Cooper<sup>1</sup>, J. A. Berger<sup>2</sup>, A. Yen<sup>3</sup>, N. Boyd<sup>4</sup>, R. Gellert<sup>4</sup>, M. A. McCraig<sup>4</sup>, and S. J. VanBommel<sup>5</sup>

<sup>1</sup>Planetary and Space Science Centre, University of New Brunswick, Fredericton, Canada

<sup>2</sup>NASA Johnson Space Center, Houston, USA

<sup>3</sup>Jet Propulsion Laboratory, California Institute of Technology, Pasadena, USA

<sup>4</sup> Department of Physics, University of Guelph, Ontario, Canada

<sup>5</sup>Department of Earth and Planetary Sciences, Washington University in St. Louis, St. Louis, USA

Corresponding author: Lucy Thompson (<a href="mailto:lthompso@unb.ca">lthompso@unb.ca</a>)

#### Contents of this file

Sections S1 to S4 Figures S1 to S24 Tables S1 to S3

#### Introduction

This supporting information document comprises:

Section S1: Details of the data and targets used in this study including Table S1, which comprises a list of targets used.

Section S2: Details of APXS data treatment, including the different statistical methods used to investigate trends and relationships. Tables of the results of statistical tests are included. Other derived datasets used to make various plots can be found in the data repository.

Section S3: Mastcam and MAHLI images of relevant pediment campaign APXS targets

Section S4: Images of previously encountered APXS targets with related compositions to pediment campaign targets

#### S1. Details of targets and data used in this study

See Table 1 in the paper for the Glasgow member, Hutton interval, Western butte cap float rock and pediment capping sandstone APXS targets and compositions. Table S1 lists other targets utilized in this study.

All MSL, raw data are available at the planetary data system:

### https://pds-geosciences.wustl.edu/missions/msl/index.htm https://an.rsl.wustl.edu/msl/mslbrowser/an3.aspx

**Table S1**: Bedrock and soil targets used in this study (GT – Glen Torridon).

List of GT Jura bedrock targets	-	List of GT Knockfarril Hill bedrock target	S	List of Mount Sharp group targets related to Hutton interval				
Name Sol		Name	Sol	Name				
Kilmarie_drill_tailings_red	2404	Ecclefechan	2465	Ricardo_raster1_DRT	805			
Kilmarie_drill_tailings_pale	2404	Tay	2463	Topanga_DRT_raster2	815			
Kilmarie_dump_offset	2402	Feshie	2462	Mescal_DRT_raster1	820			
Kilmarie_dump_centre	2402	Sligachan	2461	Puente DRT	824			
Aberlady_drill_tailings_pale	2380	Newtonhill	2458	Pickhandle_DRT	828			
Aberlady_drill_tailings_red	2380	Magnus_Bay	2452	Telegraph_Peak_DT	922			
Aberlady dump corrected	2380	Stack_of_Glencoul	2446	Oudam_tailings_APXS	1364			
Mons Graupius	2427	Beauly_DRT	2443	Mirabib_DRT	1275			
Tobermory	2427	Balnakettle	2443	Inamagando_DRT	1355			
Rutherglen	2359	Calgary_Bay	2442	List of Emerson and Naufluft plateau Stimson bedrock targets				
Longannet	2365	Blawhorn	2587	Ronan DRT 2	998			
Kilmarie	2382	Perth	2454	Ledger	1092			
Kilmarie_offset	2382	Fetterangus	2478	Conniption	1097			
Seil	2377	Fetterangus_offset	2478	Big_Sky_DRT_raster2	1114			
Aberlady_DRT	2367	Solway_Firth_DRT	2471	Big_Sky_DRT_raster1	1114			
Aberlady offset	2367	Kirbuster	2465	Big Sky mini start hole	1116			
Aberlady_triage	2367	Oykel_DRT	2458	Big_Sky_full_drill_tailings	1123			
Arbuthnott_DRT	2349	Glen_Etive_2_DRT	2483	Big_Sky_presieve_dump (off target)	1124			
Fife	2347	Glen_Etive_1_tailings	2524	Big Sky presieve dump corrected	1126			
Auchterarder	2333	Glen_Etive_1_dump_centre	2523	Big_Sky_postsieve_dump	1132			
Alloa	2333	Glen_Etive_1_DRT	2482	Ennis	1151			
Ladder_Hills	2320	Glen_Etive_1_offset	2482	Ellis_Canyon	1150			
Curlew_DRT	2318	Glen_Etive_2_tailings	2553	Exshaw	1150			
Gannet	2318	Glen_Etive_2_dump_corrected	2552	Brukkaros DRT	1294			
Tolsta	2449	Moine	2474	Sesriem_Canyon_DRT	1288			
Hill_of_Skares	2431	Mither_Tap	2474	Sperrgebiet raster2	1277			
Crakaig	2422	East Shetland DRT	2472	Sperrgebiet_raster1	1277			
Kinghorn	2422	Essendy	2472	Okoruso_DRT_centre	1130			
Galashiels	2413	Nith	2472	Okoruso DRT offset	1130			
Haddington	2413	Urr	2441	Okoruso_fulldrill_tailings	1137			
Ardnamurchan	2363	lapetus	2437	Okoruso_rundriii_tanings Okoruso_presieve_dump	1137			
Ardmillan	2361	Ben_Hope	2570	Kwakwas_centre_DRT	1341			
Crieff	2352	South_Ronaldsay_DRT	2567	Kwakwas_centre_bki Kwakwas_offset	1341			
Snorre	2356	Shetland	2564	Groendraai	1351			
	2431	High_Plains	2557	Meob_DRT	1348			
Smoogro Paible	2451		2577	Nomeib	1348			
		Pobie_Bank			1348			
Gullane	2431	Nedd	2590	List of compositionally related targets to pediment caprocks				
Hillhead	2419	Gorgie	2587	South_Park_rp_apxs_twk	694			
Kintore	2419	Inverurie_DRT	2601	Bell_Island_target9_night	117			
Maud	2363	Latheron	2601	Howells	323			
St_Fergus	2304	Everbay_DRT	2597	Eqalulik	323			
Emerald_raster2	2315	Muckle_Flugga_DRT	2591	rocknest3_rp	102			
Broad_Cairn_DRT	2415	Ard_Neakie	2591	Dismal_Lakes	304			
Loch_Ness_DRT	2301	Glen_Doll	2591	Thimble_1	706			
Puddledub	2301	Flow_Country_centre	2594	Stirling_RP	707			
Linlithgow	2300	Ratio plot target		Ravalli	1082			
Broad_Cairn_offset	2415	Lagrange	605	Little_Devil	942			
Broad_Cairn_triage	2415			Bathurst_Inlet_Top_RP	54			
				Minginish	2019			

All raw APXS data used in this study, is available at the planetary data system: <a href="https://pds-geosciences.wustl.edu/msl/msl-m-apxs-4\_5-rdr-v1/mslapx\_1xxx/data/">https://pds-geosciences.wustl.edu/msl/msl-m-apxs-4\_5-rdr-v1/mslapx\_1xxx/data/</a> and <a href="http://doi.org/10.17189/1519440">http://doi.org/10.17189/1519440</a>

For details of the APXS targets used to investigate the Mount Sharp group, pre-Glen Torridon (not including high Si targets) see Thompson et al. (2020), and: *Thompson, L. (2020). Alpha Particle X-ray spectrometer geochemistry of the Murray formation and Vera Rubin ridge, Gale crater, Mars.* <a href="https://doi.org/10.25545/ZXDJZ7">https://doi.org/10.25545/ZXDJZ7</a>, UNB, V1, UNF:6:bL/a2qTZBu6DNJlzkmGAbg==[fileUNF].

All tables within the manuscript and supporting information, as well as derived data can be found at: *Thompson, L. (2021). Alpha Particle X-ray spectrometer geochemistry of rocks associated with the Basal Siccar Point group unconformity, Glen Torridon region, Gale crater, Mars.* Doi to be supplied upon final submission

#### S2. Treatment of the data

#### S2.1. Average, median, minimum, maximum and $1\sigma$ standard deviation

Average, median, minimum, maximum and  $1\sigma$  standard deviation values were calculated for different subsets of the data using Excel. See Table 1 in the manuscript for the results of these calculations. See repository for the derived datasets. The results of these calculations are represented in various plots, all created in Excel.

#### S2.2. F- and t-tests

F-tests were performed on select groupings of analyses to determine whether they showed equal or unequal variances using the "F-Test Two-Sample for Variances" analysis tool within the Data Analysis add-in for Excel, with a 95% confidence. If F>F critical one-tail, the two groupings have unequal variances. If F<F critical one-tail, the two groupings have equal variances.

Based on the results of the F-tests, t-tests were then performed on the same datasets to determine whether they are statistically the same or different. The "t-Test: Two Sample Assuming Unequal Variances" or "t-Test: Two Sample Assuming Equal Variances" analysis tool within the Data Analysis add-in for Excel was used. The t-tests determine whether the two groupings are statistically the same or different, with a 95% confidence level. If t stat>t critical two-tail, the two groupings are statistically different. If t stat<t critical two-tail, the two groupings are statistically the same.

F- and t-tests were performed on the following datasets for Si through Zn (Br is not included as it is highly variable throughout all datasets and appears to be primarily controlled by surface processes):

- Comparison of Hutton interval targets with i) Mount Sharp group bedrock pre-Glen Torridon (GT), ii) GT Jura and Knockfarril Hill (KH) member bedrock targets (see Table S1 for the list of APXS targets), and iii) Glasgow member bedrock targets. See Table S2 for the results.
- 2) Comparison of Emerson and Naukluft plateau Stimson formation sandstones with i) basal pediment capping sandstones (platy; Gleann Beag interval), and ii) blocky pediment capping sandstones (Ladder and Edinburgh intervals). See Table S3 for the results.

#### S2.3. Log ratio plots

#### S2.3.1 Hutton interval

To examine the Hutton interval, log ratio plots were made in Excel by ratioing the data of interest to average Mount Sharp group bedrock encountered prior to Glen Torridon. The log ratioed maximum and minimum values derived for the Glen Torridon Jura and Knockfarril Hill members combined, and the Glen Torridon Glasgow member are plotted to show the range of compositions for those data subsets. Individual Hutton interval analyses and select Murray formation targets encountered earlier in the mission are plotted separately. See Figure 3a for the plot and the data repository for the derived data.

#### S2.3.1.1 Hutton interval diagenetic features

To investigate changes in chemistry associated with diagenetic features in the Glasgow member as Curiosity approached the pediment, log ratio plots were created in Excel whereby the target of interest is ratioed to a bedrock target in the same workspace (Figure 5). Derived data used for the plot can be found in the repository.

**Table S2**: Results of F- and t-tests for the Hutton interval comparisons (GT – Glen Torridon)

	Murray pre-GT vs Hutton interval GT Jura and KH vs						vs Hutton in	terval Glasgow vs Hutton interval										
	F-tests			t-tests	ests F-tests			-tests t-tests					F-tests			t-tests		
	F	F critic	al one tail	t Stat	t Critic	cal two tail	F F critical one tail		t Stat	t Critic	cal two tail	F F critical one tail		t Stat t Critical two tai		cal two tail		
SiO2	2.29	3.68	equal	-0.67	1.97	same	2.78	3.71	equal	-1.90	1.98	same	2.11	4.50	equal	-1.25	2.03	same
TiO2	1.62	3.68	equal	1.22	1.97	same	1.08	2.19	equal	4.68	1.98	different	1.07	4.50	equal	1.28	2.03	same
Al2O3	7.26	3.68	unequal	-0.10	2.31	same	2.97	3.71	equal	-2.28	1.98	different	1.85	4.50	equal	-2.21	2.03	different
Cr2O3	6.77	3.68	unequal	5.18	2.31	different	4.20	3.71	unequal	7.48	2.23	different	7.00	4.50	unequal	1.99	2.09	same
FeO	5.43	3.68	unequal	-0.68	2.31	same	2.07	3.71	equal	2.23	1.98	different	2.49	4.50	equal	-1.94	2.03	same
MnO	11.88	3.68	unequal	-3.62	2.23	different	24.37	3.71	unequal	-1.48	2.03	same	15.70	4.50	unequal	-7.65	2.05	different
MgO	1.35	3.68	equal	-2.21	1.97	different	1.22	3.71	equal	-0.79	1.98	same	1.35	4.50	equal	-1.3	2.03	same
CaO	4.10	3.68	unequal	-4.16	2.36	different	8.46	3.71	unequal	-3.51	2.13	different	3.58	4.50	equal	-0.43	2.03	same
Na2O	1.43	2.13	equal	-7.77	1.97	different	1.68	2.19	equal	-9.88	1.98	different	3.28	2.56	equal	-6.85	2.45	different
К2О	25.75	3.68	unequal	-2.56	2.13	different	64.37	3.71	unequal	1.15	1.99	same	15.60	4.50	unequal	-3.45	2.05	different
P2O5	34.72	3.68	unequal	-7.73	2.09	different	12.60	3.71	unequal	-12.90	2.09	different	5.20	4.50	unequal	-9.38	2.15	different
SO3	4.98	3.68	unequal	8.88	2.36	different	7.83	3.71	unequal	6.93	2.14	different	3.48	4.50	equal	5.81	2.03	different
Cl	5.72	3.68	unequal	3.41	2.31	different	3.04	3.71	equal	2.74	1.98	different	3.57	4.50	equal	1.21	2.03	same
Ni	13.09	3.68	unequal	8.10	2.23	different	4.90	3.71	unequal	6.35	2.20	different	18.64	4.50	unequal	5.57	2.05	different
Zn	2.19	3.68	equal	0.08	1.97	same	12.65	3.71	unequal	5.11	2.09	different	1.73	2.56	equal	-0.65	2.03	same

**Table S3**: Results of F- and t-tests for the Emerson and Naukluft plateau Stimson formation sandstones and pediment capping sandstones

							I					
	F-tests Stimson-Gleann Beag			t-tests Stimson-Gleann Beag			F-tests Stimson-Edinburgh/Ladder			t-tests Stimson-Edinburgh/Ladder		
	F	F critical	one tail	t Stat	t Critical	two tail	F	F critical one tail		t Stat	t Critical two tail	
SiO2	1.75	4.53	equal	5.19	2.04	different	1.04	2.74	equal	5.41	2.03	different
TiO2	1.02	4.53	equal	0.15	2.04	same	1.25	2.74	equal	4.81	2.03	different
Al2O3	35.35	4.53	unequal	4.34	2.05	different	8.95	2.74	unequal	4.05	2.03	different
Cr2O3	2.20	2.62	equal	0.82	2.04	same	1.04	2.25	equal	-2.5	2.03	different
FeO	1.49	4.53	equal	-0.25	2.04	same	1.7	2.74	equal	-3.88	2.03	different
MnO	5.46	2.62	unequal	0.63	2.45	same	1.23	2.74	equal	-11.11	2.03	different
MgO	1.17	4.53	equal	-0.44	2.04	same	2.56	2.74	equal	-1.39	2.03	same
CaO	3.80	4.53	equal	0.17	2.04	same	1.5	2.74	equal	0.54	2.03	same
Na2O	3.30	4.53	equal	1.99	2.04	same	1	2.74	equal	-5.11	2.03	different
K2O	1.99	4.53	equal	-1.52	2.04	same	1.82	2.25	equal	-20.78	2.03	different
P2O5	5.70	4.53	unequal	-2.8	2.06	same	1.32	2.74	equal	5.58	2.03	different
SO3	4.05	2.62	unequal	-2.21	2.45	same	1.9	2.74	equal	-0.92	2.03	same
CI	6.29	4.53	unequal	1.59	2.09	same	1.29	2.74	equal	0.03	2.03	same
Ni	6.63	4.53	unequal	-6.3	2.09	different	2.58	2.74	equal	4.59	2.03	different
Zn	2.52	4.53	equal	-3.42	2.04	different	1.54	2.25	equal	-2.5	2.03	different

#### 2.3.2 Pediment cap rocks

To examine the pediment capping sandstones, log ratio plots were made by ratioing the data of interest to Lagrange (typical Gale soil analyzed by APXS on Sol 605) in Excel. The Lagrange, Gale soil target was chosen as the ratio plot comparison owing to the Mars soil-like composition of typical Stimson formation sandstones from the Emerson and Naukluft plateaus (Thompson et al., 2016). The ratioed maximum and minimum values derived for the Stimson formation sandstones encountered at the Emerson and Naukluft plateaus are plotted to illustrate the Stimson formation range of compositions. Individual pediment capping sandstone, Western butte float caprock and select targets encountered earlier in the mission are plotted separately. See Figure 6 for the plots and the data repository for the derived data used to construct the plots.

#### S2.4. Elevation versus composition

Select oxide and element concentrations are plotted versus elevation to highlight changes in the Glasgow member, Hutton interval as Curiosity neared the pediment contact (Figure 3b). Average and  $1\sigma$  standard deviation for the Mount Sharp group pre-GT (Table 1) are shown for reference.

CaO and SO $_3$  concentrations versus elevation are plotted for the GT Mount Sharp group and Greenheugh pediment capping sandstones (Figure 12b). These plots highlight changes in Ca and S immediately below and above the Basal Siccar Point group unconformity at the pediment. Average and  $1\sigma$  standard deviation for the Mount Sharp group pre-GT and Emerson/Naukluft Stimson formation (Table 1) are shown for reference.

#### S2.5. X-Y plots

CaO versus SO<sub>3</sub> concentrations are plotted for all Mount Sharp group bedrock pre-GT, GT Jura, GT Knockfarril Hill, and GT Glasgow with the Hutton interval and select Parhump Hills and Hartmanns Valley targets highlighted (Figure 3c). A CaSO<sub>4</sub> addition trend line is also shown. See Thompson et al., 2020 Section S2 for a discussion regarding CaSO4 and the Murray formation.

Na<sub>2</sub>O versus TiO<sub>2</sub> concentrations are plotted for all Mount Sharp group bedrock pre-GT (with Pahrump Hills and gray/blue VRR Jura plotted separately), GT Jura and Knockfarril Hill, GT Glasgow and Hutton interval (Figure S1).

#### S2.6. %Increase and decrease calculations

Investigation of %increases and decreases for specific subsets of the data were computed using the following equation:

$$\%\Delta C = [(CI_x - CC_x)/CC_x]*100$$

*CI* and *CC* are concentrations of the oxide of interest (*x*) and titanium (Ti) for the targets of interest and the comparison target respectively. Various plots were made using the derived data in Excel. See the data repository for the derived data used to make plots.

%increases and decreases in  $Na_2O$  concentration were calculated for all members of the Mount Sharp Group relative to average pre-GT, Mount Sharp group  $Na_2O$  and plotted in Figure 4a. This plot highlights which Mount Sharp group strata have the highest  $Na_2O$  concentrations relative to the average.

%increases and decreases were calculated for the Gleann Beag, Ladder and Edinburgh interval sandstones relative to average Stimson formation from the Naukluft and Emerson plateaus (Figure 7).

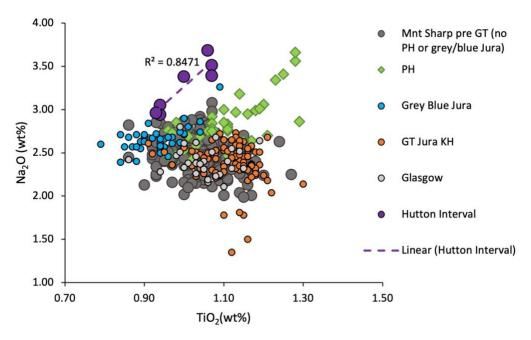


**Figure S1**.  $Na_2O$  versus  $TiO_2$  for all Mount Sharp group bedrock pre-GT (with Pahrump Hills and gray/blue VRR Jura plotted separately), GT Jura and Knockfarril Hill, GT Glasgow with the Hutton interval. Note the strong positive correlation for the Hutton interval and a number of Pahrump Hills targets.

#### S2.7. Mass balance calculations

Mass balance calculations were performed using the following equation (Brimhall & Dietrich, 1987):

$$%\Delta C = [(CI_x * CC_{Ti})/(CC_x * CI_{Ti})-1]*100$$

CI and CC are concentrations of the oxide of interest (x) and titanium (Ti) for the targets of interest and the comparison target respectively. See Thompson et al. (2020) for a discussion of the use of Ti as the conservative oxide. Calculations were made to look at gains and losses associated with the potential alteration of the Hutton interval targets versus the Glasgow DRT target, and the Gleann Beag high S, pediment capping sandstones versus Galloway Hills.

The Hutton interval targets are compared to the Glasgow DRT target, as this represents typical Glasgow member bedrock and was also a drill target (Figure 4b). The high S, capping sandstone targets exposed at the contact with the underlying Glasgow member, as well as the more nodular sandstones within the Gleann Baeg interval are compared to the relatively nodule-free Galloway Hills target, which represents the least altered Gleann Baeg interval sandstone (Figure 12a).

See the data repository for the derived data used to make plots.

#### S2.8. Errors for mass balance and %increase and decrease plots

Propagated errors for the mass balance plots and %increase and decrease plots are calculated using the general equation:

$$\frac{\delta Q}{|Q|} = \sqrt{\left(\frac{\delta a}{a}\right)^2 + \left(\frac{\delta b}{b}\right)^2} + \cdots$$

Where  $\frac{\delta Q}{|Q|}$  is the propagated error,  $\delta a$  = error associated with the concentration of the element of interest, a = first concentration,  $\delta b$  = error associated with the second concentration, b = second concentration.

## **S3.** Images of relevant pediment campaign APXS targets (Image credit for Mastcam and MAHLI images: NASA/Caltech-JPL/MSSS)

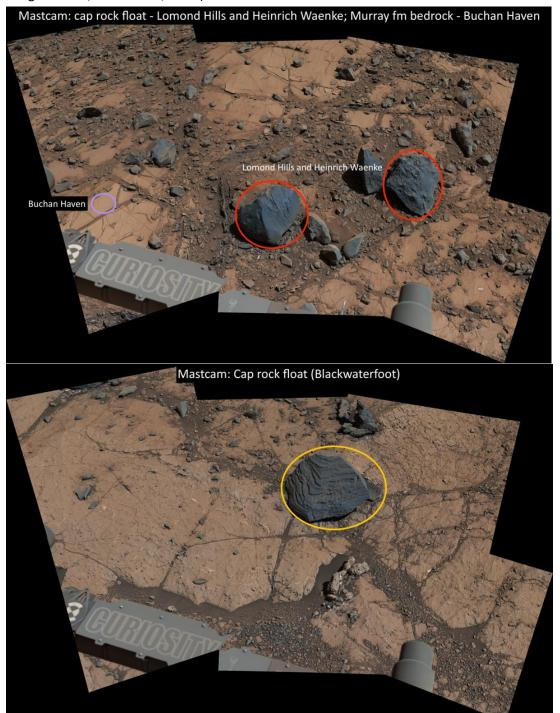


**Figure S2.** Mastcam workspace mosaics from Western butte showing: **top** - the Hutton interval bedrock target, Buchan Haven, and the two float caprock targets Lomond Hills and Heinrich Waenke (Sol 2633, mcam013793); **bottom** – the Blackwaterfoot float caprock (Sol 2618, mcam013759)

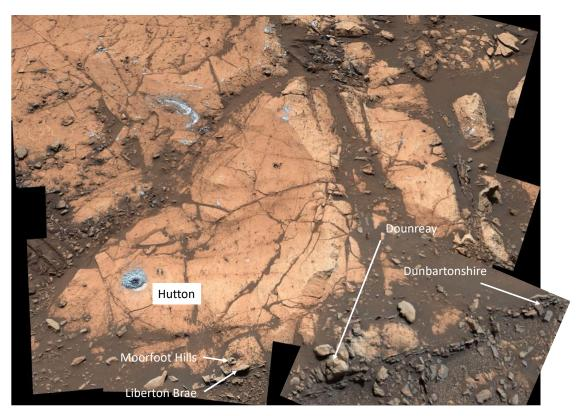


**Figure S3**. Mastcam mosaics (Sol 2680, mcam014031; Sol 2666, mcam013985) of the Hutton drill site workspace, including the diagenetic targets; Moorfoot Hills, Liberton Brae, Dounreay and Dunbartonshire.

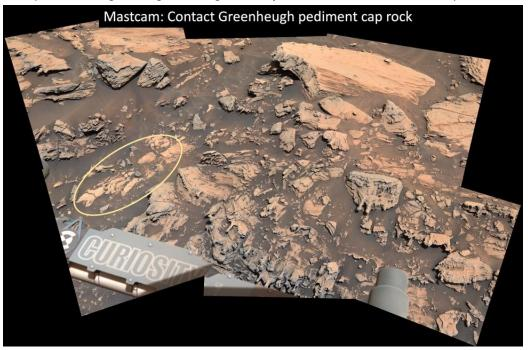


**Figure S4.** Mastcam workspace mosaic (Sol 2693, mcam014090) showing the location of the Gleann Beag interval, high S, APXS targets (Clach Glas and Huttons Section).



**Figure S5**. Mastcam workspace mosaic (Sol 2695, mcam014100) of the Galloway Hills, Gleann Beag interval sandstone target.

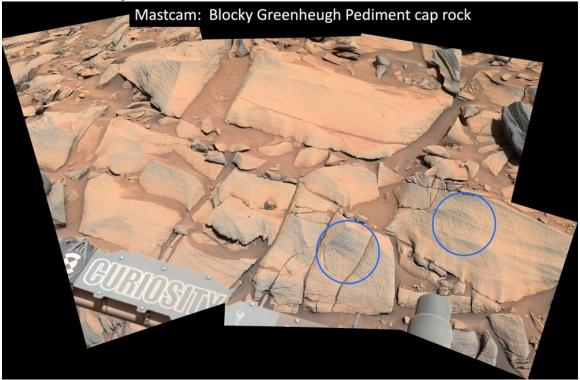


**Figure S6**. Mastcam workspace mosaic (Sol 2698, mcam014122) of the Ladder interval sandstone targets Forsinard Flows (right) and Machir Bay (left).

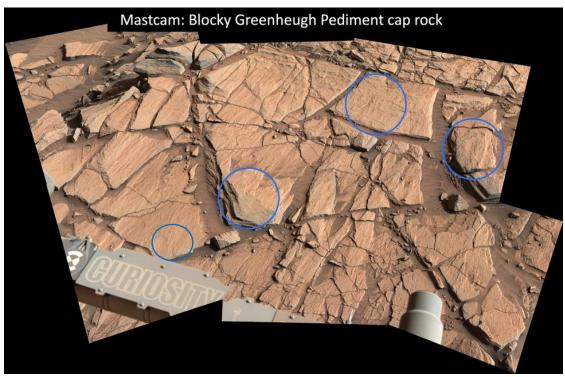


**Figure S7**. Mastcam workspace mosaic Sol 2700, mcam014136 of the Ladder interval sandstone targets Glen Feshie (left), Assynt Window (middle), Edinburgh (top), and Eshaness (right).



**Figure S8**.  $\sim$ 5 cm standoff MAHLI images of the Hutton interval targets Buchan Haven (Western butte – left) and Hutton (right) after DRT

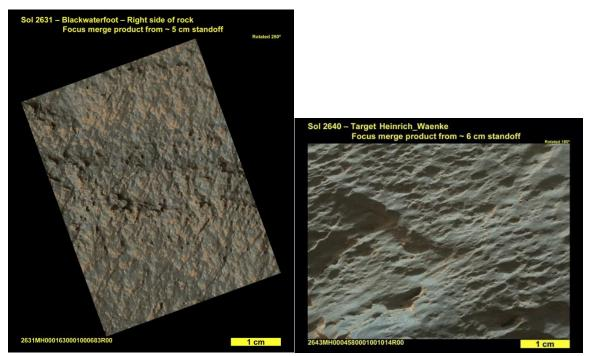


**Figure S9**. ~5-6 cm standoff MAHLI images of Western butte float cap rock targets Blackwaterfoot (left) and Heinrich Waenke (right).



**Figure S10**. ~5-6 cm standoff MAHLI images of diagenetic features within upper Glasgow member bedrock; Abernethy (Western butte, Buchan Haven workspace, left), Moffat Hills (Trossachs workspace, middle), Bogmill Pow (Cullivoe workspace).

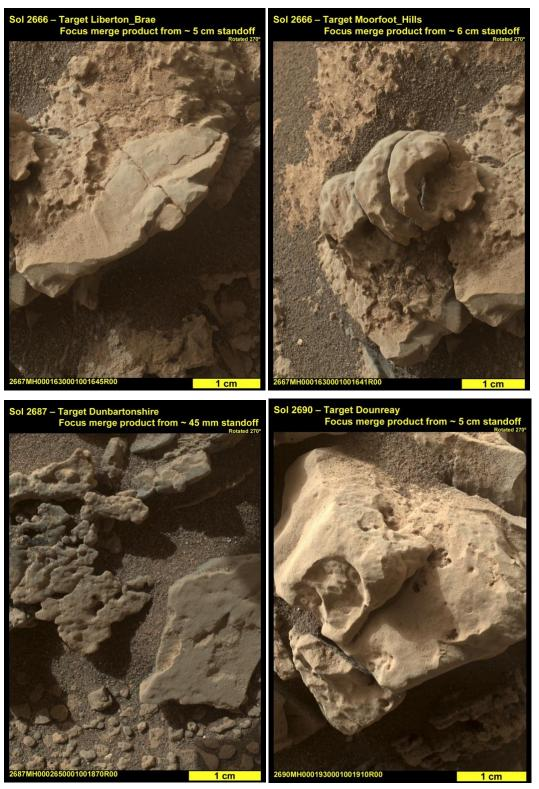


**Figure S11**. ~4.5-6 cm standoff MAHLI images of diagenetic features within Hutton workspace; Liberton Brae, top left), Moorfoot Hills (top right), Dunbartonshire (bottom left), and Dounraey (bottom right).

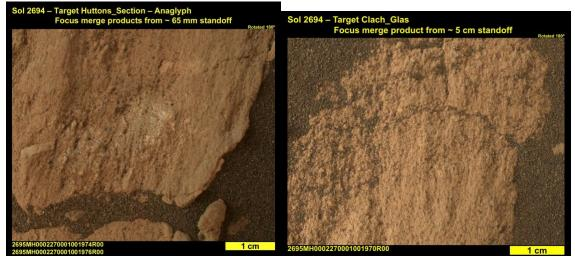


**Figure S12**. ~5 - 6 cm standoff MAHLI images of Gleann Beag pediment capping sandstone immediately at the contact with the underlying Hutton interval; Huttons Section (left) and Clach Glas (right).

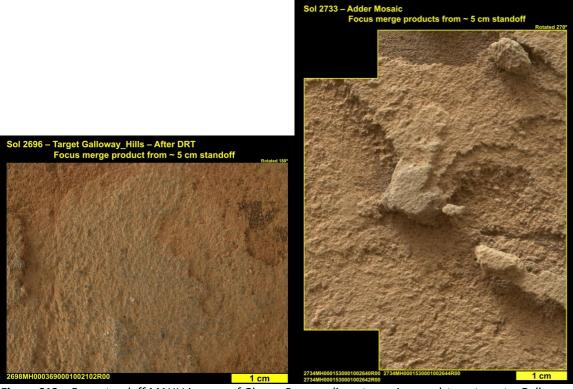


**Figure S13**.  $^{\sim}$ 5 cm standoff MAHLI images of Gleann Beag pediment capping sandstone targets; Galloway Hills (left) and nodular Adder (right).

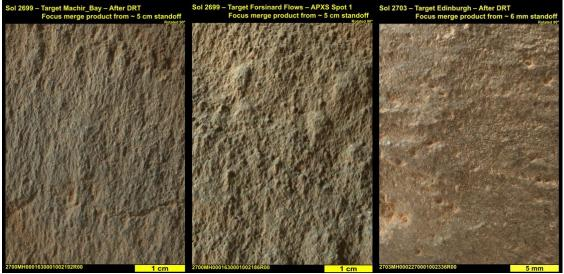


**Figure S14**. ~5-6 cm standoff MAHLI images of Ladder and Edinburgh interval pediment capping sandstone targets; Machir Bay(left), Forsinard Flows (middle), and Edinburgh (right).

Section S4: Images of previously encountered APXS targets with related compositions to pediment campaign targets (Image credit for Mastcam and MAHLI images: NASA/Caltech-JPL/MSSS)

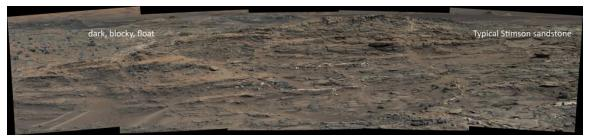


**Figure S15.** Mastcam mosaic (mcam04764) showing an outcrop is typical Stimson formation sandstone on the Emerson Plateau and associated dark, block float rocks.

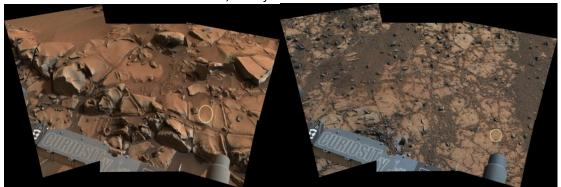


**Figure S16.** Mastcam mosaics showing workspaces for lower Mount Sharp group targets Mescal (left, mcam03600), and Telegraph Peak (right, mcam03953).

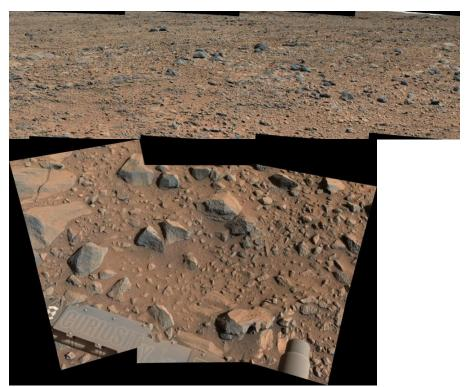


**Figure S17.** Mastcam mosaics showing: context for the Bradbury group, South Park cap rock target (top, mcam02925); and the South Park workspace (bottom, mcam02931).



**Figure S18.** Mastcam mosaics showing: context for the Bradbury group, Thimble and Stirling cap rock targets (top, mcam02977); and their workspace (bottom, mcam02994).



Figure \$19. Mastcam mosaic showingcontext for the Bradbury group, Bathurst Inlet target (mcam00240).



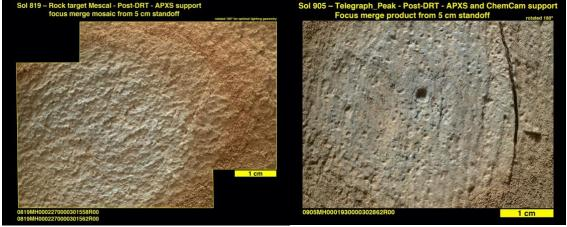
**Figure S20.** Mastcam mosaic showing context for the Bradbury group, Shaler outcrop, Eqaluik target (mcam01304).



Figure S21. Mastcam mosaic showing context for the Bradbury group, Rocknest 3 target (mcam00666).



**Figure S22.** Mastcam mosaic showing context for the Little Devil float cap rock target derived from the Salsberry Peak capping sandstones at Pahrump Hills (mcam04132).



**Figure S23.** ~5 cm standoff MAHLI images of the lower Mount Sharp group, Pahrump Hills targets; Mescal (left), and Telegraph Peak (right).

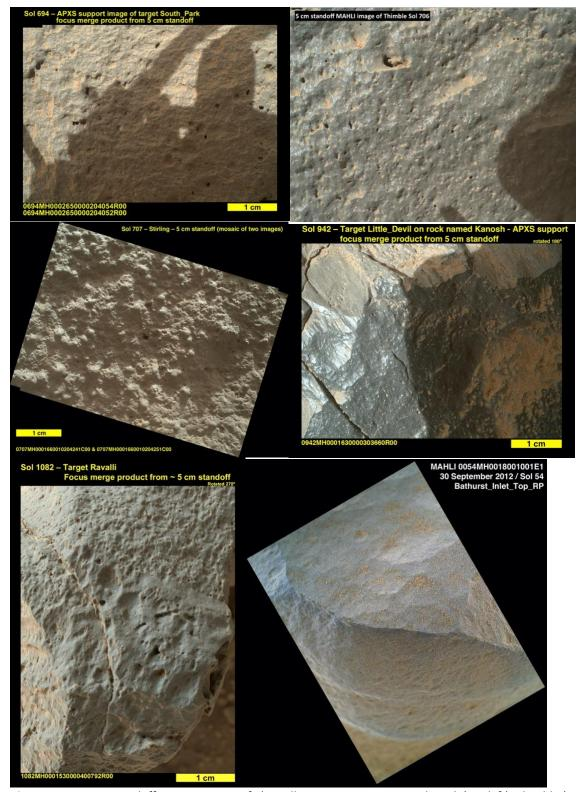


**Figure S24.** ~5 cm standoff MAHLI images of 1) Bradbury group targets: South Park (top left), Thimble (top right), and Stirling (middle left), 2) float rock targets encountered along the Mount Sharp group traverse: Little Devil (middle right), and Ravalli (bottom left), 3) Bradbury group Bathurst Inlet sandstone target (bottom right).